Deposition and Diagenesis of the Hibernia Member, Jeanne d'Arc Basin, Offshore Newfoundland

by

Colleen E. Fitzgerald

©

Submitted in partial fulfillment of the requirements
for the degree of Master of Science
at
Dalhousie University
Halifax, Nova Scotia
July 1987

DEPOSITION AND DIAGENESIS OF THE HIBERNIA MEMBER,

JEANNE d'ARC BASIN, OFFSHORE NEWFOUNDLAND

by

Colleen E. Fitzgerald

Submitted in partial fulfillment of the requirement for the degree of Master of Science at Dalhousie University, Halifax, Nova Scotia, July 30, 1987.

DALHOUSIE UNIVERSITY

Date: July 1987

Author : Colleen E. Fitzgerald

Title : Deposition and Diagenesis of the Hibernia Member, Jeanne d'Arc Basin, Offshore Newfoundland

Department or School : Geology

Degree : M. Sc. Convocation : October 1987

Permission is herewith granted to Dalhousie University to circulate and to have copied for non-commercial purposes, at its discretion, the above title upon the request of individuals or institutions.

_____

Signature of Author

THE AUTHOR RESERVES OTHER PUBLICATION RIGHTS, AND NEITHER THE THESIS NOR EXTENSIVE EXTRACTS FROM IT MAY BE PRINTED OR OTHERWISE REPRODUCED WITHOUT THE AUTHOR'S WRITTEN PERMISSION.

THE AUTHOR ATTESTS THAT PERMISSION HAS BEEN OBTAINED FOR THE USE OF ANY COPYRIGHTED MATERIAL APPEARING IN THIS THESIS (OTHER THAN BRIEF EXCERPTS REQUIRING ONLY PROPER ACKNOWLEDGMENT IN SCHOLARLY WRITING) AND THAT ALL SUCH USE IS CLEARLY ACKNOWLEDGED.

TABLE OF CONTENTS

List of Figures		v
List of Plates		vi
List of Enclosures		vii
Abstract		viii
Acknowledgements		ix
I	Introduction	1
II	Tectonic, Structural and Stratigraphic Evolution of the Jeanne d'Arc Basin: A Summary of Previous Work	6
III	Regional Chronostratigraphy (Time-Space Diagram)	13
IV	Sedimentology of the Hibernia Member	24
V	Paleoenvironmental Interpretation and Provenance of the Hibernia Member	47
VI	Burial History of the Jeanne d'Arc Basin	55
VII	Thermal History of the Jeanne d'Arc Basin	66
VIII	Maturation of Organic Matter and Hydrocarbon Migration	76
IX	Petrography and Diagenesis of the Hibernia Member	89
X	Conclusion	123
Appendix		126
References		133

LIST OF FIGURES

		Page
Figure 1 :	Index Map	2
Figure 2 :	Generalized Stratigraphy of the Jeanne d'Arc Basin	3
Figure 3 :	Tectonic Elements of the Grand Banks	7
Figure 4 :	Late Triassic - Early Jurassic Rift Basins of the Present North Atlantic	9
Figure 5 :	Early and Late Mesozoic Basins of the Present North Atlantic	11
Figure 6 :	Stratigraphic Relationships to Fault Blocks	22
Figure 7 :	Isopach Map: Hibernia Member	25
Figure 8 :	Isolith Map: Hibernia Sandstone	27
Figure 9 :	Compositional Classification of the Hibernia Sandstone	29
Figure 10:	Thermal-Burial History Curves: Hibernia P-15	58
Figure 11:	Thermal-Burial History Curves: Hibernia B-08	59
Figure 12:	Thermal-Burial History Curves: Hibernia K-18	60
Figure 13:	Thermal-Burial History Curves: Hebron I-13	61
Figure 14:	Thermal-Burial History Curves: Ben Nevis I-45	62
Figure 15:	Thermal-Burial History Curves: Nautilus C-92	63
Figure 16:	Thermal-Burial History Curves: Hibernia O-35	64
Figure 17:	Thermal-Burial History Curves: Egret K-36	65
Figure 18:	Diagrammatic Structure and Sediment Thickness Map: Jeanne d'Arc Basin	67
Figure 19:	Average Geothermal Gradient: Jeanne d'Arc Basin	68
Figure 20:	Vertical Changes in Geothermal Gradient, Wells Nautilus C-92, Hibernia K-18, Hibernia B-08, and Hibernia O-35	70
Figure 21:	Vertical Changes in Geothermal Gradient, Wells Hibernia P-15, Egret K-36, Hebron I-13, and Ben Nevis I-45	71
Figure 22:	Surface Heat Flow Versus Time for a Scotian Basin Model	74
Figure 23:	Correlation of Time-Temperature Index and Vitrinite Reflectance	77
Figure 24:	Isopach of the Oil Window: Jeanne d'Arc Basin	79
Figure 25:	Organic Maturation Profiles based on Vitrinite Reflectance, Wells Nautilus C-92, Hibernia K-18, Hibernia B-08, and Hibernia O-35	81
Figure 26:	Organic Maturation Profiles based on Vitrinite Reflectance, Wells Egret K-36, Flying Foam I-13, Ben Nevis I-45, and Hebron I-13	82
Figure 27:	Grain Size Compared to Porosity of Hibernia Sandstone	91

Table

Table 1:	Source of Data Used in This Study	5

LIST OF PLATES

Page

Core Photographs

Plate 1 : Hibernia Sandstone Reservoir 31
Plate 2 : Basal Conglomerate 32
Plate 3 : Deformed Shale Clasts in the Hibernia Sandstone 33
Plate 4 : Coal-rich Hibernia Sandstone 34
Plate 5 : Coal Seam Overlain by Hibernia Sandstone 37
Plate 6 : Silty Shale in Sharp Contact with Overlying Sandstone 38
Plate 7 : Finely Laminated Shale and Siltstone 39
Plate 8 : Bioturbated Siltstone 40
Plate 9 : Bioturbated Sideritic Shale 41
Plate 10: Siltstone with Concentrations of Shells, Shale Clasts, and Quartz Pebbles 42
Plate 11: Fault Breccia 45
Plate 12: Silty Shale and Argillaceous Siltstone Rubble 46

Photomicrographs

Plate 13: Conglomerate with Abundant Detrital Nodules of Siderite and Pyrite 95
Plate 14: Secondary Porosity Outlined by Pre-Dissolution Clay 97
Plate 15: Dolomite Rhombs 98
Plate 16: Ferroan Calcite Cementation and Replacement of Plagioclase 99
Plate 17: Calcite Cementation and Replacement of Plagioclase 101
Plate 18: Extensive Pyrite and Ferroan Calcite Cement 102
Plate 19: Honeycombed Feldspar and Patchy Ferroan Calcite Cement 103
Plate 20: Siltstone with Detrital Quartz Overgrowths Partially Replaced by Kaolinite 104
Plate 21: Sedimentary Rock Fragments Partially Replaced by Kaolinite and Pyrite 106
Plate 22: Siltstone Clast Replaced by Ferroan Calcite 107
Plate 23: Ferroan Calcite and Clay Associated with Secondary Porosity 108
Plate 24: Grain Replacement 109
Plate 25: Diagenetic Front Between Ferroan Calcite and Clay 110
Plate 26: Grain Molds 111
Plate 27: Ghost Grain and Corroded Quartz Overgrowths 113
Plate 28: Laumontite Cement 114
Plate 29: Laumontite Cement 115

LIST OF ENCLOSURES

Enclosure 1 : Time - Space Diagram, Jeanne d'Arc Basin
Enclosure 2 : Stratigraphic Column: Hibernia K-14
Enclosure 3 : Stratigraphic Column: Hibernia K-18
Enclosure 4 : Stratigraphic Column: Hibernia B-08
Enclosure 5 : Stratigraphic Column: Hibernia B-27
Enclosure 6 : Stratigraphic Column: Hebron I-13
Enclosure 7 : Stratigraphic Column: Ben Nevis I-45
Enclosure 8 : Lithofacies Relationships Within the Hibernia Member
Enclosure 9 : Structural Fence Diagram: Hibernia Member
Enclosure 10: Depth Versus Sandstone Porosity
Enclosure 11: Petrographic Data: Hibernia K-14

ABSTRACT

The Jeanne d'Arc Basin was formed during Late Triassic to Early Cretaceous time by two episodes of rifting that caused repeated movement on one set of basin-forming faults. This resulted in up to 14 km of sediments, some of which contain huge reserves of hydrocarbons. The Hibernia member, the subject of this thesis, is a sandstone dominated zone within this basin-fill that contains a high proportion of the discovered hydrocarbons.

Deposition of the Hibernia member is a result of two simultaneous and related events during Tithonian to Berriasian time: 1. deep erosion of upthrown sides of the fault blocks, and 2. a global eustatic rise of sea-level. The provenance and depositional environment are interpreted from the examination of cores, cuttings, microfossils, and thin sections. The siliciclastics were derived from a southern source of sediments and sedimentary rocks that had an original metamorphic origin. They were deposited in a non-marine to brackish water environment of channels and associated floodplains in an anastomosed fluvial system. Rates of sedimentation and subsidence were high, and coupled with a contemporaneous eustatic sea level rise resulted in rapid aggradation and a thick sequence.

The center of the basin currently has the highest geothermal gradient and thinnest oil window. Burial and thermal history curves show that the source rocks reached maturity first at the Ben Nevis well; early-formed hydrocarbons may have been lost during tectonic movements in Albian time. The source rocks underlying the Hibernia field are presently at peak oil-generating capability. Organic acids formed during the maturation of organic matter have produced excellent secondary porosity in the sandstones of the Hibernia field. However, at Ben Nevis, subsequent thermal degradation of carboxylic acids allowed late-stage cementation by ferroan calcite cement, destroying the reservoir porosity.

ACKNOWLEDGEMENTS

I am especially grateful to Mobil Oil Canada for providing relevant summer employment and partially funding my graduate work.

I would also like to thank my supervisory committee: Dr. P.E. Schenk (Dalhousie University) and Drs. L.F. Jansa and K.D. McAlpine (Atlantic Geoscience Centre, Bedford Institute of Oceanography).

Phil Moir was very helpful in retrieving well logs from the A.G.C. computer data base and Dr. D.B. Scott and S. Thibideau kindly assisted with microfossil identification.

I. INTRODUCTION

The Hibernia member of the Upper Jurassic to Lower Cretaceous Missisauga Formation is one of four principal reservoirs of the giant Hibernia oil field (Arthur et al., 1982). The Hibernia member has been encountered only in the subsurface by 16 exploratory wells, all located within the Jeanne d'Arc Basin, offshore Newfoundland, Canada. (Fig. 1)

Due to its economic significance, the general stratigraphic framework of the Jeanne d'Arc Basin has been the focus of previous studies by oil companies, government scientists and consultants (Fig. 2). The sedimentology and diagenesis of the Hibernia member was studied by Robertson Research (unpublished consultant report, 1985) and D. Brown (M.Sc. thesis, Carleton University, 1985).

The purpose of this thesis is to study the stratigraphic, sedimentologic, and diagenetic aspects of the Hibernia member in the context of basin evolution. A multi-disciplinary approach is used to show how deposition, preservation, and diagenetic alteration of the Hibernia reservoir was affected by a prolonged period of basin formation.

Recent advances in basin modelling have provided a theoretical basis for basin analysis (e.g. 1986 Atlantic Geoscience Society Symposium on Basins of Eastern Canada). Masson and Miles (1984) contributed an updated plate

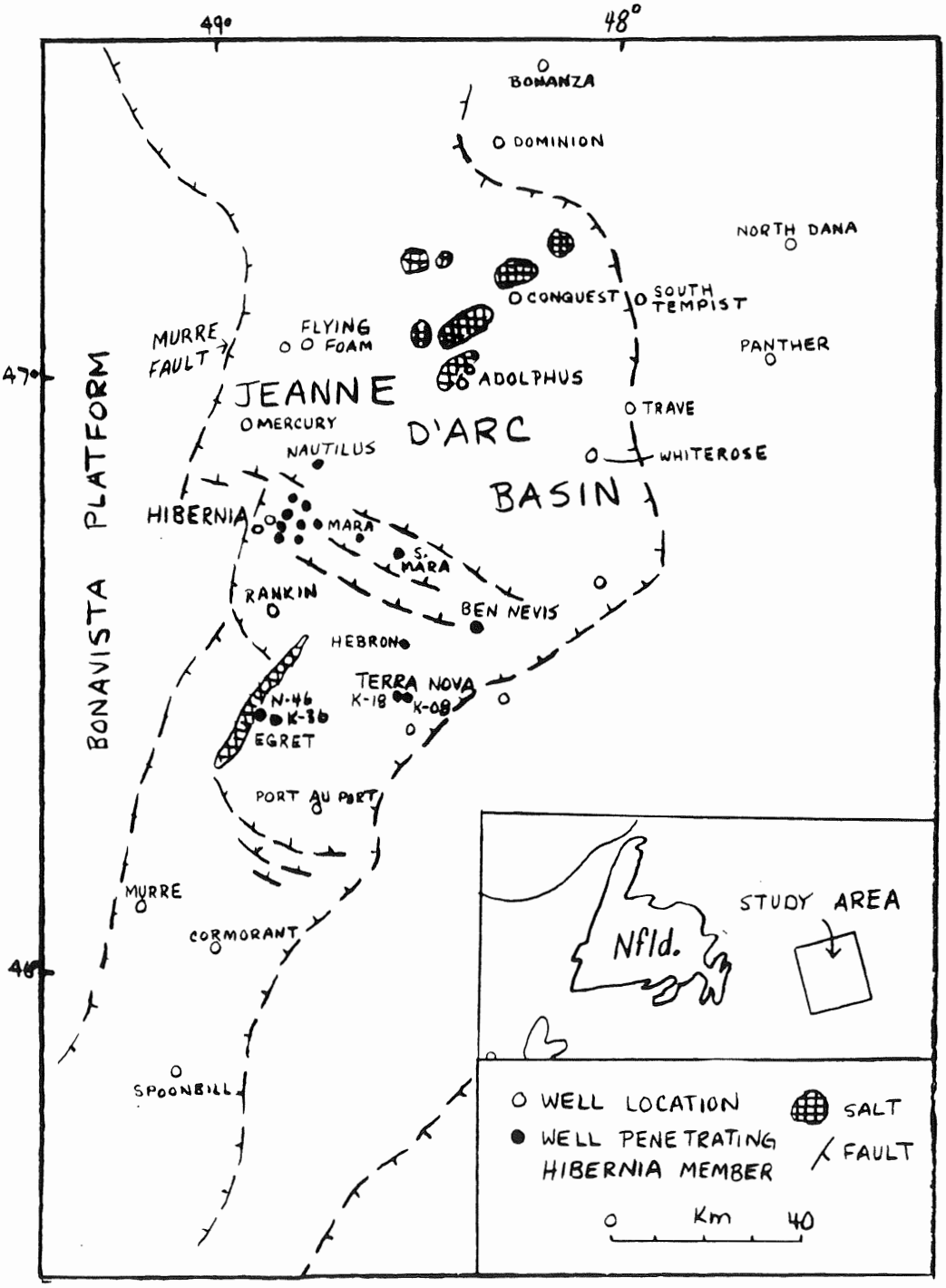

Figure 1: Diagrammatic structure map of the Jeanne d'Arc Basin showing the location of wells penetrating the Hibernia member (modified from Grant et al., 1986).

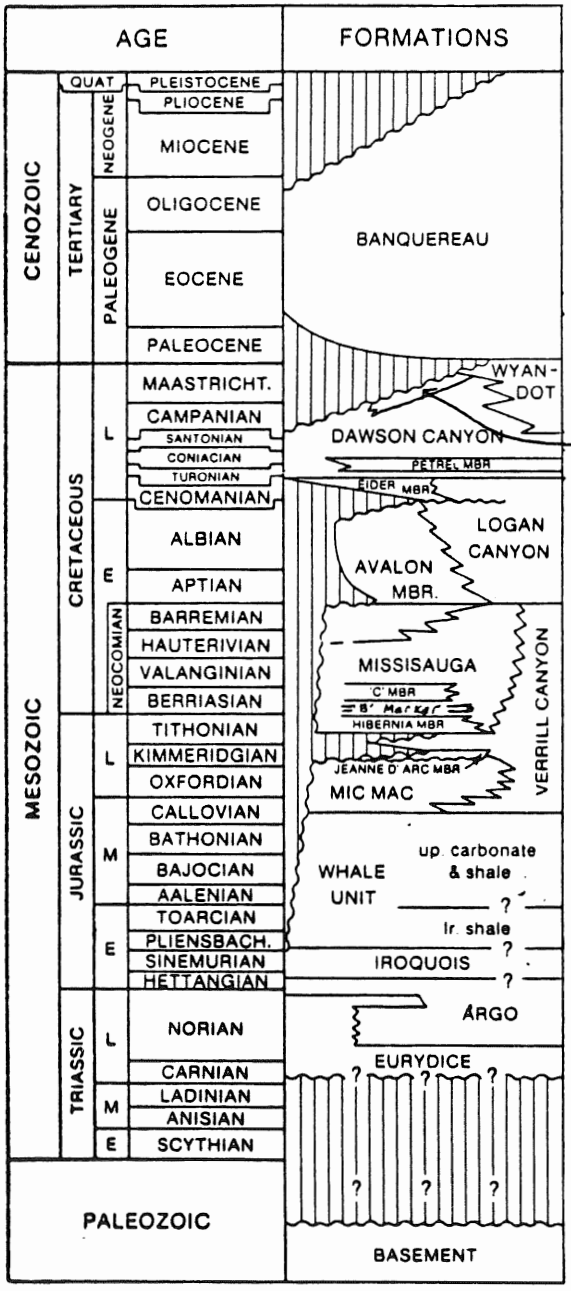

Figure 2: Generalized stratigraphy of the Jeanne d'Arc Basin (modified from Grant et al., 1986). The Jeanne d'Arc, Hibernia, "C", and Avalon members are informal units introduced by Arthur et al., 1982.

reconstruction of the North Atlantic area prior to continental drift. Quantitative thermo-mechanical models of deep crustal structure and extensional development of rifted basins have recently been developed (e.g. Keen et al., 1982). A tectonic model based on simple shear has subsequently been proposed to explain the structural and stratigraphic framework of the Jeanne d'Arc Basin (Tankard and Welsink, in press). This study will further consider the effect of tectonics on diagenesis.

The material from which data was obtained is summarized in Table 1. It consists of all information released to the date of this study from wells penetrating the Hibernia member. The material was obtained from the Canadian Oil and Gas Lands Administration and the Atlantic Geoscience Centre, Bedford Institute of Oceanography, Dartmouth, Nova Scotia.

The thesis begins with a summary of the tectonic evolution of the Jeanne d'Arc Basin, based on recent literature. The author's contribution begins in chapter III, where chronostratigraphic correlations are explained in terms of syndepositional tectonics. Such correlation is used in turn to interpret the regional geologic framework. Chapter IV documents sedimentologic data for the Hibernia member and Chapter V develops an interpretation of paleoenvironment and provenance, consistent with the interpreted basinal history. Chapters VI and VII describe the burial and thermal history of the basin and Chapter VIII discusses the maturation of

organic matter and hydrocarbon migration. Aspects of the basin analysis are used to explain the diagenetic history of the Hibernia member in chapter IX. An understanding of the tectonic control on basin development is necessary in order to predict the occurrence of porous, hydrocarbon-bearing Hibernia sandstone.

WELL	PETROPHYSICAL LOGS	PETROPHYSICAL CORE	CUTTING SAMPLES AT 5M INTERVALS	THIN SECTIONS	BIOSTRATIGRAPHIC DATA FORAMINIFERA	BIOSTRATIGRAPHIC DATA PALYNOMORPHS	BIOSTRATIGRAPHIC DATA OSTRACODS
Ben Nevis I-45	X		128	24	a	d	
Hebron I-13	X		110	26	a	e	f
Hibernia K-14	X	115 m	32	68			
Hibernia K-18	X	81 m		21	a	e	e,f
Hibernia B-27	X	74 m					
Hibernia B-08	X	40 m		32	a	e	f
Hibernia P-15	X				a		f
Hibernia O-35	X				a	e	f
Hibernia C-96	X						
Nautilus C-92	X				a		
Terra Nova K-08	X				f		f
Egret K-36	X			12	a,b	c	b
Flying Foam I-13	X				a	d	
		310 m	270	183			

a: Williamson, 1987
b: F. Gradstein
c: G. Williams
d: J.P. Bujak
e: E.H. Davies
f: P. Ascoli

Table 1: Source of data used in this study.

II TECTONIC, STRUCTURAL AND STRATIGRAPHIC EVOLUTION OF THE JEANNE D'ARC BASIN: A SUMMARY OF PREVIOUS WORK

The Jeanne d'Arc Basin is one of a series of fault-bounded Mesozoic basins beneath the Grand Banks (Fig. 3). It lies between the stable Bonavista Platform to the west, composed of metamorphosed Precambrian and Paleozoic rocks, and the Outer Ridge Complex to the east, which contains highly faulted Early Mesozoic sediments (Avery et al., 1986). Continental crust underlies the entire area. The post-Paleozoic geologic record reveals essentially a history of intracratonic development, although various episodes of continental rifting are responsible for the timing of events in the tectonic evolution (Grant et al., 1986).

Until the mid-Mesozoic, the Grand Banks area was located within the supercontinent of Pangea. This area consisted of lithologically distinctive accretionary terrains of the Appalachian Orogen. Subsequent tectonism related to the development of the North Atlantic Basin was influenced by this complexity.

The evolution of the sedimentary basins on the Grand Banks probably began with a Late Triassic phase of rifting (Jansa and Wade, 1975; Masson and Miles, 1986). Red bed and evaporite sequences of Late Triassic and Early Jurassic age have been identified in rift basins on the Grand Banks, Scotian Shelf, along the western margins of Europe, and in Northwest Africa. In the Jeanne d'Arc Basin, the continental

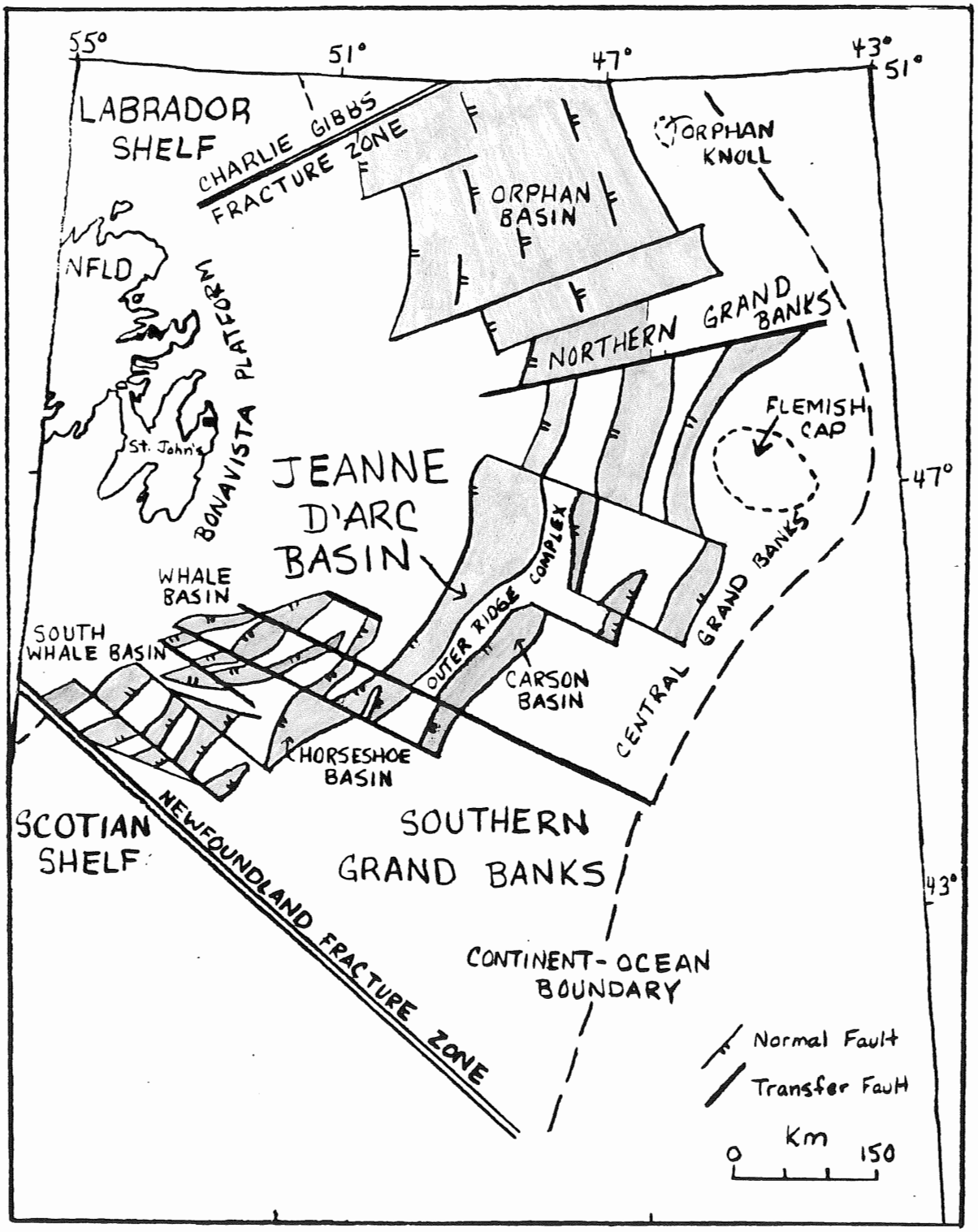

Figure 3: Tectonic elements of the Grand Banks (modified from Tankard and Welsink, in press).

red beds of the Eurydice Formation and evaporites of the Argo Formation record this earliest phase of taphrogenic subsidence (Jansa and Wade, 1975; Fig. 2). Figure 4 shows the distribution of these early rift basins plotted on a North Atlantic plate reconstruction by Masson and Miles (1984). The basins are components of a northeast-southwest trending rift system in which the Grand Banks basin complex is correlated with sediments of the Porcupine Basin, through one or two basins between Flemish Cap and Orphan Knoll (Masson and Miles, 1986).

The clastic sediments in the Scotian Basin record an Early Jurassic tectonic episode due to the initial rifting between Africa and North America (Sherwin, 1973; Jansa and Wade, 1975). Masson and Miles (1986) suggest that the entire rift system was caused by this tension.

During the Early and Middle Jurassic epochs, the area north of the Newfoundland - Azores - Gibraltar Fracture Zone was tectonically quiet (Masson and Miles, 1986). At this time, the environment changed from continental or restricted to normal marine conditions which produced the dolomite and limestone of the Iroquois Formation and the shale and carbonate of the Whale Unit (Fig. 2). During the Middle Jurassic (Bajocian) oceanic crust began to form in the area south of the Newfoundland Fracture Zone as the African and North American plates completely separated (Pitman and Talwani, 1972). Lateral movement between Europe-North

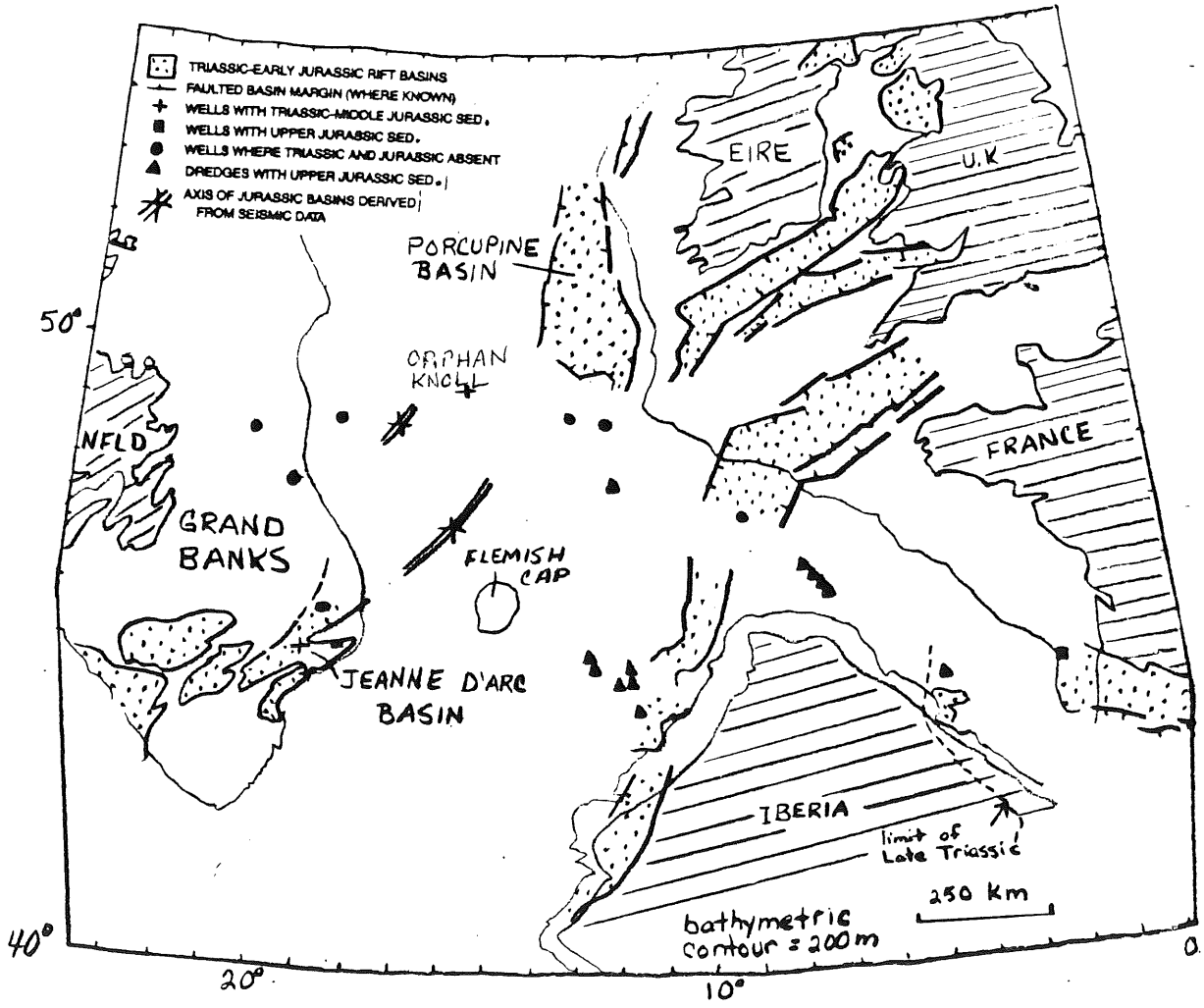

Figure 4: Distribution of Early Mesozoic rift basins plotted on a North Atlantic plate reconstruction (modified from Masson and Miles, 1986).

America and North Africa was accommodated by the transform fault along the southern margin of the Grand Banks (Le Pichon, et al., 1977), relieving the tension in the north.

During the Late Jurassic and Early Cretaceous, a major phase of rifting occurred north of the Newfoundland Fracture Zone (Masson and Miles, 1986). This second episode of rifting produced basins which trend parallel to the present western and eastern margins of the Atlantic Ocean.

Figure 5 shows both the early and later Mesozoic rift basins as defined by Masson and Miles (1986). Only in the Grand Banks - Iberia area did the later rifts follow earlier northeasterly trends. In the south and central Grand Banks, the orientation of the basin-forming faults may have been controlled by inherited Paleozoic structures which in part coincided with regional stress patterns (Tankard and Welsink, in press). Reactivation of the faults may have overdeepened the Jeanne d'Arc Basin which contains up to 14 km of sediment (Avery et al., 1986).

Both of the extensional episodes were accommodated by northeast trending listric and planar normal faults with strikes parallel to the basin axis. Southeast trending transfer faults compensated for different amounts and rates of extension by opening the Jeanne d'Arc Basin to the north (Tankard and Welsink, in press).

During the later rifting episode (Late Callovian to Aptian), 80% of the sedimentary fill in the Jeanne d'Arc

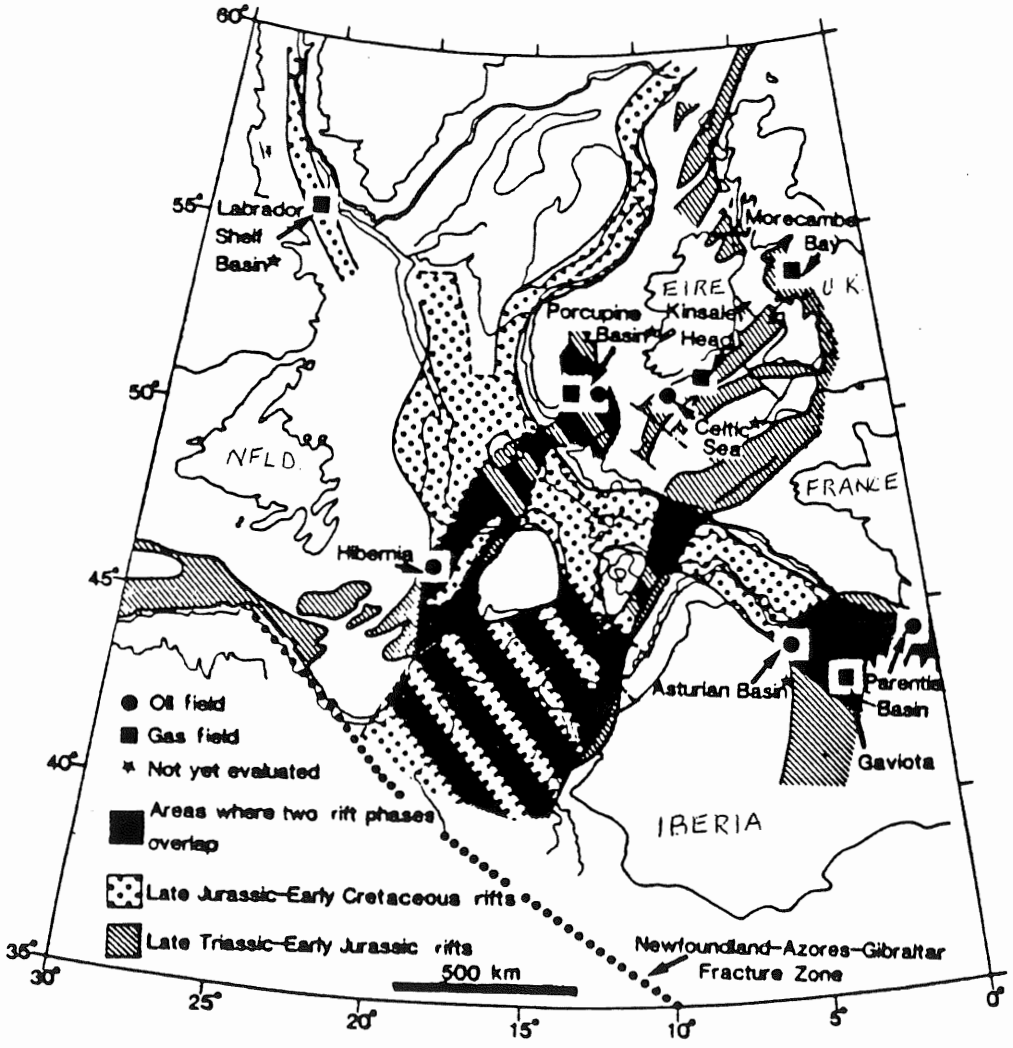

Figure 5: Early and Late Mesozoic basins plotted on a North Atlantic plate reconstruction (after Mason and Miles, 1986).

Basin was deposited (Tankard and Welsink, in press). Large amounts of clastics were deposited on the down-thrown sides of fault blocks. This was contemporaneous with a eustatic sea level rise (Vail and Mitchum, 1978) and resulted in complex facies development, discussed in Chapter III. These synrift sediments contain all of the hydrocarbon discoveries to date.

During middle Cretaceous time, oceanic crust began to develop between the Iberian Peninsula and the Grand Banks (115 Ma) and between Galicia Margin and Flemish Cap (100 ma) (Masson and Miles, 1984). These events are associated with structural adjustments in the Jeanne d'Arc Basin, reflected in the widespread pre-Aptian and Avalon unconformities Tankard and Welsink (in press) believe that the net slip on the older faults was normal so that the basin deepened to the northeast. Increasingly northward plunge of the basin and gravity processes may have generated a new set of listric normal faults which detached and rotated the upper parts of the transfer blocks.

By Late Cretaceous time, faulting had ceased and slow thermal subsidence resulted in the deposition of an undisturbed section of marine siliciclastics and chalky limestone. The unconformity at the base of the Tertiary section coincides with the separation of Europe and Greenland, the last tectonic event to be recorded in the basin.

III REGIONAL CHRONOSTRATIGRAPHY (TIME-SPACE DIAGRAM)

Enclosure 1 is a time-space diagram showing the chronostratigraphic relationships between 12 wells in the Jeanne d'Arc Basin. The diagram was constructed using biostratigraphic age determinations to date the lithologic boundaries in each well. The lithologic boundaries were plotted and correlated on a vertical axis of time; the distance between wells was plotted on the horizontal axis. Fossil data helped to ascertain the stratigraphic location of the major unconformities. The time and space represented by each unconformity was shown as a lacuna.

The diagram is based on unpublished biostratigraphic studies of foraminifera, polynomorphs, and ostracoda (Table 1), as well as the published results of a quantitative biozonation by Williamson (1987). Unfortunately, much of the biostratigraphic data existing for the Jeanne d'Arc Basin is imprecise. Occasional contradictions occurred between the palynomorph data and the foraminifera and ostracoda data. Palynology seemed to provide better stratigraphic resolution for the non-marine parts of the Upper Jurassic section, whereas foraminifera and ostracoda data were generally more useful for dating the remaining marine sections. Three problems are associated with the use of the microfossil data:

(1) Microfossils are extracted mainly from cuttings samples which can be cavings from an overlying unit. In non-marine lithologies, caved fossils dilute the rare, in-place fossils.

(2) Erosion of sediment from uptilted fault blocks at the pre-Aptian and Avalon unconformities yield reworked fossils, causing erroneous dates in adjacent wells.

(3) Biozones are usually defined by European and Scotian Shelf assemblages. These faunal provinces may not always have been in communication. Most ostracod species do not have planktonic larvae and cannot cross physical or oceanographic barriers (such as temperature and salinity differences). They are only of limited use for intercontinental or interregional stratigraphy, especially in the Cenozoic (Pokorny, 1978).

Because of these drawbacks, much of the time-space diagram is based on Williamson's (1987) quantitative biozonation of the Early Cretaceous and Late Jurassic of 13 wells in the Jeanne d'Arc Basin. His scheme is independent of zonal schemes developed for Western Europe or the Scotian Basin and specifically compares the fauna in wells of the Jeanne d'Arc Basin.

Williamson used a ranking and scaling (RASC) computer programme to sift objectively through last occurrence data (extinction points) of 113 species of foraminifera. The program records the frequency with which each fossil event

occurs above, below, and simultaneously with each other event, and so develops an optimum or average sequence. Using the cross-over frequency of pairs of events in the optimum sequence, the events are scaled along an axis with the assumption that, the greater the cross-over frequency, the closer together they are stratigraphically. Using a few well-established fossil dates, he was able to substitute the RASC distances with an absolute time scale (Kent and Gradstein, 1984).

There are three main advantages of Williamson's scheme: (1) The method facilitates the use of foraminifera species which may be of limited use for global correlations but are significant in developing local zonal schemes.

(2) Anomalous events could be recognized by comparison to the optimum sequence. Reexamination of identified abnormalities in terms of the state of preservation of the observed event, the taxonomic certainty of the original identification, the abundance of the event, and the co-occurrence of other misplaced events, enabled these abnormalities either to be removed from the data set, or to be reassigned to another level in the well.

(3) Each biozone was ascribed a measure of reliability, an important feature for its application to the time-space diagram. Biozones with a large standard deviation were given less consideration than dates implied by more conventional biostratigraphy.

The time-space diagram is a synthesis of the biostratigraphic data based on subjective judgements of the accuracy of the fossil data. Dates obtained from different microfossils were averaged for some horizons, whereas clearly anomalous dates were disregarded. From preliminary correlations, it was noted that each major lithologic unit (eg. Verrill Canyon Shale) had a consistent sedimentation rate. This rate would include any short-lived erosional events associated with the non-marine facies. These average "accumulation rates" were used to extrapolate ages to specific rock boundaries and to help to establish the time frame of the lacunas. Other chronostratigraphic interpretations are certainly possible, although no similar diagrams are known to the author.

The diagram implies a chronology of geologic events, consistent with published interpretations based mainly on seismic data. The diagram will be interpreted with reference to the literature, in order to introduce the stratigraphic framework of the Jeanne d'Arc Basin.

Enclosure 1 shows four main sequences separated by the Late Cretaceous lacuna, the Avalon lacuna, the Pre-Aptian lacuna, and the short-lived Kimmeridgian lacuna. Within each sequence, net transgressive or regressive stratigraphic transitions are classified according to the dominant process responsible for shoreline translation (following Curray, 1964). The most important of these variables are eustatic sea level change, sediment supply, and subsidence rate.

The first sequence consists of undifferentiated limestones and shales immediately below the Kimmeridgian Unconformity. Only five wells shown on the diagram penetrated this sequence. During 10 Ma of slow subsidence, organic-rich Kimmeridgian shales were deposited. They are a source rock for oil in the Jeanne d'Arc Basin (Powell, 1984). These shales are coeval with an Oceanic Anoxic Event which produced widespread, organic-rich marine black shales in the North Atlantic region (Demaison and Moore, 1980). Tectonically, the sequence may reflect the lower plate distension that precedes brittle deformation of the continental crust, according to a simple shear extensional model (Tankard and Welsink, in press). Alternatively, the widespread steady subsidence may have been a continuation of thermal contraction of the mantle following the first phase of rifting.

The second sequence was deposited during the Late Jurassic to Early Cretaceous taphrogenic episode; it consists of the Jeanne d'Arc sandstones, and the Verrill Canyon and Missisauga formations. Over two kilometers of sediment were deposited during 50 Ma of rifting. Seismic data show that this sequence is highly faulted and penetrated by salt, in contrast to the overlying undisturbed sequences (McKenzie, 1981). This second sequence contains the four principal reservoir rocks (the Jeanne d'Arc, Hibernia, Catalina and Lower Avalon sandstones) and numerous structural traps.

The Jeanne d'Arc member consists of immature fluvial sediments with conglomerate clasts up to 10 cm in diameter. In the Hibernia P-15 well, the conglomerate clasts consist of limestone, chert, mudstone, shaly sandstone, and metaquartzite. They show little evidence of weathering and have a low degree of roundness and sphericity. This suggests high local relief and short transport distances (Arthur, et al.,1982). The time-space diagram shows a lacuna in the Egret area while the Jeanne d'Arc sandstone was being deposited elsewhere. Perhaps the Mic Mac Formation in the Egret area supplied the sedimentary conglomerate clasts. The metaquartzite clasts may have been sourced from the Avalon terrain to the west.

The average accumulation rate for the Jeanne d'Arc member was approximately 90 m/Ma, the highest rate calculated from the chronostratigraphic data. There are probably minor discontinuities in this non-marine member, so the true sedimentation rate may have been higher.

Seismic lines show a westward thickening of this interval toward the basin-bounding Murre Fault. This has been attributed to growth faulting during sedimentation (Arthur, et al., 1982). Relatively high sedimentation rates and growth faulting may explain why the Jeanne d'Arc member is currently overpressured in the Hibernia field.

High local relief, short transport distances, high sedimentation rates and growth faulting, together suggest

that the Jeanne d'Arc Basin was receiving large volumes of sediment from upthrown fault blocks, causing a depositonal regression. A contemporaneous "global" eustatic sea level rise (Vail and Mitchum, 1978), eventually caused a net transgression.

The "J" seismic marker is a prominent chalky limestone on well logs and in seismic data. Biostratigraphic data suggest that it is synchronous across the basin. It may represent a time of maximum transgression and was used as a time marker to aid correlation on the time-space diagram.

The Verrill Canyon Shale to Hibernia sandstone transition is a regressive succession, representing a change from marine to non-marine conditions. A second order eustatic sea level fall at 150 Ma (Vail and Mitchum, 1978) was coincident with an abundant sediment supply. This was followed by a resumption of eustatic sea level rise while the Hibernia member was being deposited.

The time-space diagram shows that there are two separate cycles of sandstone deposition. Marine shales were deposited in the Ben Nevis area while the non-marine Hibernia interval was forming on the western basin margin (146 Ma). Deposition of the Hibernia member in the west, began at the Hibernia O-35 well location, adjacent to the Murre Fault. In the Egret-Terra Nova area, initial progradation of the Hibernia sandstones may have filled the shallower part of the basin so that it remained above sea level at 146 Ma.

By approximately 144 Ma, sea level rise surpassed sediment supply along the western basin margin. Perhaps relief at the Murre Fault was diminishing, allowing a net transgression. Meanwhile, the Hibernia member was aggrading in the Ben Nevis area, reflecting movement at the adjacent faults.

The remainder of the sequence, from the "B" limestone to the top of the Missisauga Formation, is mainly transgressive. The sediment supply was probably diminishing as sea level continued to rise. Whereas the Hibernia member accumulated at an average rate of 70 m/Ma, the remainder of the Missisauga Formation subsided at a rate of 55 m/Ma. However, the Murre Fault was still active; growth faulting caused anomalously high sedimentation rates (70 m/Ma) at the Hibernia O-35 well location.

The Catalina sandstones are finer grained than the Hibernia sandstones. Decreased current velocities may have resulted from decreased relief of the uptilted fault blocks. Alternatively, the source of clastics may have been farther away at this time. Tankard and Welsink (in press) believe that the shoreline was located outside the confines of the half graben. The presence of limestone in the Upper Missisauga Formation is consistent with a diminishing supply of clastics.

The third sequence, containing the Upper Avalon sandstone reservoir, occurs after the Pre-Aptian lacuna and

before the Avalon lacuna. The episodes of erosion coincide with the separation of the Grand Banks from Iberia (115 Ma) and Flemish Cap from Galicia Margin (100 Ma) (Masson and Miles, 1984). The sea-floor spreading in the east apparently caused structural adjustment in the Jeanne d'Arc Basin.

Seismic records show that northward tilting of the basin occurred in Aptian time (Arthur et al., 1982). Tankard and Welsink (in press) argue that an intrabasinal detachment converted the upper parts of older transfer faults into listric normal faults, deepening the basin to the northeast. Progressive rotation of the fault blocks would have caused suites of unconformities that converge toward the northern uptilted edges of these blocks (Fig. 6). The differential erosion represented on the time-space diagram is consistent with this interpretation.

A complete holostrome may be represented in the Ben Nevis well. Lower Avalon sandstones were deposited in this subsiding area while the adjacent Hebron fault block was being eroded. An erosional episode began much earlier in the Egret area, presumably due to salt movement.

Although the Upper Avalon sandstone is more continuous across the basin than the Lower Avalon, it is very thin or absent over the uptilted fault blocks (eg. Hibernia B-08 well). The Avalon lacuna began much earlier in the B-08 well and lasted much longer than in the down-thrown fault blocks (eg. Nautilus C-92).

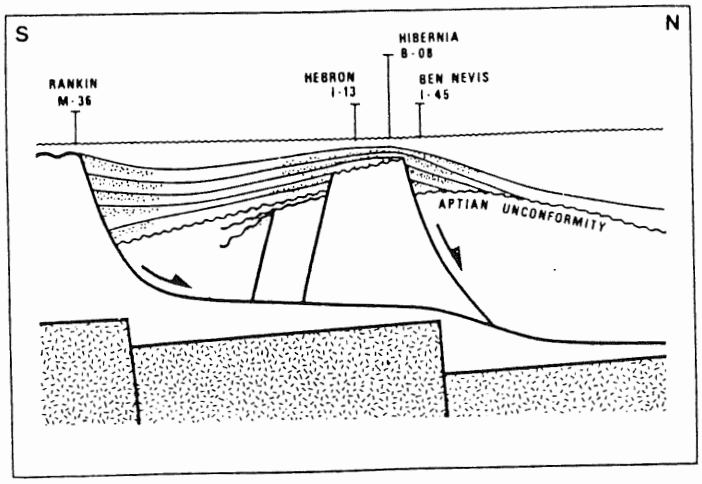

Figure 6: In the late Barremian and Aptian, structural rearrangement was associated with sea floor spreading to the east. Older transfer faults were converted into listric normal faults. This caused the pre-Aptian and Avalon unconformities to converge at the crests of transfer blocks (also see time-space diagram) and created onlapping stratigraphy (seen on seismic). (From Tankard and Welsink, in press)

The fourth sequence, of Late Cretaceous age, is a tectonically undeformed succession of marine shales, calcareous siltstones, very fine to fine sandstones, and a chalky limestone (Arthur et al., 1982). Accumulation rates decreased from an average of 43 m/Ma for the Logan Canyon Formation to 22 m/Ma for the rest of the Upper Cretaceous section. This may reflect decreasing subsidence due to decreasing thermal contraction of the lithosphere following rifting.

The upward lithologic change is transgressional until the Petrel Member. This chalky, microcrystalline limestone has been correlated across the Grand Banks and Scotian Shelf (Swift et al., 1975; Jansa and Wade, 1975). Although it may be regionally diachronous, the biostratigraphic data suggest that it is a local time marker.

The Dawson Canyon Formation to the Upper Cretaceous sandstone is a regressive succession which precedes the uppermost lacuna of the time-space diagram. The diagram shows that erosion occurred earliest at the Ben Nevis, Hebron, and Terra Nova wells which are located in the southern half of the northward-plunging basin. This southern area may have been the source of clastics for the Upper Cretaceous sandstone deposited to the north. The lacuna marks the end of major tectonic events in the Jeanne d'Arc Basin.

IV SEDIMENTOLOGY OF THE HIBERNIA MEMBER

The Hibernia member is an informal lithostratigraphic unit defined as the interval from 3744 m to 3924 m in the Hibernia P-15 discovery well (Arthur et al., 1982). It is a distinctive, sandstone-dominated rock unit, overlain and underlain by shales in the Hibernia P-15 well. The unit is easily correlated to similar sections throughout the Hibernia field, although its thickness ranges from 122 m at the Hibernia K-18 well to 282 m at the Hibernia O-35 well.

Correlation of the Hibernia member across the basin is more difficult. The more recent Ben Nevis I-45 and Hebron I-13 wells encountered additional sandstone units which do not occur in the Hibernia field. The entire section between the "B" marker limestone and the Verrill Canyon Shale (Fig. 2) is thicker at the Ben Nevis (685 m) and Hebron (588 m) wells than at the Hibernia field (average is 491 m). The additional sandstone units are considered to be part of the Hibernia member which is defined in this thesis as the sandstone-dominated rock unit occurring stratigraphically above the Verrill Canyon Shale and below the "B" marker limestone.

Geometry

Figure 7 is an isopach map of the Hibernia member penetrated by 13 wells in the Jeanne d'Arc Basin. It shows the fault-controlled erosional limits in the south, east, and west, which are evident on seismic data (Arthur et al.,

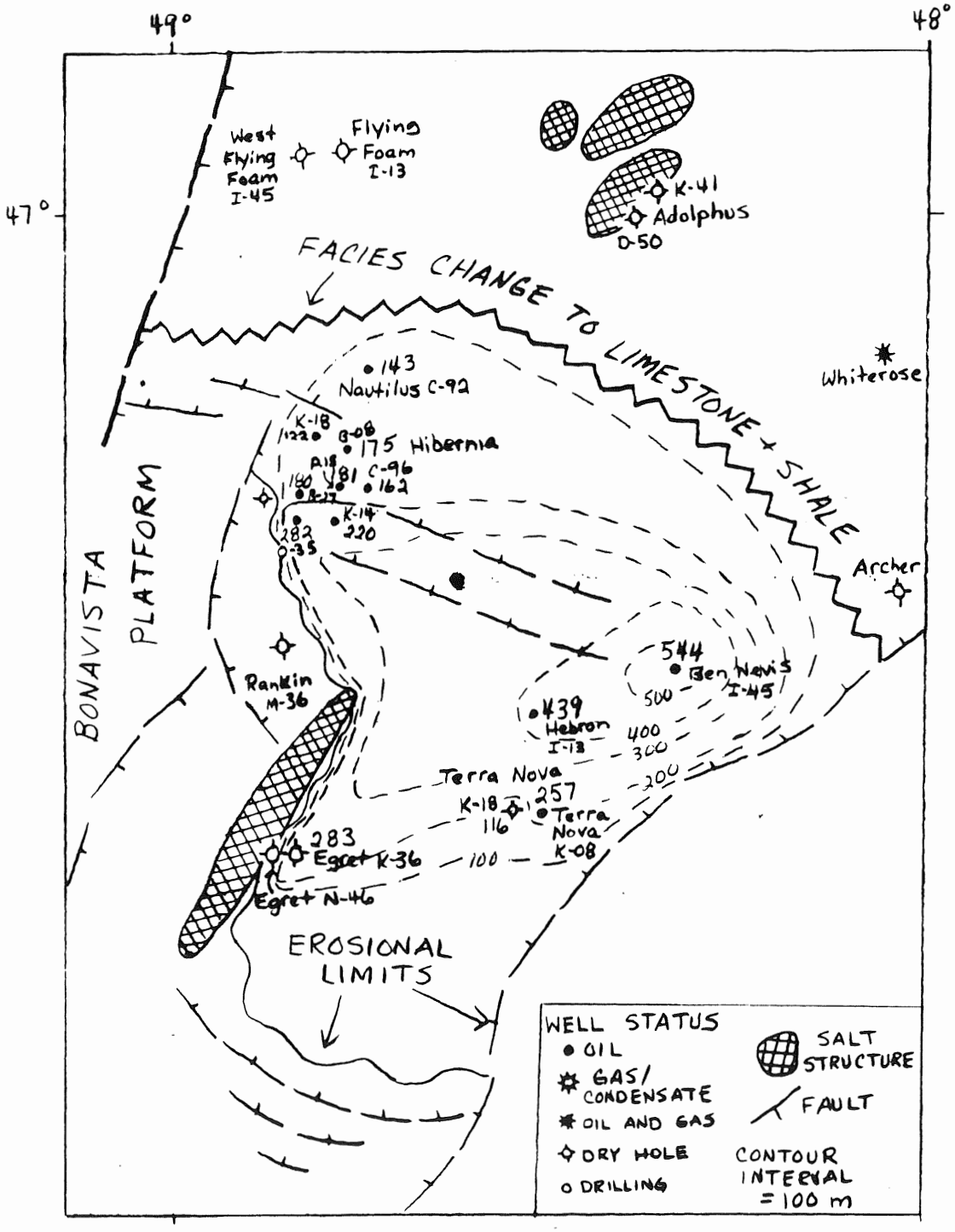

Figure 7: Isopach map of the Hibernia member, Jeanne d'Arc Basin.

1982). From the chronostratigraphic relationships between the Flying Foam and the Nautilus wells (Enclosure 1), a sandstone depositional limit is inferred to the north. The thickness of the Hibernia member is highly variable; the mean is 239 ± 27m.

Figure 8 is an isolith map of the Hibernia sandstones, obtained by adding the thicknesses of sandstones in each well as determined by a gamma ray or SP log. Wells with core in the Hibernia member helped to define appropriate cut-off values for sandstone. The percentage of sandstone in the Hibernia member varies from 82% in the Terra Nova K-18 well to 29% in the Hebron well. There is a large variation, even in the Hibernia wells: 78% sandstone in the P-15 well to 36% in the O-35 well. For all thirteen wells, the mean is 55 ± 16% sandstone in the Hibernia member.

Lithofacies

Enclosures 2 to 7 are stratigraphic columns of the Hibernia member penetrated by two wells in the eastern part of the basin (Hebron I-13 and Ben Nevis I-45) and four western basin margin wells (Hibernia K-14, K-18, B-08, and B-27). The most valuable sedimentologic data was obtained from Hibernia K-14 which contains 115 metres of continuous core; cuttings samples were used to complete this stratigraphic column. Data on cements and porosity are visual estimates from core and cuttings; porosity values were also measured from the sonic log.

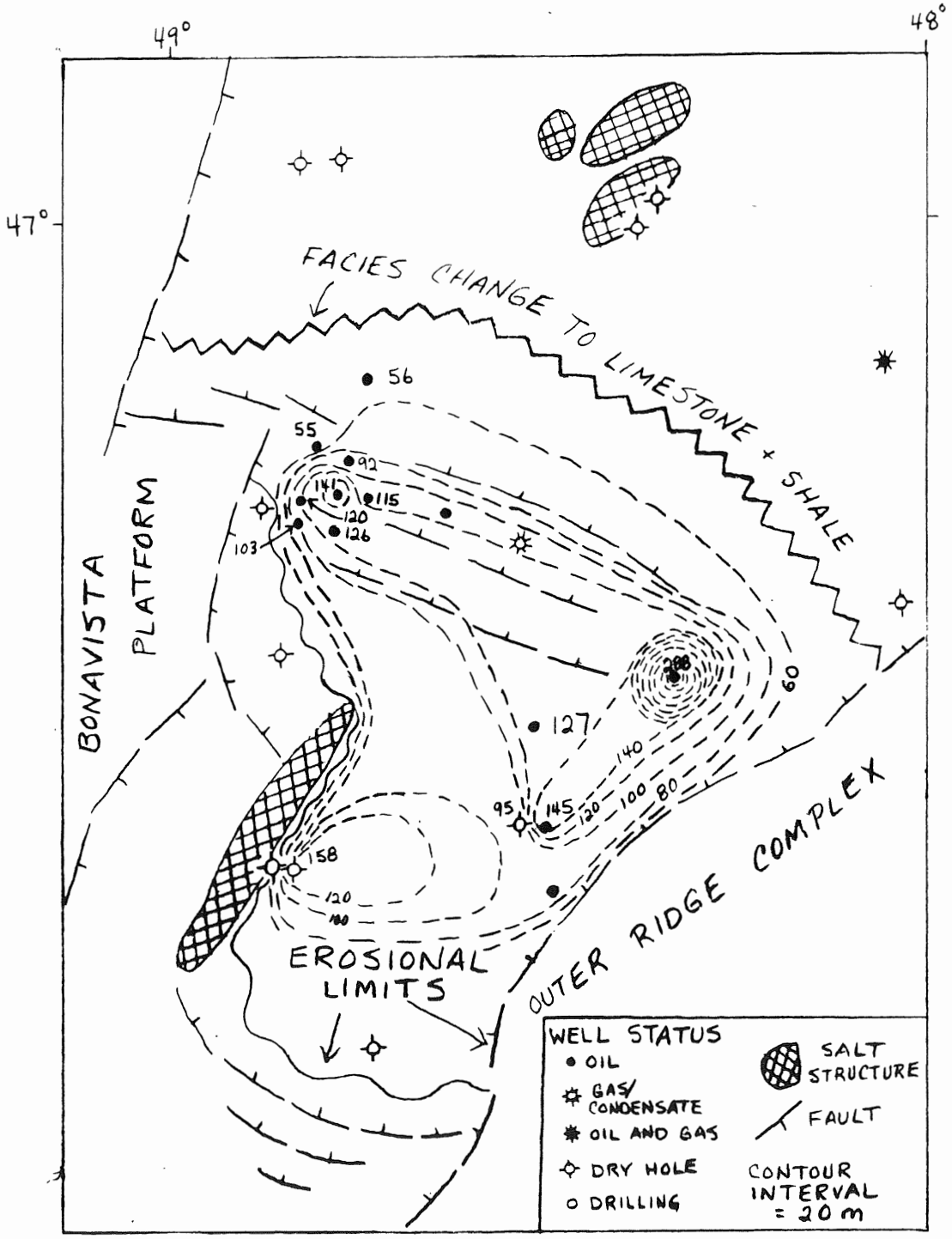

Figure 8: Isolith map of the Hibernia sandstone, Jeanne d'Arc Basin.

No core was cut from the Hibernia member in the Hebron and Ben Nevis wells. Cuttings samples, taken at five metre intervals, were correlated with the well logs to produce the lithologic column. The type and amount of cement and percent porosity in the sandstones were estimated from cuttings, thin sections, and well logs. Many of the sandstone units in the Hebron well yielded samples consisting of unconsolidated quartz grains. This is a drilling effect which preferentially occurs in the coarser-grained and more porous sandstones (Graves, 1986); it was used as an additional porosity indicator.

From the lithostratigraphic columns, three main lithofacies are distinguished in the Hibernia member: (1) fining upward sandstone units, (2) coarsening upward siltstone to sandstone units, and (3) a very fine sandstone--siltstone--shale--coal association.

(1)The fining upward sandstone units comprise about half of the Hibernia member and are the main reservoir rocks in the Hibernia field. Commonly, they are oil stained with porosities ranging from 14-22%. The thickness of individual sandstone units ranges from 1 to 60 m; the average is 7 $\pm$ 10 m (for 119 units measured).

The sandstones are very uniform in composition and classify as sublithic arenites (Folk, 1974). (Fig. 9) Their average composition is: 92% quartz, 8% sedimentary and metamorphic rock fragments, and a trace of feldspar. The

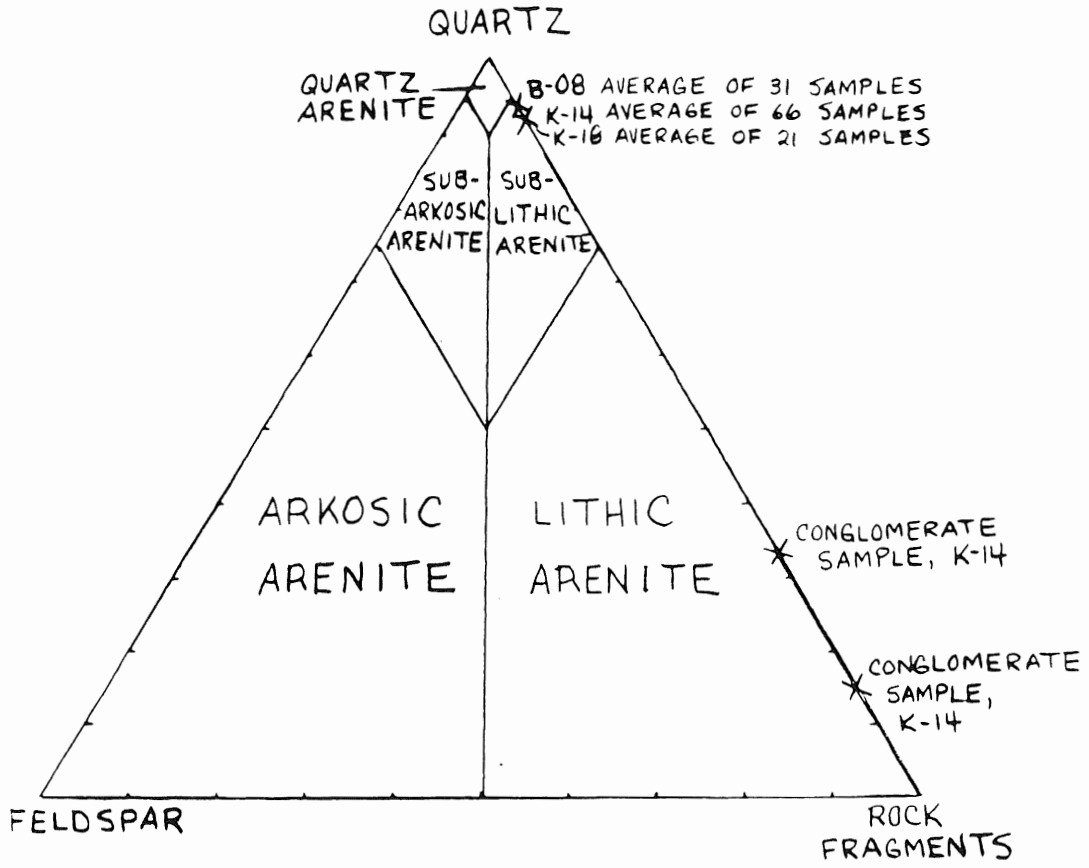

WELL	QUARTZ	FELDSPAR	ROCK FRAG.
B-08	93.6 ± 3.9	0.1 ± 0.4	6.2 ± 3.9
K-14	91.4 ± 2.5	0.2 ± 0.7	8.4 ± 2.5
K-18	91.7 ± 2.2	0	8.3 ± 2.2

Figure 9: Hibernia sandstones are sublithic arenites according to Folk's (1974) classification scheme. The rock fragments include: chert, shale, siltstone, siderite nodules (SRF) and polycrystalline quartz (MRF). Based on thin section petrography.

sedimentary rock fragments include chert, siltstone, shale, and detrital siderite nodules. Polycrystalline quartz grains commonly show subgrain development or a polygonal granoblastic texture and appear to be metamorphic rock fragments. The sandstones contain no glauconite and only trace amounts of detrital clay.

The sandstones also have trace amounts of the ultrastable heavy minerals: tourmaline, zircon, and rutile. These hard and inert minerals are equally abundant in cemented and uncemented sandstones. They are locally concentrated in very thin laminae and have grain sizes appropriate for their hydraulic ratio.

The sandstone units have sharp, commonly erosional lower contacts, observed in cored intervals (Plate 1). They rarely have a conglomeratic base with clasts of siderite and shale (Plate 2). Intraclasts of deformed shale are found locally within sandstone units (Plate 3) and all of the sandstones have scattered coaly or carbonaceous lenses, becoming locally very abundant (Plate 4).

Grain size ranges from very coarse-grained near the base to very fine-grained near the top of individual strata; most range from coarse- to medium- to fine-grained. Overall, they are rather poorly sorted; however, at the scale of a thin section, they are moderately poorly-sorted to moderately well-sorted. Sphericity and roundness of the grains are highly variable and have been modified by overgrowths and solution.

Plate 1: Hibernia sandstone reservoir. Medium to coarse-grained oil-stained sandstone in sharp contact with the underlying gray shale. Some of the oil has been extracted for laboratory testing. 3925 m, core 12, Hibernia K-14.

Plate 2: Matrix-supported basal conglomerate. Clasts of orange, sideritic shale and gray shale in moderately-sorted, medium-grained matrix. 3964 m, core 14, Hibernia K-14.

Plate 3: Fine to medium-grained sandstone with very angular, deformed shale clasts. 3905 m, core 10, Hibernia K-14.

Plate 4: Very coaly, poorly sorted sandstone with patchy calcite cement and poor porosity. 3960 m, core 14, Hibernia K-14.

Sedimentary structures are barely visible in the homogenous sandstone units. Vague parallel bedding at a 70° angle to the core is outlined by heavy minerals and is possibly large-scale cross-bedding. Some parallel beds at a 90° angle to the core were also noted.

(2)A coarsening-upward siltstone to sandstone unit is present at the base of the Hebron I-13 and Ben Nevis I-45 lithologic sections. The unit is 33 m thick in the Hebron well, where it is poorly sorted and grades upward from siltstone to coarse-grained sandstone. The coarsening-upward unit is 93 m thick in the Ben Nevis well, moderately sorted, and grades from interbedded shale, siltstone, and very fine sandstone to very fine to fine sandstone. The top of the sequence has tested oil and gas in the Ben Nevis well.

Thin sections cut from chip samples of the Hebron and Ben Nevis wells were of poor quality. However, the coarsening upward sandstones appear to have similar petrographic compositions to the fining upward sandstones. They are very quartz-rich, contain 6-8% sedimentary rock fragments, minor metamorphic quartz, and up to 2% feldspar. Coaly or carbonaceous lenses were also visible in some consolidated sandstone chip samples.

(3)The very fine sandstone-siltstone-shale-coal lithofacies comprises up to 80% of the Hibernia member. The association is most common in the upper part of the Hibernia member in the Hibernia wells.

The coal is black, vitreous, sub-bituminous and argillaceous. It most commonly occurs with gray, siliceous shale beneath the fining upward units (Plate 5, discontinuous core). The maximum thickness of pure coal recovered by coring is 13 cm. However, several coal-rich intervals are thick enough to be resolved by petrophysical logs. The coal-rich horizons are difficult to trace from well to well and are probably discontinuous.

Very fine to fine, well-sorted sandstones are found in places in sharp contact with underlying shales (Plate 6). They have a "blocky" appearance on gamma ray logs and contain minor argillaceous and carbonaceous streaks. Small-scale cross-bedding is rarely visible.

Interbedded very fine sandstone to siltstone and shale are commonly associated with the well-sorted sandstones. They may be finely laminated with planar beds, small-scale cross beds, or climbing ripples (Plate 7). More commonly, the interbedded units are extensively deformed by bioturbation (Plates 8 and 9), load casts, sand balls, and water escape structures.

Thick, monotonous sequences of quartz-rich siltstone are very common. They have rare burrows filled with siderite and are light gray in colour. Locally, sideritic, argillaceous siltstones have concentrations of calcareous shells, sideritic shale clasts, and quartz pebbles (Plate 10). These siltstones usually have gradational contacts with

Plate 5: Argillaceous coal seam and gray shale overlain by fine to medium-grained, oil stained sandstone, 3910 m, core 10, Hibernia K-14.

Plate 6: Gray silty shale in sharp contact with overlying well-sorted, very fine to fine sandstone (photo - left). The overlying sandstone unit has very common argillaceous streaks, an 8 cm thick lens of interbedded siltstone and shale, and a coal stringer (photo - right). 3855 m, core 6, Hibernia K-18.

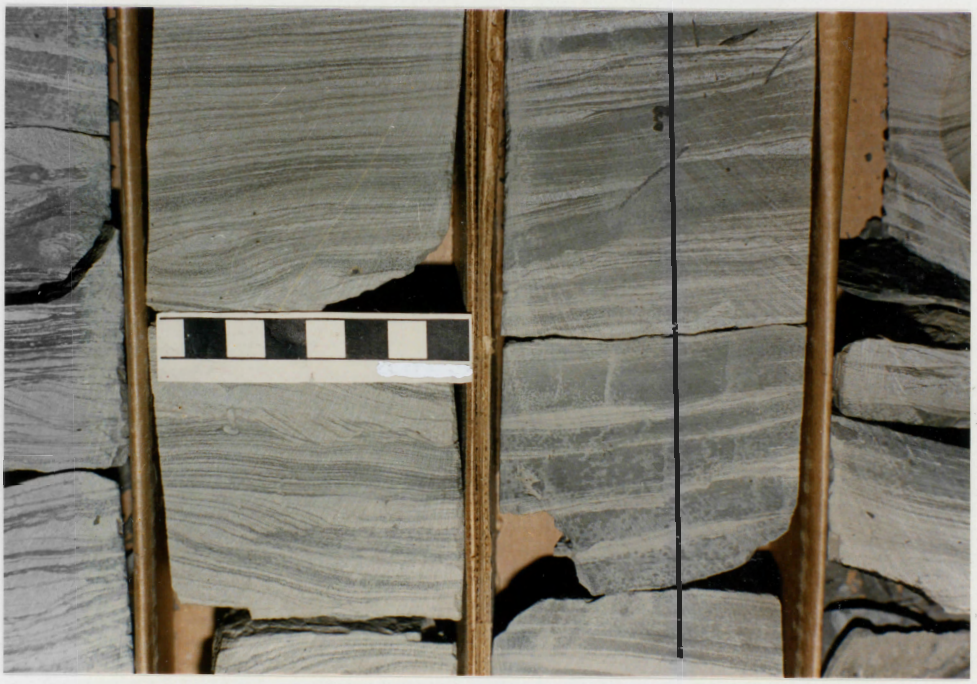

Plate 7: Finely laminated dark gray shale and light gray siltstone/very fine sandstone showing: planar laminations, small-scale cross-bedding, climbing ripples, and small-scale tensional faults. 3890 m, core 8, Hibernia B-27.

Plate 8: Bioturbated white, siliceous siltstone and gray, argillaceous siltstone. 3966 m, core 14, Hibernia K-14.

Plate 9: Bioturbated dark gray, sideritic shale. 3897 m, core 9, Hibernia K-14.

Plate 10: Sideritic, argillaceous, bioturbated siltstone with concentrations of calcareous shells, sideritic shale clasts and quartz pebbles. 3490 m, core 2, Hibernia B-08.

the other fine-grained units and appear to be genetically related.

Porosity in the very fine sandstones to siltstones averages 6%. Depending on both the amount of calcite and siderite cement, and the abundance of argillaceous partings, porosity ranges from 0-18%. These fine sediments are composed mainly of quartz with variable amounts of detrital clay and organic matter. Ultrastable heavy minerals comprise approximately 1%; rutile is the most abundant, comprising 2% of one siltstone sample. Rutile appears to have a positive correlation with detrital clay and may be formed authigenically by the decomposition of ilmenite (Scholle, 1979).

Micropaleontology

Previous micropaleontologic studies have identified rather few microfossils in the Hibernia member (Gradstein, pers. comm.; Williamson, pers. comm.). A few agglutinated, possibly brackish water forms were noted by Williamson. Nonetheless, 14 previously processed samples from the Hibernia K-14 well were reexamined (courtesy of M. Williamson). They were found to be barren, except for one sample at 3850 m. It contained a Milamina species, a marsh foraminifera (D. Scott, pers. comm.). This prompted the collection of four more samples from the Hebron I-13 and Ben Nevis I-45 wells. With the help of S. Thibideau and Dr. Scott, several specimens of unidentified thecamoebians were found.

"Thecamoebians" is an informal term used to characterize a group of testate protozoans belonging to the subphylum Sarcodina, that includes mainly forms of fresh-water origin (Medioli and Scott, 1986). A few species of foraminifera, typical of an upper estuary, were also found: Ammobaculites (13 specimens) and Trochammina (3 specimens). Although this data is quantitatively insufficient to make a definitive paleoenvironmental interpretation, it strongly suggests an estuarine environment.

Additional Core Data

Evidence of faulting was found in core from the Hibernia B-27 and K-14 wells. Plates 11 and 12 show a fault breccia and red staining in slickensided, silty shale/argillaceous siltstone rubble. Due to thickness and lithologic variations of the Hibernia member, the amount of missing section is uncertain.

Small-scale faults offset the fine laminae shown in Plate 7. It is difficult to judge whether these small-scale faults are a common occurrence. Most of the finer-grained portion of the Hibernia member is bioturbated or disturbed by water escape structures. The faults would only be visible in finely laminated sections.

Plate 11: Fault breccia (below scale) with sideritic pebbles in clay-rich, slickensided rubble. 3910 m, core 10, Hibernia B-27.

Plate 12: Silty shale and argillaceous siltstone rubble: very friable and soft with slickensides and red staining. 3892 m, core 9, Hibernia K-14.

V PALEOENVIRONMENTAL INTERPRETATION AND PROVENANCE OF THE HIBERNIA MEMBER

Paleoenvironmental Interpretation

The Hibernia member has previously been interpreted as a deltaic deposit (Benteau and Sheppard, 1982; Handyside and Chipman, 1983; Robertson Research, 1985; Brown, 1985; Tankard and Welsink, in press), a deltaic shoreline deposit (McKenzie, 1981; McMillan, 1982) and a "distal braided fluvial fan delta complex" (Rayer, 1981). The evidence presented in this thesis indicates that the Hibernia member was deposited in a non-marine, fresh to brackish water environment, close to sea level.

The main evidence for a non-marine interpretation is the presence of fresh water, marsh, and upper estuarine microfossils. Marine fauna was not found. Reducing conditions were probably imposed by an elevated water table in a coastal marsh. Both coal and siderite nodules are produced and best preserved in a non-marine, reducing environment (Curtis and Coleman, 1986).

The fining-upward sandstone units contain ubiquitous transported coal matter and have sharp, erosional lower contacts. Clasts of siderite nodules, sideritic shale, and angular, deformed shale (Plate 3) were derived from a nearby, semi-consolidated source. An intraformational origin is most likely. Similar fining-upward units are frequently found to be channel sandstones (Cant, 1982; Walker and Cant, 1979).

The coarsening upward sandstones at the base of the Hibernia member in the Hebron I-13 and Ben Nevis I-45 wells also contain coaly fragments and rare shale clasts (Enclosures 6 and 7). They are interpreted as initial progradational mouth bars formed at the mouth of a paleoriver.

The very fine to fine-grained, well-sorted sandstones have small-scale cross-bedding and less coaly material than the other lithologies (Plate 6). The sandstones are interbedded with very fine sandstone to siltstone and shale, and have a "blocky" appearance on gamma ray logs. They are found in places in sharp contact with underlying shales. Soft sediment deformation features are also common in the underlying sediment. The sandstones are rarely overlain by finely laminated siltstone and shale. The laminae may reflect seasonal variations of energy conditions on the floodplain. Climbing ripples in the silty layers attest to rapid deposition following flooding; as clays fall out of suspension, the argillaceous laminae are deposited. Bioturbation often destroys these features. The well-sorted sandstones are most likely crevasse splay deposits, encased in fine-grained sediment of the floodplain.

The monotonous siltstone units are well-sorted and well-winnowed and contain rare concentrations of shell debris, intraclasts, and quartz pebbles. The shell debris was not identifiable and could indicate a marine incursion.

However, no marine microfossils were found in samples from this facies. The monotonous siltstone units are very similar to the other fine-grained sediments. Their thickness and stratigraphic range are variable and they are overlain by channel and overbank sediments. "Sheet floods", during times of particularly high water levels in the flood basin, may have allowed widespread deposition outside of channels.

The coals are very thin, argillaceous, and often occur in gray siliceous shale below channel sandstones (Plate 5). Although several coal-rich intervals are thick enough to be detected by petrophysical logs, they are uncorrelatable and probably discontinuous. Peat formation may have been interrupted by sedimentation or high water levels in the floodplains. The channel sandstones also contain abundant transported coal (Plate 4). Some coal at the base of the sandstones may have been formed from rafted logs or other organic material that collected in local depressions on the channel bottom, as observed in modern rivers (Crawford, 1972).

To summarize, the Hibernia member is interpreted as a non-marine to brackish water deposit. It contains fresh water, marsh, and upper estuarine microfossils, and presumably in situ coal. The Hibernia member consists of channel sandstones and well-sorted crevasse splay sandstones, encased in fine-grained swampy floodplain

material. No other interpretation explains all of the observed data. The lithofacies have some features common to turbidites such as: graded bedding, soft sediment deformation, generally poor sorting (within the fining upward sandstone units), and transported terrestrial organic matter. However, the lack of marine microfossils in the fine-grained sediment, widespread geometry of the Hibernia member, and the presence of coal within the shales, make this interpretation unlikely.

Deposition of the Hibernia member was influenced by an overall eustatic sea level rise and an abundant sediment supply caused by faulting at the basin margins.

Most of the Hibernia member was built by rapid vertical aggradation of the swampy floodplain and lateral accretion in the paleochannels. Sediment supply was able to keep pace with rapid subsidence (70 m/Ma) and a resumption of eustatic sea level rise. Eventually, a net transgression occurred and the "sheet floods" became more common until the river channels became estuaries and a distinctly marine influence prevailed. Biostratigraphic studies (Table 1) generally report that the Hibernia interval is barren, whereas abundant marine microfossils have been found in the overlying sediments.

The particularly thick sandstones at the top of the Hibernia member in the Hebron and Ben Nevis wells contain coal fragments and shale clasts, typical of channel

sandstones. However, the sandstones are not interbedded with floodplain deposits and probably accumulated by vertical aggradation instead of lateral accretion. The rising sea level, coupled with high subsidence rates, would allow vertical stacking of channel sandstones. This could have resulted in amalgamated sandstone bodies with only minor overall grain size range, causing a "blocky" log motif (Enclosures 6 and 7). In other words, a rising base level means that there is no need for extensive meandering or channel avulsions.

The Hibernia member does not represent a Mississippi River type of deltaic sequence. Progradation of many of the lobes of the Mississippi delta was followed by substantial subsidence and a marine transgression (Coleman and Prior, 1980). In the Jeanne d'Arc Basin, subsidence and a sea level rise were contemporaneous with deposition of the Hibernia member. The sediment load was deposited mainly in channels, at areas of greatest subsidence. This may also explain the anomalous thickness and aereal extent of the Hibernia member. The large supply of clastics coupled with high rates of syndepositional subsidence and a eustatic sea level rise allowed rapid vertical aggradation. Only in the Egret - Terra Nova area did sediment supply exceed base level rise, causing a datable period of erosion.

At least some of the subsidence was accommodated by syndepositional movement on the Murre fault; the

paleodrainage pattern may have been localized along active fault zones. This would explain the great variation in sediment thickness (Fig. 7 and 8). There is a facies change to limestone and shale in the northern part of the basin. A lack of sediment coupled with the persistent sea level rise would have resulted in a net transgression. However, data from more wells are needed to define the paleodrainage pattern and to confirm the facies boundary.

The proposed origin of the Hibernia member is reminiscent of the genesis of anastomosed fluvial systems. Modern examples form on low topographic gradients caused by a downstream rise in base level and/or subsidence of the depocenter relative to a down-river reach (Smith, 1983). During deposition of the Hibernia member sea level was rising and the depocenter was subsiding rapidly.

Anastomosing fluvial systems are characterized by rapid vertical accretion in stable channels and surrounding wetlands (Smith and Putnam, 1980; Smith, 1983). Based on cores through modern anastomosed fluvial deposits, Smith (1983) suggested subsurface facies associations. A three dimensional model would show multiple, interconnected, low sinuosity stringers of channel sand (greater than 10m thick) with occasional sheets of splay sand (2-3 m thick) extending laterally. The sand would be encased in fine-grained sediment and peat of the wetland environments.

Enclosure 8 shows the lithofacies relationships between four wells in the Hibernia field. The datum is that suggested by the time-lines of the time-space diagram, although the biostratigraphy is not precise enough for fine-scaled correlations. The diagram shows that the Hibernia member in the K-18 well is not composed solely of overbank material (as implied by Tankard and Welsink, in press). It also suggests that the Hibernia sandstones are not continuous sheets and not directly correlatable. However, the channel nature of the sandstones implies hydrodynamic continuity.

Enclosure 8 suggests that deposition of the Hibernia member began in the southern part of the field; the paleocurrent direction may have been south to north, along the Murre Fault Zone. Transgression of the Hibernia member by marine facies would have occurred first at the areas with greatest subsidence and least sediment supply (e.g. Hibernia B-27).

Provenance

The Hibernia member had a sedimentary source. The most direct evidence is the presence of clasts of chert, siltstone, and quartz grains with rounded overgrowths. The shale and detrital siderite nodules are probably intraclasts and would not reflect extrabasinal provenance. Transported coal lenses are most probably locally derived.

Secondly, the Hibernia sandstones have a high chemical maturity and a rather low mechanical maturity. The chemical maturity is evident from the very quartz-rich composition and ultrastable heavy mineral suite (Crawford, 1972). The chemical maturity may be a function of source composition, transport distance, or diagenesis. The rather poor mechanical maturity is evident from the poor sorting of most of the sandstone units. A nearby sedimentary source would provide chemically mature, mechanically immature detritus.

The presence of metamorphic quartz indicates that a metamorphic terrain (eg. Avalon) may have been an original source of sediment. A second generation of sediment may have been eroded from the upthrown sides of fault blocks. The Egret-Terra Nova area was being eroded while the Hibernia member was being deposited in the Hibernia field area (Enclosure 1). A south to north transport direction would also be consistent with Enclosure 8 and a northerly facies change to limestone and shale.

VI BURIAL HISTORY OF THE JEANNE D'ARC BASIN

In the following two chapters, the burial history and thermal history of the Jeanne d'Arc Basin are assessed. The thermal-burial history exerts important controls on both diagenetic reactions and petroleum source rock maturation. Geodynamic (tectonic) models (e.g. Keen, 1979) have shown that subsidence is largely controlled by the cooling (contraction) of the lithosphere following its initial heating by upwelling asthenosphere. Therefore, thermal- burial histories are intimately related and the importance of considering diagenesis in the context of basin analysis becomes apparent.

The biostratigraphic data (Table 1) was used to construct burial history curves for eight wells in the Jeanne d'Arc Basin (Figs. 10-17). The curves reflect the "sedimentation rates" and lacunas displayed on the time-space diagram. In general, steep slopes on the curves are due to rapid burial caused by a high sedimentation rate in an overlying unit. Horizontal segments of the curves represent zero net burial at lacunas.

As mentioned in Chapter 3, the "sedimentation rates" include any diastems that are shorter than the resolution of the fossil data. The burial history curves also reflect "accumulation rates" after compaction. For highly compacted shales, the true sedimentation rates would be much higher.

For the overpressured shales in the Mic Mac Formation (McAlpine, pers. comm.), the distinction is insignificant.

The present depth to the sea floor was used as a datum for the burial history curves. A datum defined by the locus of depths to the sea floor with time, would have resulted in more accurate sedimentation rates. This correction for paleobathymetry was not made because sea level fluctuations were less than 100m (Williamson, 1987) and would not have noticeably affected the curves (eg. Keen, 1979).

Fewer biostratigraphic data are available for the Tertiary section than for the Cretaceous. In particular, the length of the Early Tertiary lacuna needs to be more clearly defined. This limits the accuracy of the most recent burial history, the most critical time for high temperature diagenetic reactions. However, the earlier burial history imposes constraints on the time available for Tertiary sedimentation, so the potential error would not be too serious.

The burial history curves show a significant decrease in sedimentation rate from Jeanne d'Arc time until the early Tertiary. The observed subsidence can be interpreted as resulting from the thermal contraction of the lithosphere following rifting. Sediment loading and eustatic sea level changes were shown to be minor contributors to subsidence in the Scotian Basin (Keen, 1979). Thermal models predict an exponential decrease in subsidence following rifting.

The first phase of rifting (Triassic to Lower Jurassic) is not represented on the burial history curves since most of the wells reach total depth in the Upper Jurassic section. The second phase of rifting is represented by the Jeanne d'Arc to Upper Cretaceous sandstones. Initial high subsidence rates can be attributed to movement on the major, basin-forming faults. This will explain the rapid deposition of the Jeanne d'Arc member. Subsidence and sedimentation rates were moderately high during the deposition of the Missisauga Formation, then decreased until the Early Tertiary lacuna because of diminishing thermal effects of rifting. The unconformity at the base of the Tertiary section probably marks the end of rift-related sedimentation.

Tectonic subsidence was variable across the basin. A comparison of the subsidence history at the eight well locations shows that the total subsidence at the Ben Nevis and Nautilus wells is much greater than at the Hibernia and Hebron wells. This was due mainly to faulting which caused differential erosion at the Pre-Aptian and Avalon Unconformities. The high subsidence rate at the Hibernia O-35 well is attributed to growth faulting at the listric, normal, Murre Fault. Subsidence rates were lower at the Egret K-36 well where salt movement, triggered by structural deformation, caused extensive erosion during the middle Cretaceous.

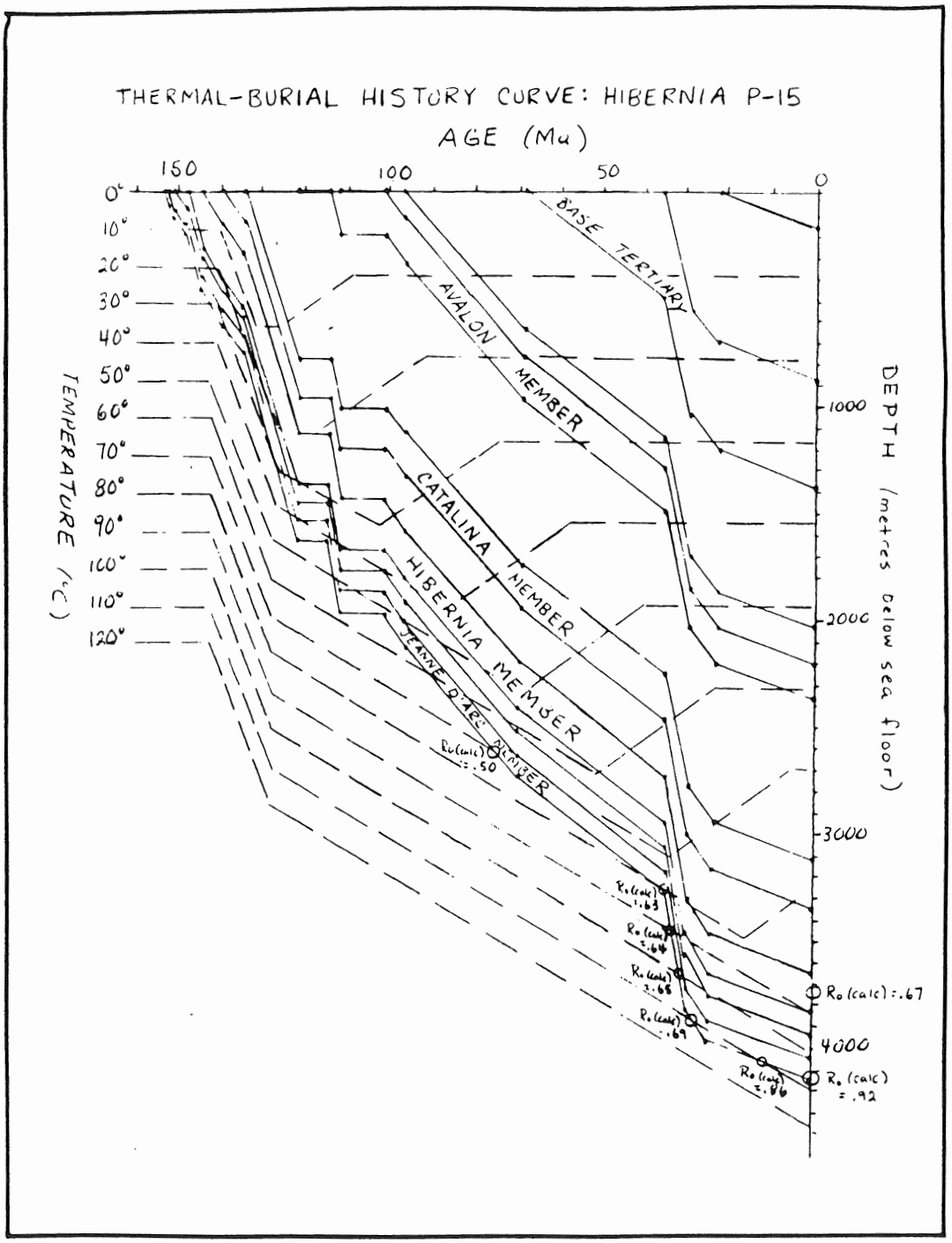
THERMAL-BURIAL HISTORY CURVE: HIBERNIA P-15
AGE (Ma)
150
100
50
0
0°
10°
20°
30°
40°
50°
60°
70°
80°
90°
100°
110°
120°
TEMPERATURE (°C)
BASE TERTIARY
AVALON MEMBER
CATALINA MEMBER
HIBERNIA MEMBER
JEANNE D'ARC MEMBER
Ro(calc) = .50
Ro (calc) = .63
Ro (calc) = .64
Ro (calc) = .66
Ro (calc) = .69
Ro (calc) = .86
Ro (calc) = .67
Ro (calc) = .92
1000
2000
3000
4000
DEPTH (metres below sea floor)

Figure 10

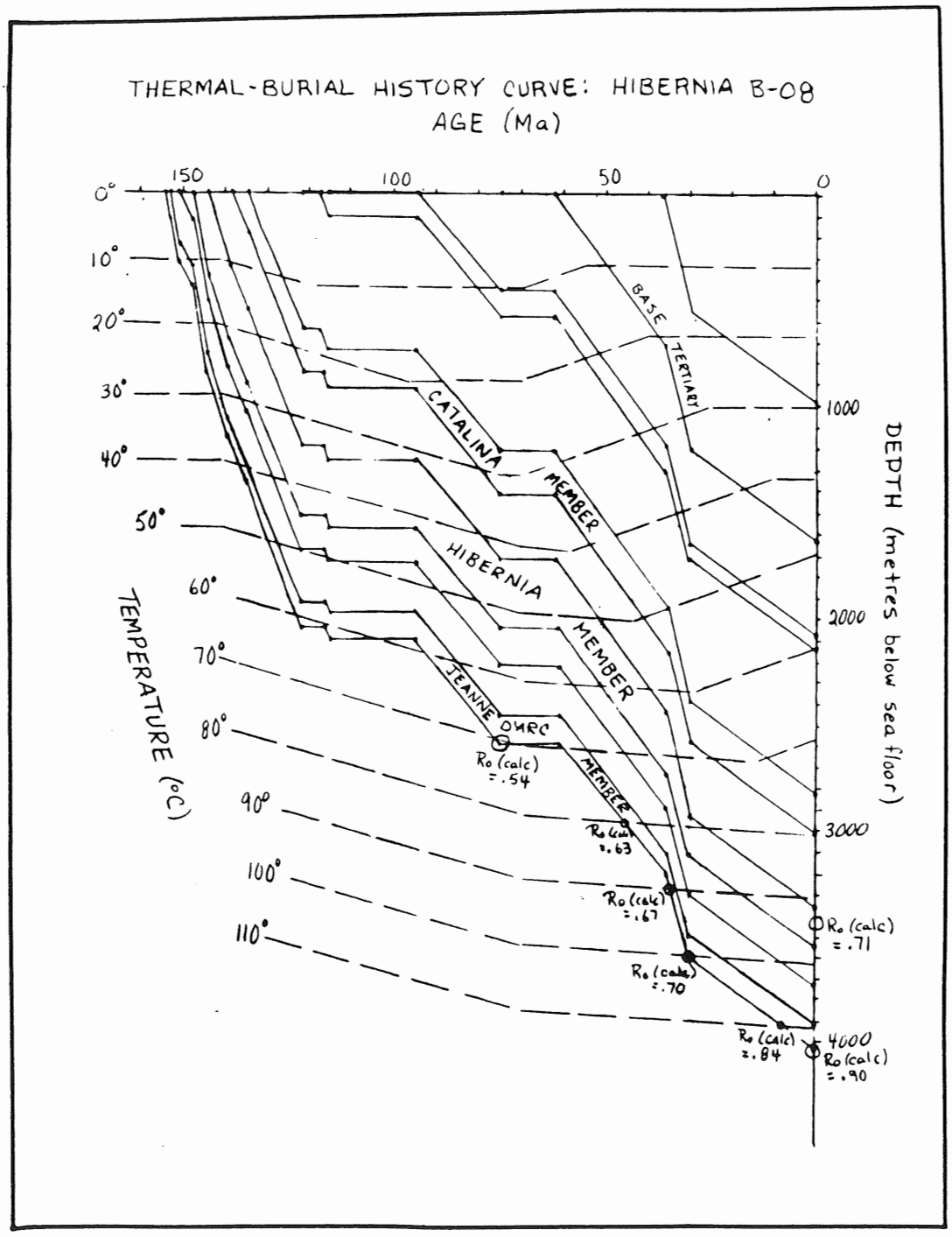
THERMAL-BURIAL HISTORY CURVE: HIBERNIA B-08
AGE (Ma)
150
100
50
0
0°
10°
20°
30°
40°
50°
60°
70°
80°
90°
100°
110°
TEMPERATURE (°C)
BASE TERTIARY
CATALINA MEMBER
HIBERNIA MEMBER
JEANNE D'ARC
Ro (calc) = .54
Ro (calc) = .63
Ro (calc) = .67
Ro (calc) = .70
Ro (calc) = .71
Ro (calc) = .84
Ro (calc) = .90
1000
2000
3000
4000
DEPTH (metres below sea floor)

Figure 11

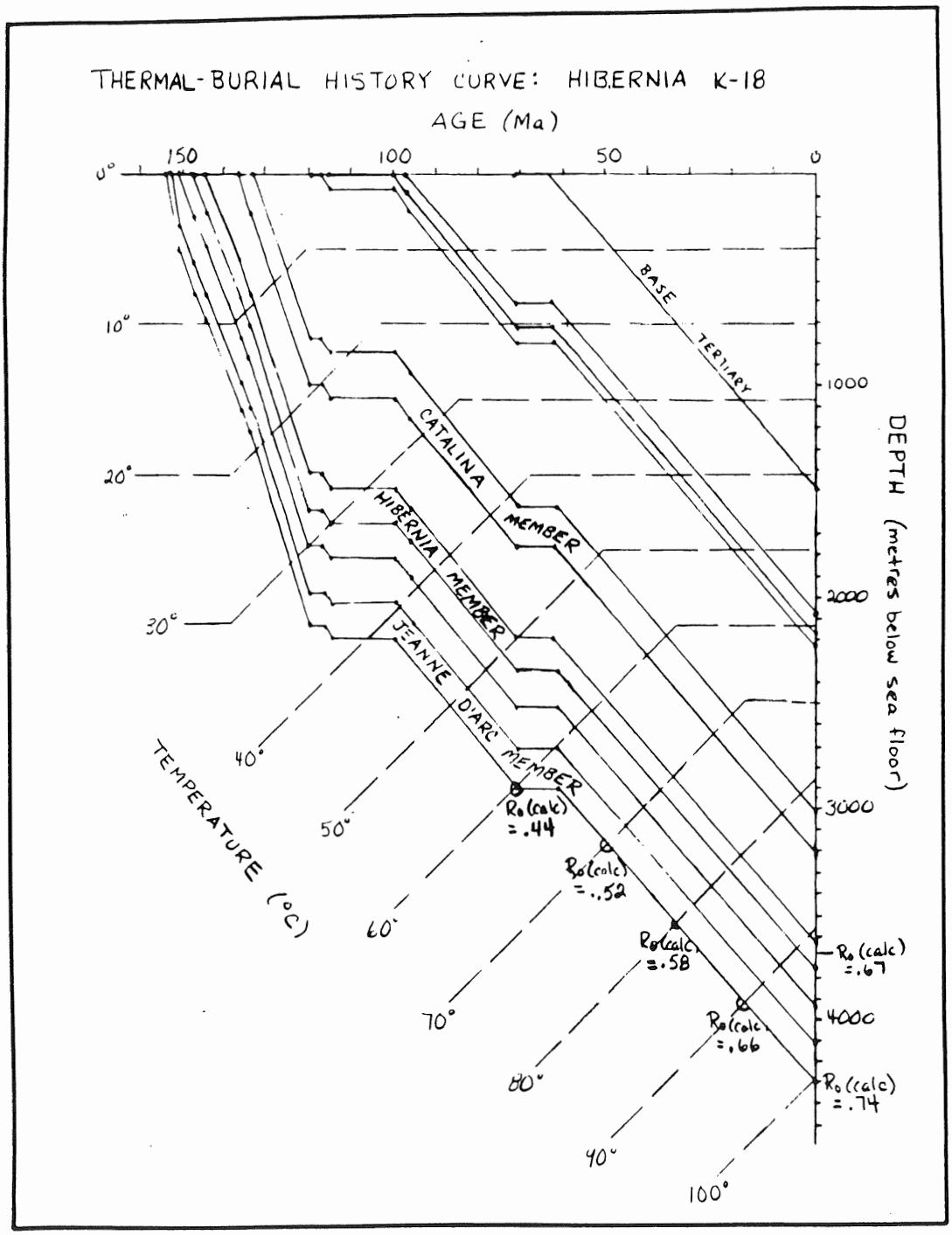
THERMAL-BURIAL HISTORY CURVE: HIBERNIA K-18
AGE (Ma)
150
100
50
0
0°
10°
20°
30°
40°
50°
60°
70°
80°
90°
100°
TEMPERATURE (°C)
BASE TERTIARY
CATALINA MEMBER
HIBERNIA MEMBER
JEANNE D'ARC MEMBER
1000
2000
3000
4000
DEPTH (metres below sea floor)
Ro(calc) =.44
Ro(calc) =.52
Ro(calc) =.58
Ro(calc) =.66
Ro(calc) =.74
Ro(calc) =.67

Figure 12

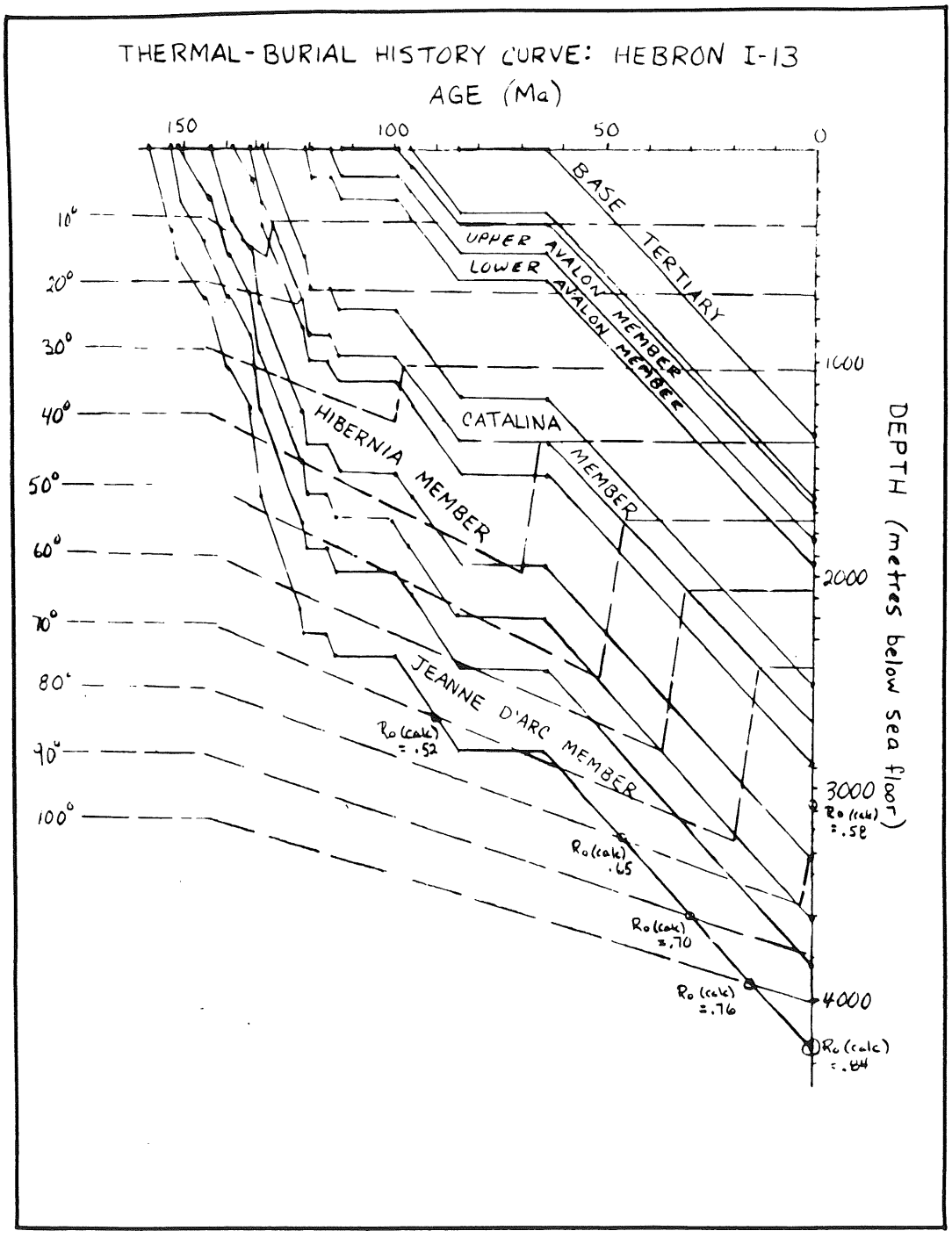
THERMAL-BURIAL HISTORY CURVE: HEBRON I-13
AGE (Ma)
150
100
50
0
10°
20°
30°
40°
50°
60°
70°
80°
90°
100°
BASE TERTIARY
UPPER AVALON MEMBER
LOWER AVALON MEMBER
CATALINA MEMBER
HIBERNIA MEMBER
JEANNE D'ARC MEMBER
Ro (calc) = .52
Ro (calc) .65
Ro (calc) = .70
Ro (calc) = .76
Ro (calc) = .84
1000
2000
3000
Ro (calc) = .58
4000
DEPTH (metres below sea floor)

Figure 13

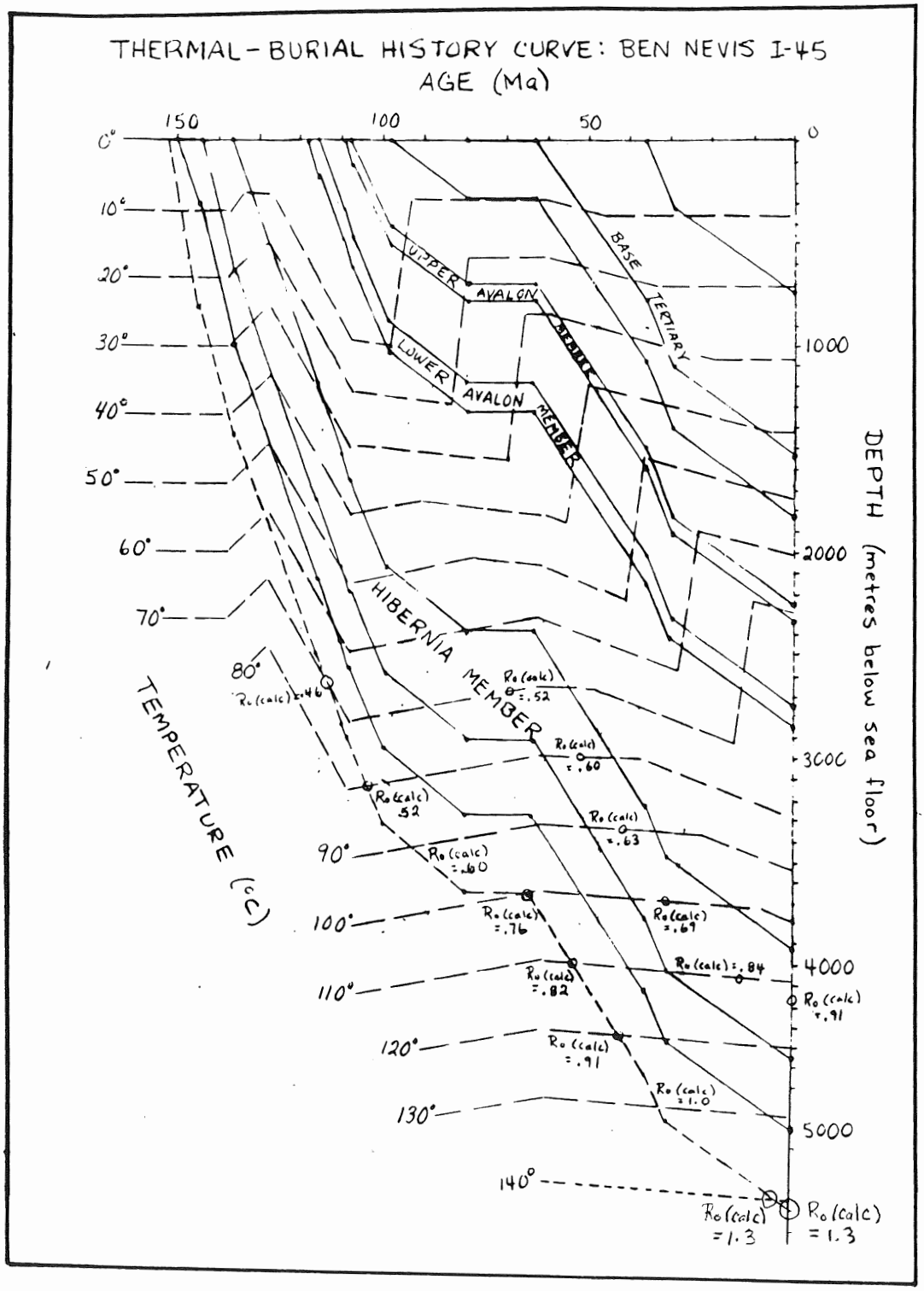
THERMAL-BURIAL HISTORY CURVE: BEN NEVIS I-45
AGE (Ma)
150
100
50
0
C°
10°
20°
30°
40°
50°
60°
70°
80°
90°
100°
110°
120°
130°
140°
TEMPERATURE (°C)
DEPTH (metres below sea floor)
1000
2000
3000
4000
5000
UPPER AVALON
LOWER AVALON
MEMBER
SHALE
BASE TERTIARY
HIBERNIA MEMBER
Ro (calc) =.46
Ro (calc) =.52
Ro (calc) =.60
Ro (calc) =.52
Ro (calc) =.63
Ro (calc) =.60
Ro (calc) =.76
Ro (calc) =.69
Ro (calc) =.84
Ro (calc) =.82
Ro (calc) =.91
Ro (calc) =.91
Ro (calc) =1.0
Ro (calc) =1.3
Ro (calc) =1.3

Figure 14

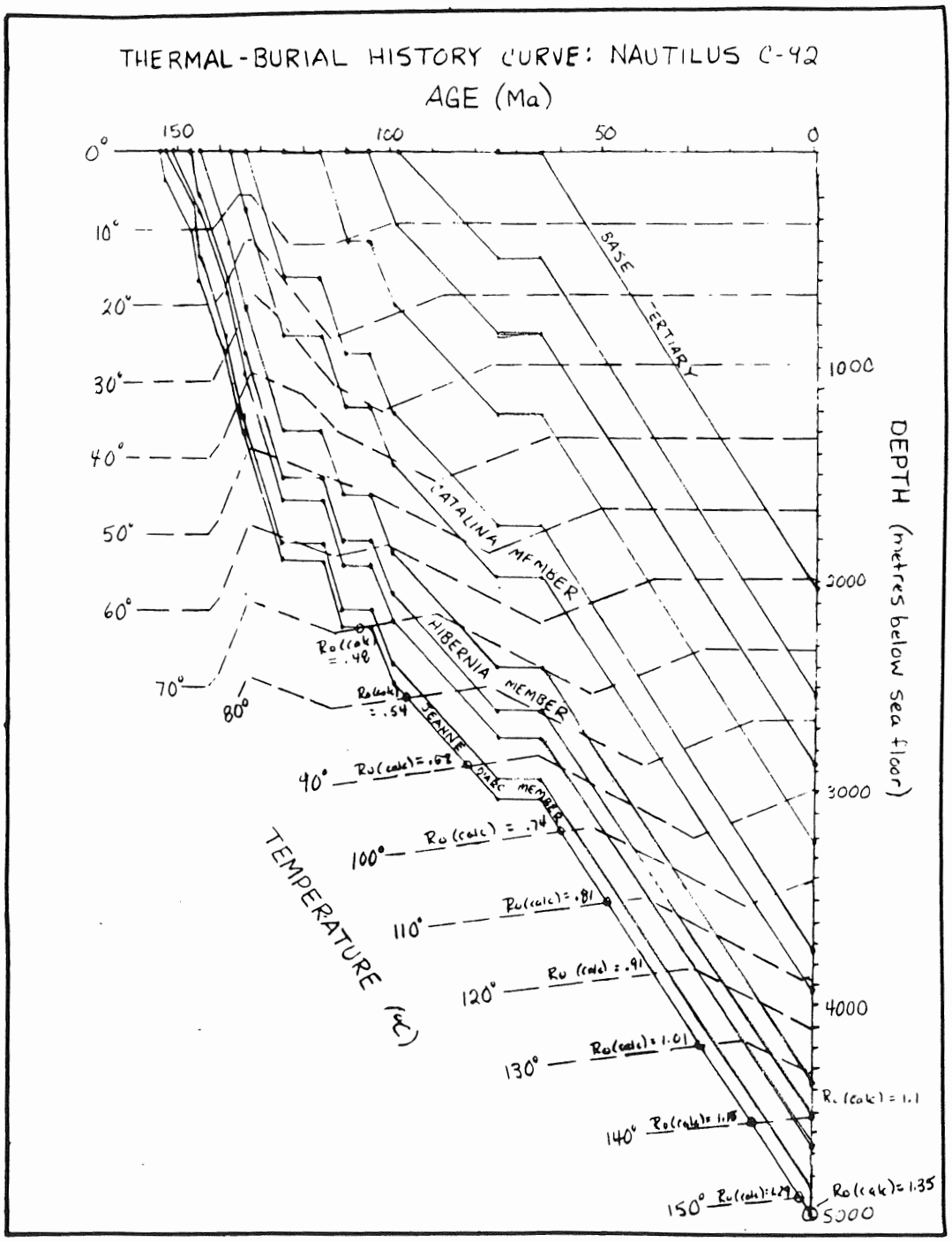
THERMAL-BURIAL HISTORY CURVE: NAUTILUS C-42
AGE (Ma)
150
100
50
0
0°
10°
20°
30°
40°
50°
60°
70°
80°
BASE TERTIARY
CATALINA MEMBER
HIBERNIA MEMBER
JEANNE D'ARC MEMBER
Ro(calc) = .48
Ro(calc) = .54
Ro(calc) = .68
Ro (calc) = .74
Ro(calc) = .81
Ro (calc) = .91
Ro(calc) = 1.01
Ro(calc) = 1.18
Ro(calc) = 1.29
Ro(calc) = 1.35
1000
2000
3000
4000
5000
DEPTH (metres below sea floor)
TEMPERATURE (°C)
40°
100°
110°
120°
130°
140°
150°

Figure 15

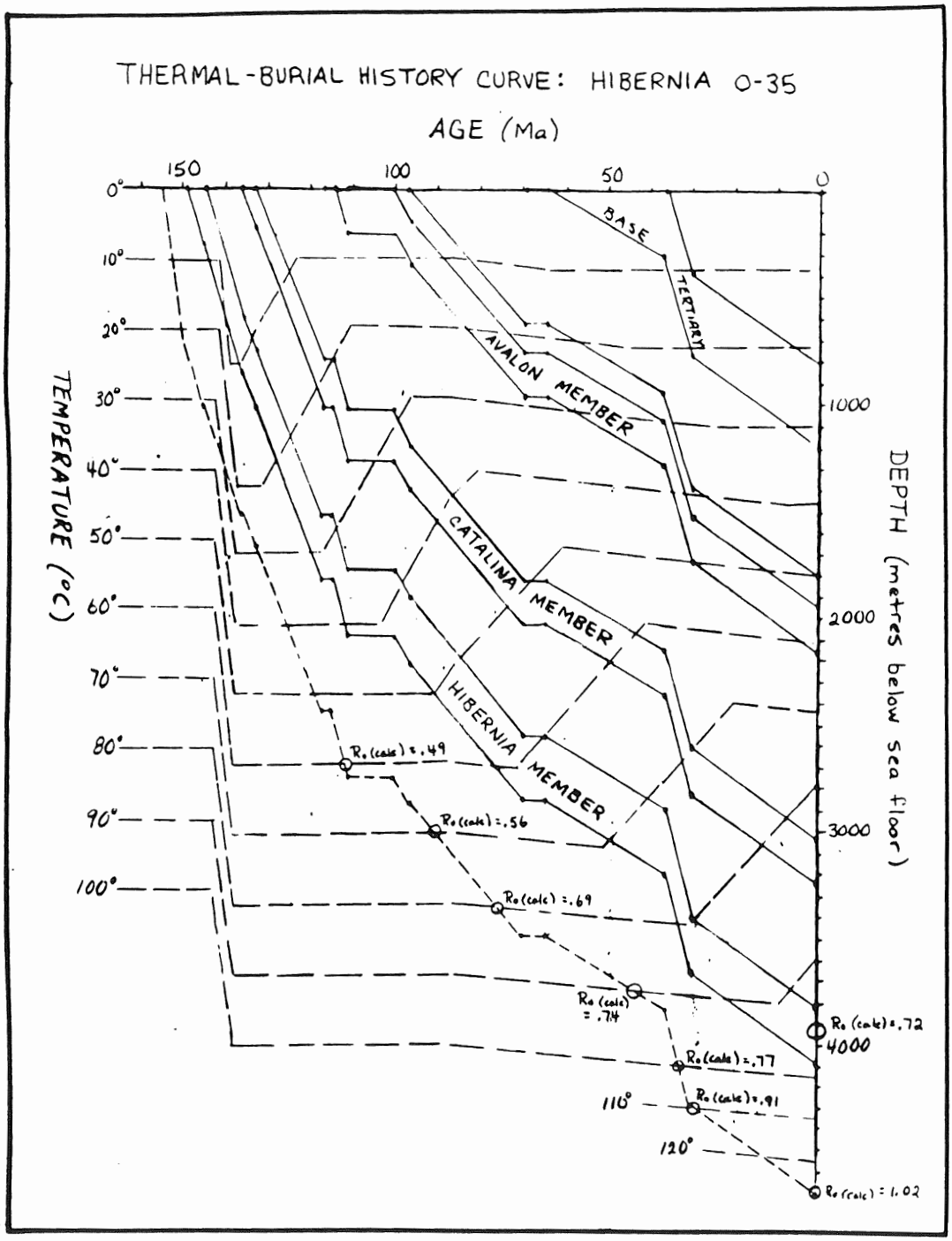
THERMAL-BURIAL HISTORY CURVE: HIBERNIA O-35
AGE (Ma)
150
100
50
0
TEMPERATURE (°C)
0°
10°
20°
30°
40°
50°
60°
70°
80°
90°
100°
110°
120°
BASE
TERTIARY
AVALON MEMBER
CATALINA MEMBER
HIBERNIA MEMBER
Ro (calc) = .49
Ro (calc) = .56
Ro (calc) = .69
Ro (calc) = .74
Ro (calc) = .77
Ro (calc) = .91
Ro (calc) = 1.02
Ro (calc) = .72
1000
2000
3000
4000
DEPTH (metres below sea floor)

Figure 16

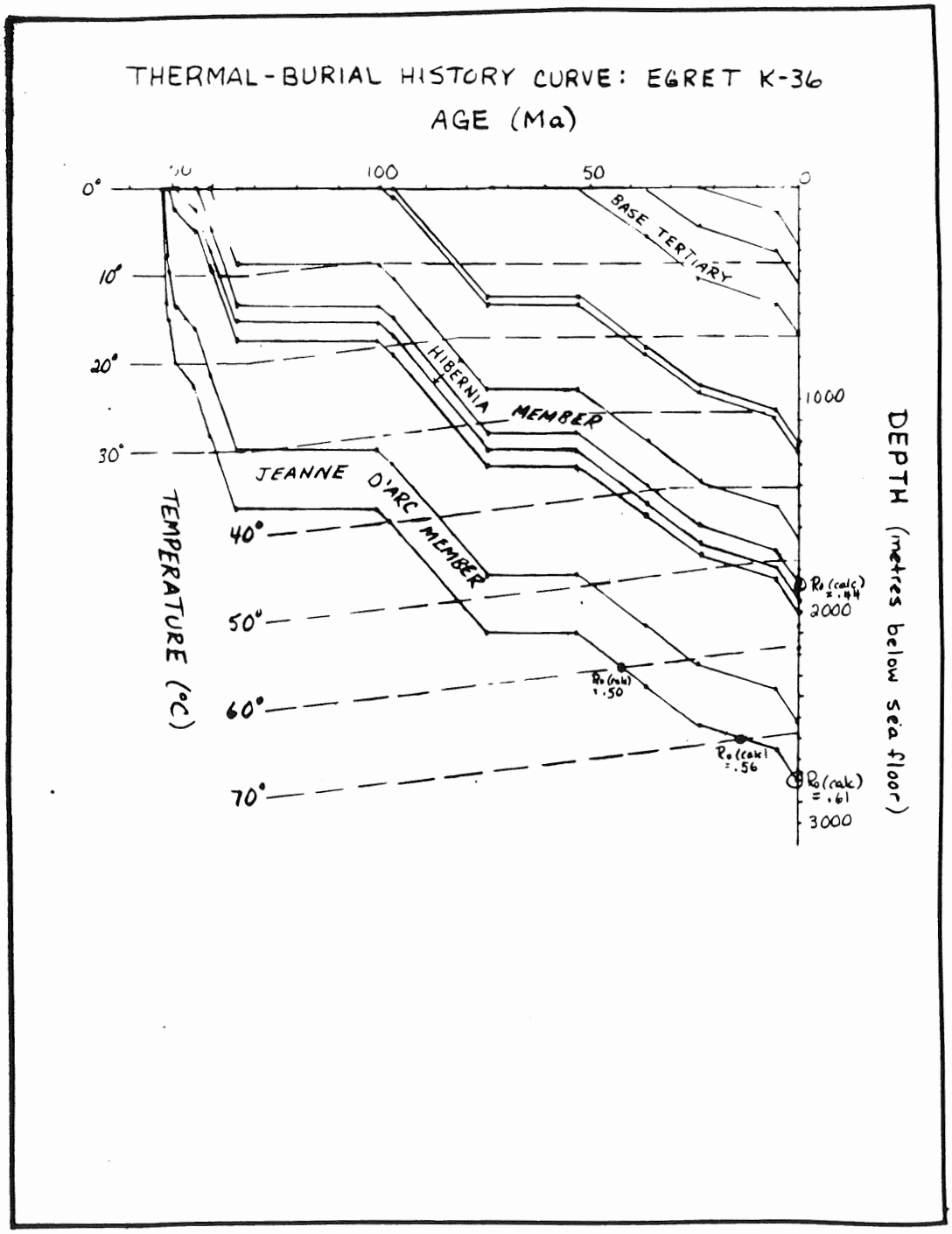
THERMAL-BURIAL HISTORY CURVE: EGRET K-36
AGE (Ma)
100
50
0
0°
10°
20°
30°
40°
50°
60°
70°
TEMPERATURE (°C)
BASE TERTIARY
HIBERNIA MEMBER
JEANNE D'ARC MEMBER
1000
2000
3000
DEPTH (metres below sea floor)
Ro (calc) = .50
Ro (calc) = .56
Ro (calc) = .61

Figure 17

VII THERMAL HISTORY OF THE JEANNE D'ARC BASIN

The present thermal structure of the Jeanne d'Arc Basin may provide clues to the geothermal history of the basin. Ervine (1985) used corrected borehole temperatures to calculate average geothermal gradients at 23 well locations in the Jeanne d'Arc Basin. Figures 18 and 19 show a positive correlation between sediment thickness and geothermal gradient; geothermal gradients increase with increasing depth to the basement. Studies of the Scotian and North Sea basins have shown a similar relationship (Issler, 1984; Ervine, 1985).

Conductivity contrasts cannot account for this pattern. Since the conductivity of basement rock is higher than that of sediments (Gretener, 1981), the basin margins should receive more heat from the basement. In the Jeanne d'Arc Basin, the basin margins have a lower geothermal gradient than the basin axis.

Radiogenic heat production in the thicker sediment pile of the basin axis (14 km versus 5 km) may have caused the higher geothermal gradients. Keen and Lewis (1982) measured radiogenic heat production from sediments of the Scotian Basin and found that it increased the total heat flow by about 15%. Depending on the parent rocks, Jeanne d'Arc Basin sediments may have similar radioactivities.

Ervine's temperature data indicate that the geothermal gradient also changes in the vertical direction. In

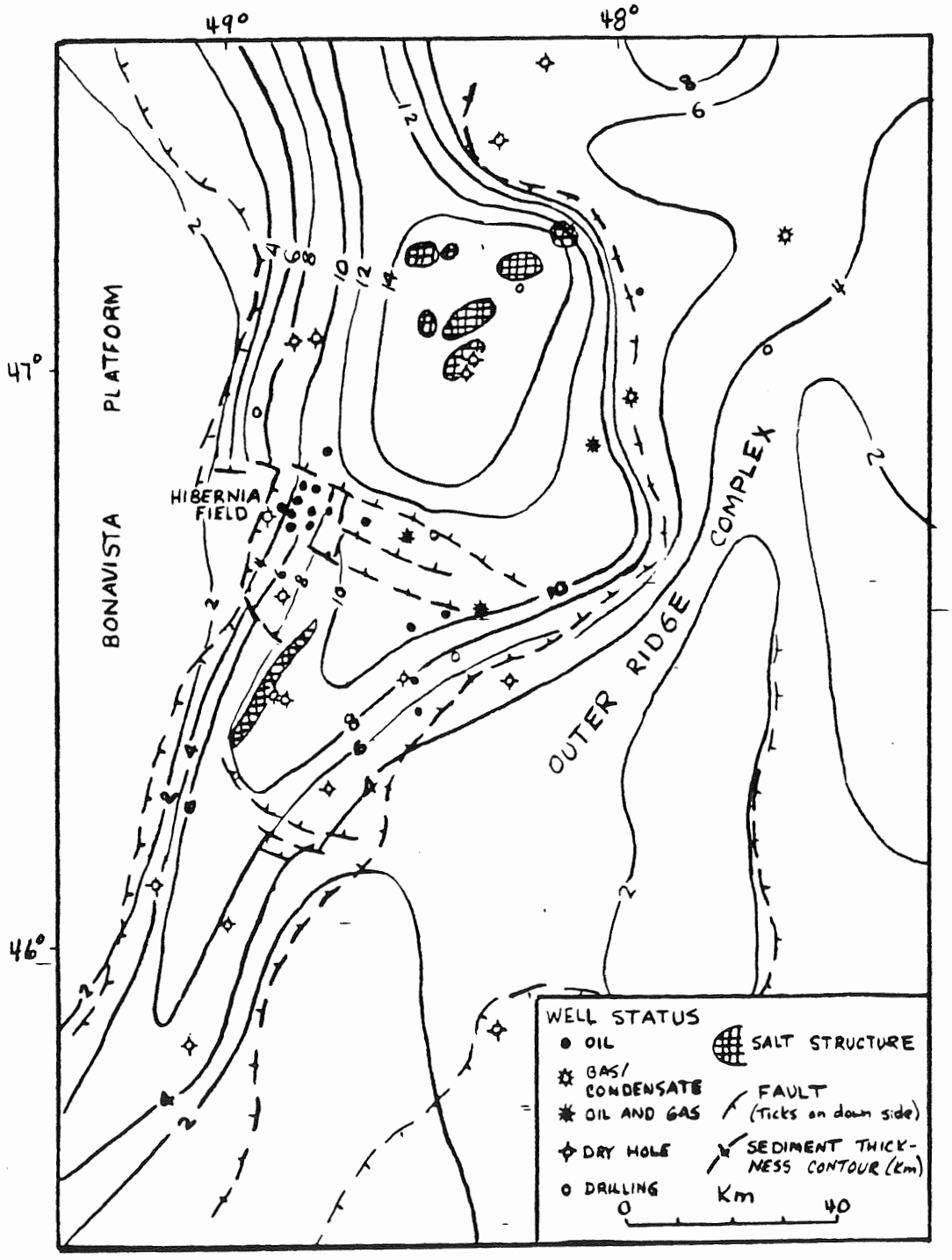

Figure 18: Diagrammatic structure and sediment thickness map of the Jeanne d'Arc Basin (from Grant, et al, 1986).

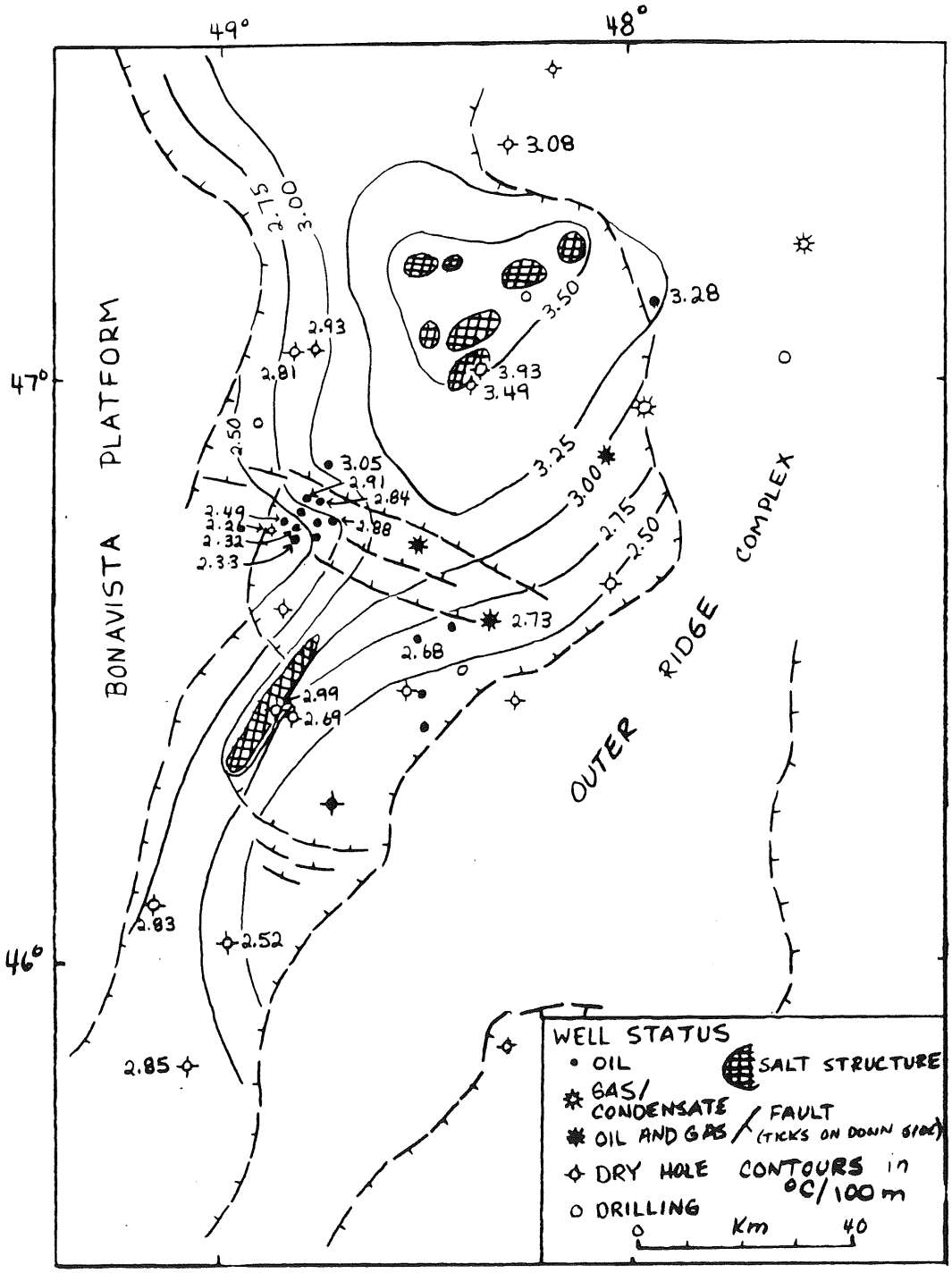

Figure 19: Average geothermal gradient across the Jeanne d'Arc Basin (from Ervine, 1985).

particular, a change from higher to lower geothermal gradients often coincide with the Verrill Canyon - Missisauga Formation boundary, which usually marks the top of the overpressured zone (Figs. 20 and 21).

Vertical variations in the geothermal gradient are probably also influenced by radiogenic heat production from varying lithologies. In their Scotian Basin study, Keen and Lewis (1982) obtained heat production measurements of 1.4 to 1.8 uWm^{-3} in the shales of the Mic Mac and Verrill Canyon Formations, and values of only 0.3 to 0.6 uWm^{-3} from the limestones of the Abenaki Formation. Values from the Missisauga Formation ranged from 0.8 to 1.5; it is comprised of various lithologies. Their results show that radiogenic heat production differences can change the total heat flow by several degrees (depending on the thickness of the units and appropriate conductivities).

Conductivity differences between Verrill Canyon and Mic Mac shales (low) and Missisauga sandstones and limestones (higher) will affect the geothermal gradient in the same direction as heat production. Gretener (1981) noted that the tops of overpressured zones are commonly the locus of a sharp increase of the geothermal gradient. For siliciclastic sequences, he attributes this to the sharp change in sand/shale ratio, hence conductivity contrast. In fact, some of the excess pore pressure may be caused by increasing the temperature (by burial) of an isolated formation (Gretener, 1981).

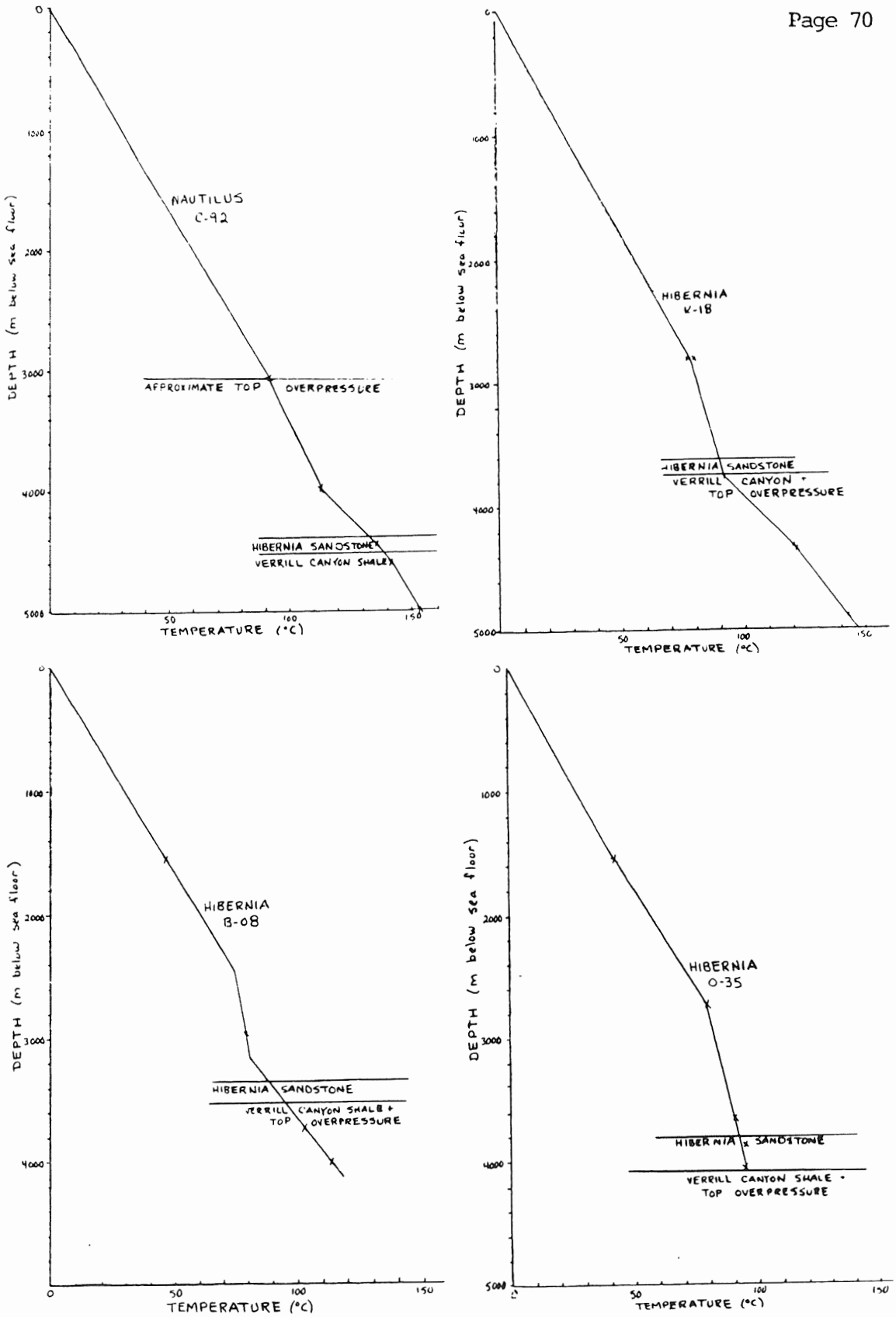

Figure 20: Vertical geothermal gradients compared across the Jeanne d'Arc Basin. Data from Ervine, 1985.

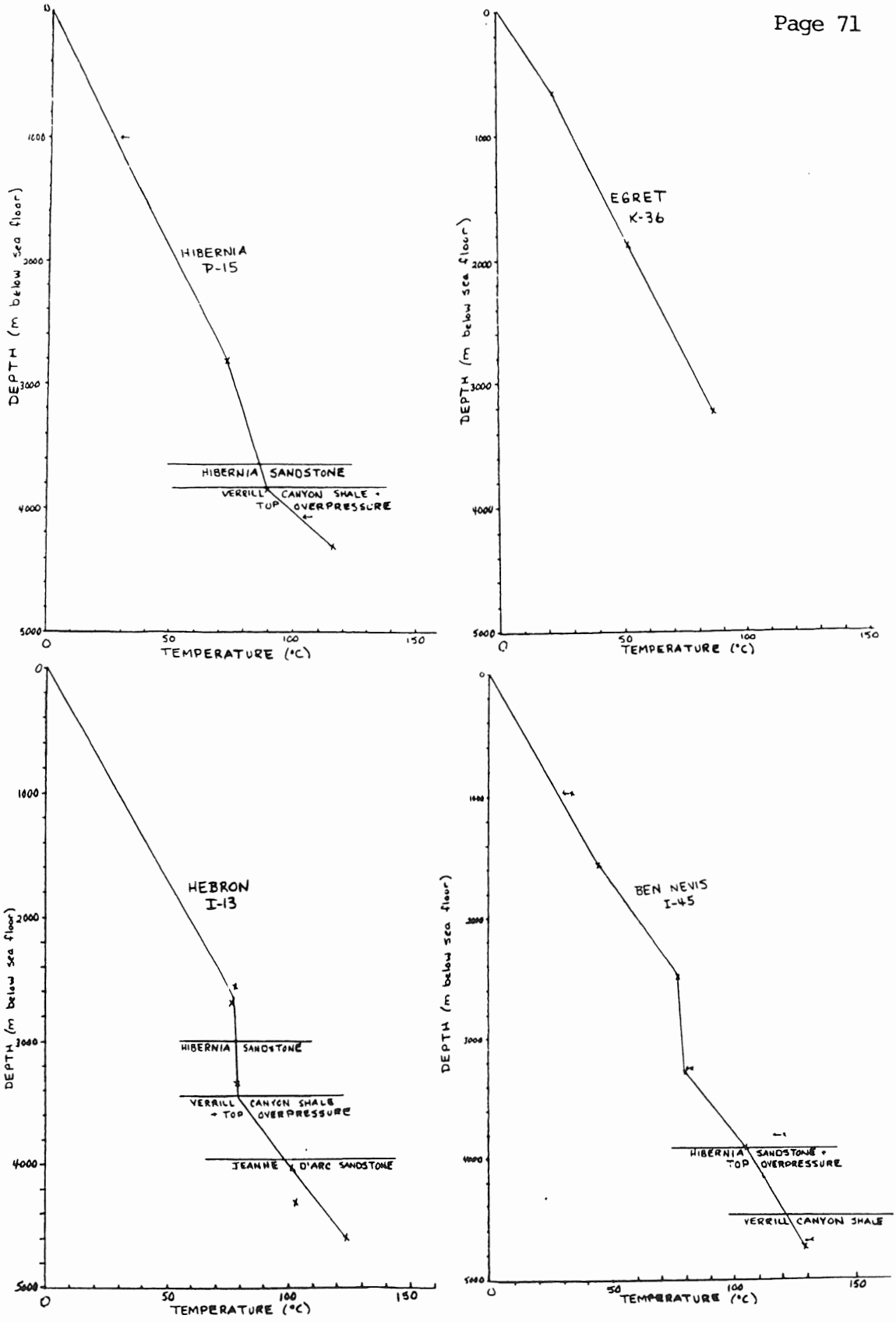

Figure 21: Vertical geothermal gradients compared across the Jeanne d'Arc Basin. Data from Ervine, 1985.

The thick overpressured section (Verrill Canyon and Mic Mac Formations) contains the hydrocarbon source rock in the Jeanne d'Arc Basin. The shale is probably a very good source of radiogenic heat. This heat, and heat from below, would be "trapped" in the overpressured zone by its low conductivity and the impeded circulation of pore fluids. However, the overpressured zone may periodically relieve pressure buildup through fractures (such as those shown in Plate 7?), locally increasing the heat flow to the overlying Hibernia member, by convection of warmer fluids. This has important implications for the maturation of organic matter, hydrocarbon migration, and mineral diagenesis.

The underlying principle is that vertical and basinwide differences in the present geothermal gradient are mainly due to lithology. Different rocks have different heat-production and heat-distribution capabilities. Since the relative positions of all of the lithologies have remained constant through time, each lithologic unit should have retained a characteristic geothermal gradient appropriate for its place in the stratigraphic succession. For example, the Verrill Canyon Shales were always hotter, and the Hibernia Member always cooler than an "average" geothermal gradient would predict.

This partially justifies the use of Ervine's (1985) curves which show the geothermal history at several well locations in the Jeanne d'Arc Basin. Figures 10-17 are the

burial history curves based on the time-space diagram, with Ervine's geothermal history curves superimposed. Each segment of the geothermal gradient is assumed to be constant for that lithology through time. Thermal influences from overpressured zones are thus accounted for and assumed to be operative since deposition. The importance of considering vertical variations in the geothermal gradient is only recently being emphasized (e.g. Chapman and Willett, 1986; Weir and Furlong, 1986).

However, Ervine's method does not take into account net differences in the heat flow from the basement with time. Current research has produced models of the cooling history of Eastern Canadian rift basins following extension (Keen, 1979; Keen, Beaumont, and Boutilier, 1982; Keen and Barrett, 1981; Royden and Keen, 1980). By calculating the amount of crustal thinning, the authors estimate the amount of initial lithospheric heating produced by upwelling of hot asthenosphere and trace its cooling history. The thermal model predicts an approximately exponential decrease in heat flow due to rifting, with time. This is valid for tens of millions of years following rifting.

Figure 22 shows the surface heat flow versus time for a Scotian Basin thermal model. Most of the excess heat flow generated during rifting would have dissipated by early Tertiary time. If radiogenic heat production were

negligible, the heat flow would decay to an equilibrium value corresponding to heat flux from the base of the lithosphere. (Keen and Lewis, 1982)

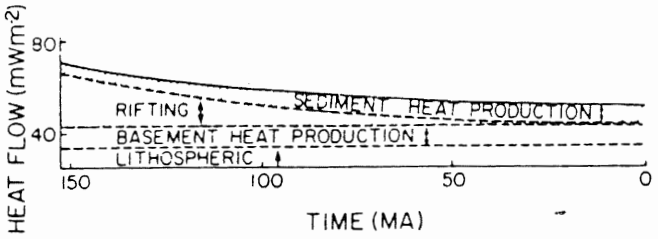

Figure 22: Surface heat flow versus time for a Scotian Basin model (from Keen and Lewis, 1982).

Therefore, Ervine's curves are probably lower than the early post-rift geothermal gradient. There were two phases of rifting in the Jeanne d'Arc Basin, compounding the error at the left-hand side of the thermal history curves. Fortunately, most of the important diagenetic organic reactions occur during the later part of the thermal-burial history; the rate of organic reactions is extremely slow during early diagenesis.

A more accurate thermal history of the Jeanne d'Arc Basin may evolve through the use of geodynamic models. In their Scotian and Labrador Basin studies, Keen (1979) and Keen and Lewis (1982) successfully predicted the present level of organic maturation as measured by vitrinite reflectance. A similar thermal history model for the Jeanne d'Arc Basin will have to consider two phases of rifting and must input radioactivity/conductivity values which are appropriate for each lithology (including overpressured shales) in the Jeanne d'Arc Basin. Keen and Lewis (1982) further note that the relative roles of conductive and convective heat transport must be better known.

VIII MATURATION OF ORGANIC MATTER AND HYDROCARBON MIGRATION

The maturation of organic matter results from its thermal and burial history. Chemical reaction rates involving organic matter vary linearly with time, but exponentially with temperature (Lopatin, 1971, in Ervine, 1985). Different types of organic matter respond differently to heat through time. The reflectance of vitrinite within kerogen systematically increases with maturity; it is used often as the most objective maturation scale for comparing coalification, kerogen maturation to hydrocarbons, colour alteration of spores and pollen, and several other thermal maturation indicators (summarized by Heroux et al., 1979).

Vitrinite reflectance (Ro) measurements provide a means of testing the predictive power of the thermal burial history curves. A time-temperature index (TTI) was calculated from the curves using Lopatin's (1971) method (in Ervine, 1985); the TTI is a measure of maturity that doubles with every 10°C increase in temperature or with a doubling of exposure time. TTI values were calculated for horizons representing the Hibernia member and source rocks (Fig. 10-17); these were compared to measured Ro values (Fig. 23). On logarithmic graph paper, there is a linear relationship. Since the thermal history curves are taken from Ervine (1975), his data, from several horizons, are also shown. There is a reasonably good correlation.

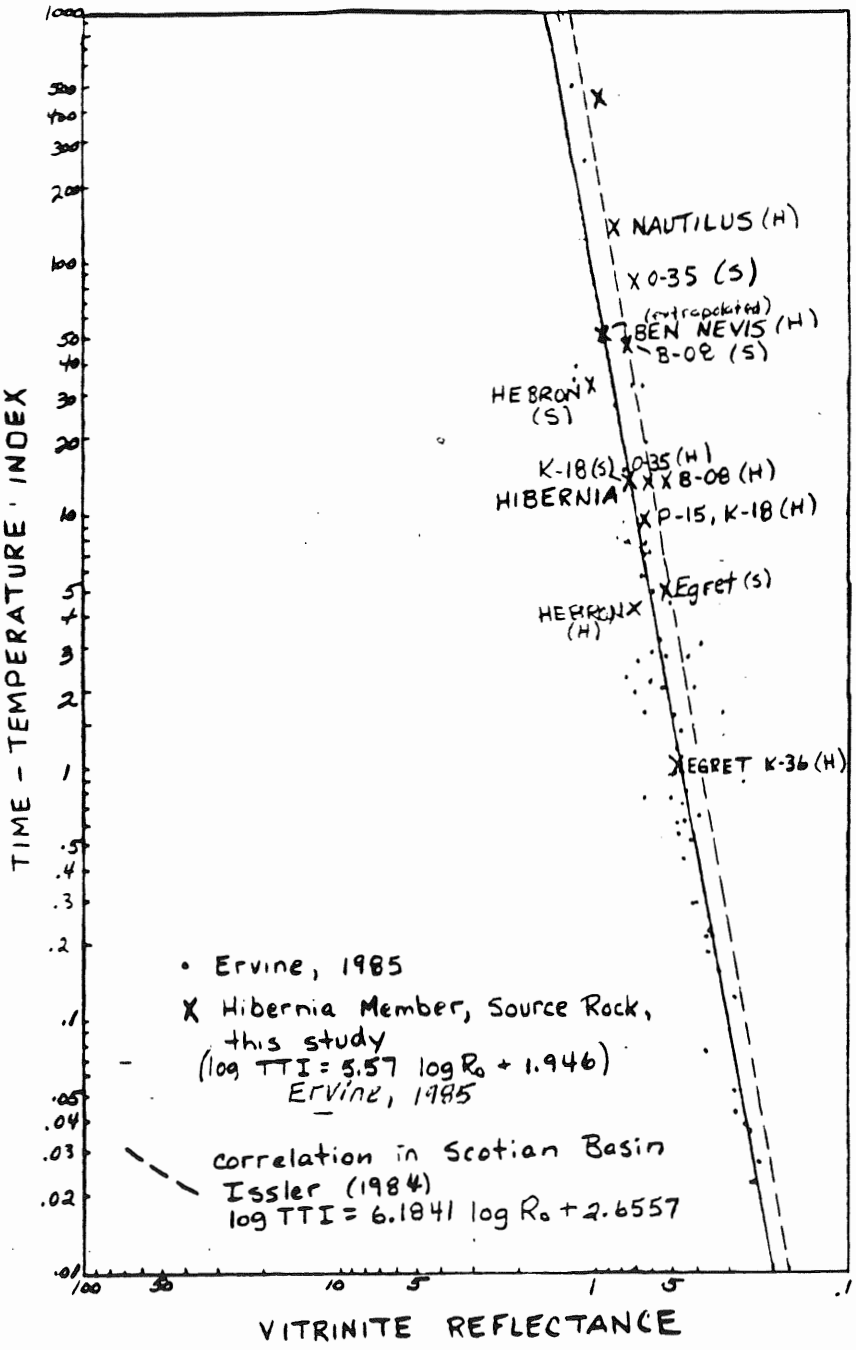

Figure 23: Correlation of calculated TTI valves and measured Ro.

Issler (1984) obtained a different correlation between Ro and TTI in his Scotian Basin study (Fig. 23). The thermal histories used in both studies neglect the exponential decrease in temperature following rifting. Since the Scotian Basin had a greater initial heat flow due to greater crustal extension, a different calibration with vitrinite reflectance was needed.

Vitrinite reflectance data from Avery et al. (1986), Avery (pers. comm.), and well history reports were used to compare organic maturity across the basin. Figure 24 shows that the thickness of the oil window (0.5 to 1.35 Ro) increases toward the basin margins. It is over 6 km thick in the Hibernia field area, where present geothermal gradients are lower due to a thinner sedimentary section. Paleogeothermal gradients may also have been lower due to less crustal thinning at this basin margin (proposed by Tankard and Welsink, in press). The very thick oil windows allow organic reactions to be effective over longer periods of time.

The oil window is compressed in the center of the basin, where the present geothermal gradient is highest, the sedimentary section is thickest, and thermal subsidence was greatest (compare Fig. 24, 18 and 19).

The thickness of the oil window around the salt domes (measured at the Adolphus and Egret wells) is consistent with the regional trend. Keen (1983) showed that the high

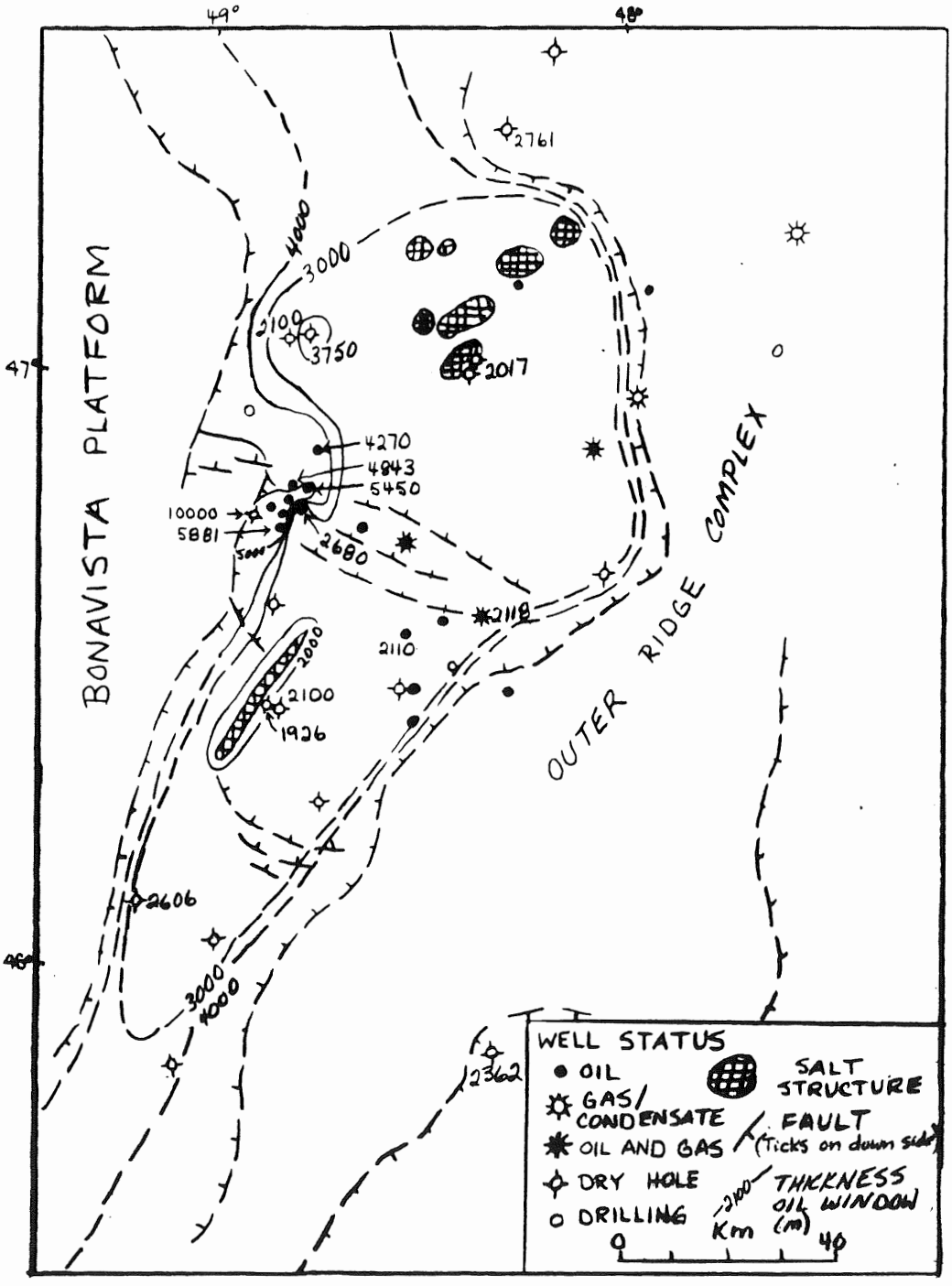

Figure 24: Thickness of the oil window, Jeanne d'Arc Basin, based on vitrinite reflectance data from Avery et al., 1986; Avery, pers. comm.; and well history reports.

conductivity of salt in the Scotian Basin, does not raise temperatures in the sediments enough to cause a significant increase in the level of maturity.

Vitrinite reflectance profiles also vary in the vertical direction. Figures 25 and 26 show maturation profiles for eight wells in the Jeanne d'Arc Basin. There appears to be the same correlation with lithology as noted for the temperature profiles (Figs. 20 and 21); namely, higher temperatures and resulting greater organic maturation are associated with the overpressured Verrill Canyon Shales.

Heroux et al. (1979) note that at the same maturation stage, reflectance of vitrinite increases from sandstone to siltstone to shale to coal. It is possible that this is an apparent effect of radiogenic heat production. However, a few of the calculated TTI values agree more closely with a least squares, linear fit of the data points (eg. Hibernia K-18). The accuracy of the reflectance method may obscure any correlation between maturation gradient and lithology. For example, Avery (pers. comm.) notes that bitumen staining or adsorption may cause lowering of the observed Ro valves in the Verrill Canyon Formation of the Hibernia B-08 well.

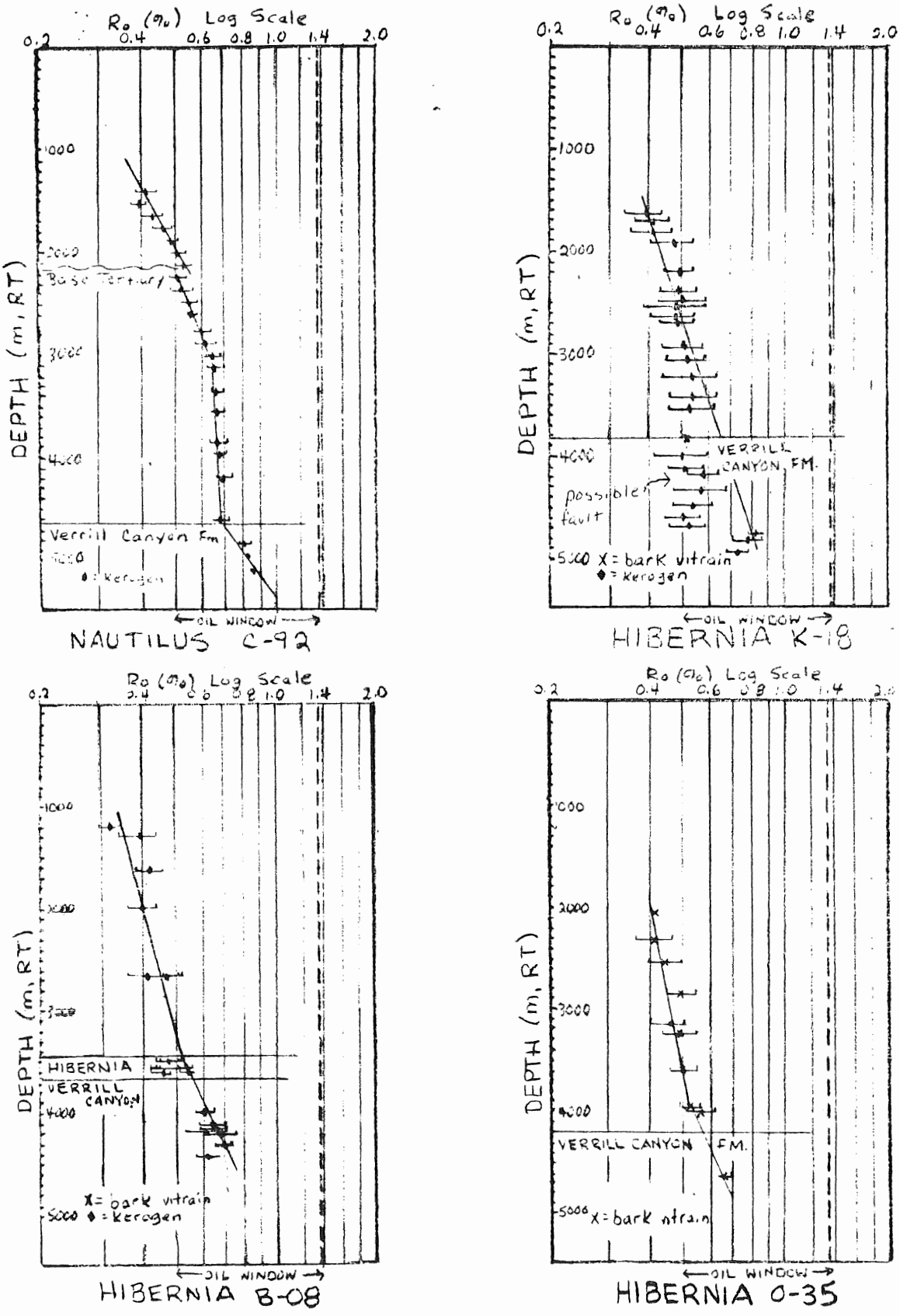

Figure 25: Maturation profiles based on vitrinite reflectance data from Avery et al., 1986.

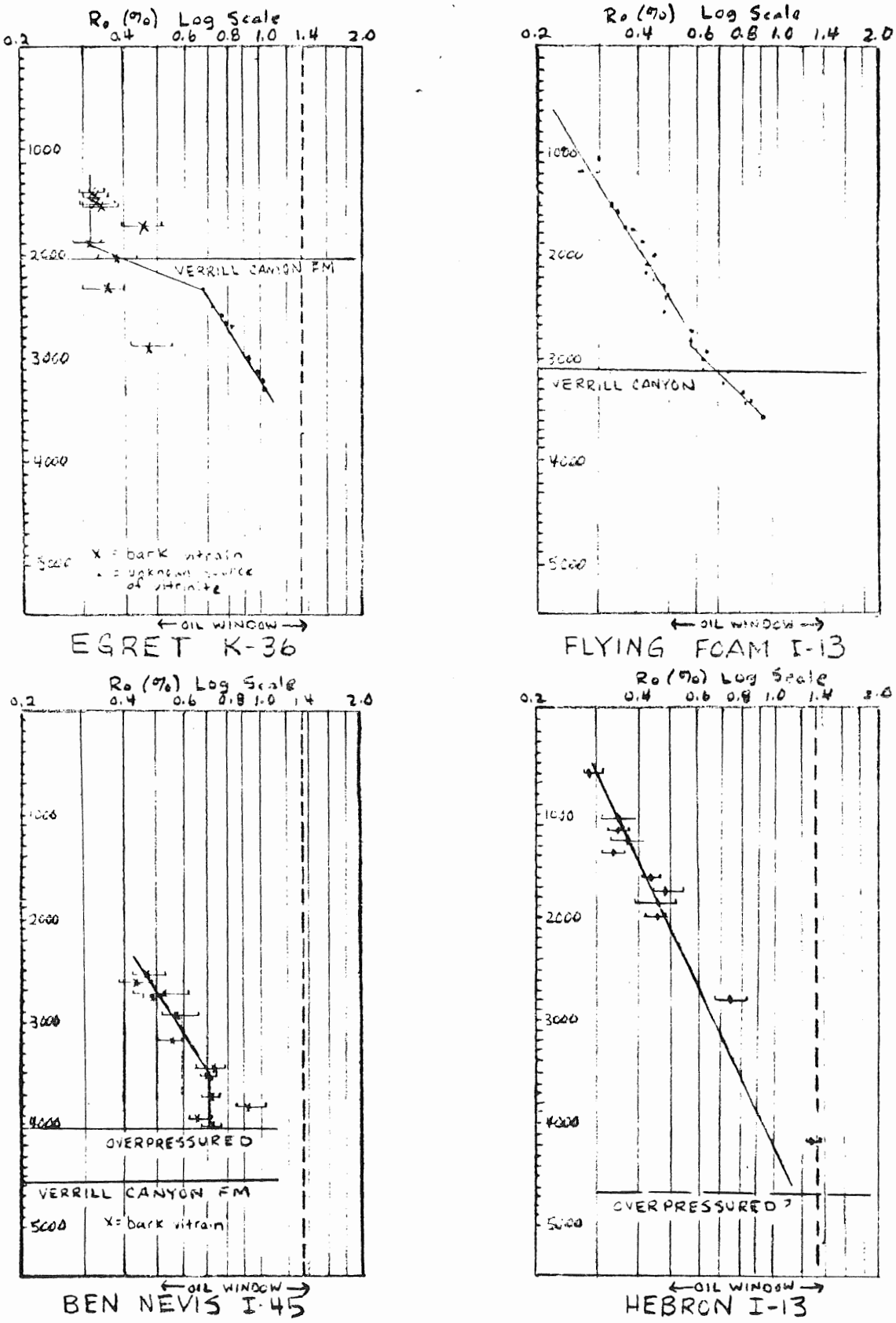

Figure 26: Maturation profiles based on vitrinite reflectance data from Avery, pers. comm. and well history reports.

Hydrocarbon Generation

Powell (1984) used gasoline range data to show that most of the oil in the Jeanne d'Arc Basin was sourced from Type II organic matter in Upper Jurassic shales. Up to 9% organic carbon was found in Kimmeridgian shales at the Hibernia P-15 and K-18 well locations. He found that the hydrocarbons belong to a general genetic family but differ in the level of maturity at which they were generated.

In order to ascertain the timing of oil maturation, time-temperature index (TTI) values were calculated from the thermal-burial history curves for the base of the Jeanne d'Arc Sandstone (Figs. 10-17). This horizon is within the source zone identified by Powell (1984). The TTI values were converted to vitrinite reflectance values, using the correlation established in Figure 22 by Ervine (1985).

The calculations show that the potential source rocks first reached maturity at the Ben Nevis I-45, Nautilus C-92, and Hibernia 0-35 well locations. (Since the Ben Nevis well reached total depth at the base of the Verrill Canyon, the depth and age of the base of the Jeanne d'Arc sandstone was estimated by stratigraphic comparison with the Hebron well.) For all three wells, the threshold for oil generation (0.5 R_0) was reached during the Albian (106-104 Ma) and the peak of oil generation (0.8 Ro) occurred during the Eocene to Oligocene (55-30 Ma). These results agree with Grant et al. (1986).

The Ben Nevis and Nautilus wells are located near the centre of the basin where the geothermal gradients are highest and the sedimentary pile is thickest. These wells showed the highest subsidence rates on the burial history curves. The Hibernia O-35 well is next to the Murre Fault which caused rapid burial of the source rocks beneath the Lower Cretaceous section.

The threshold for oil generation was reached slightly later, during the Cenomanian (94 Ma), in the Hebron well. Peak oil generation did not occur until the Pliocene (5 Ma). This well is also near the basin axis but is located on a fault block which was extensively eroded during the Pre-Aptian and Avalon lacunas. Therefore, the source rocks were not buried as deeply at this location.

The source rock in the Hibernia P-15 and B-08 wells reached the threshold for oil generation during the Campanian (80-75 Ma) and reached peak generation capacity during the Miocene (20 Ma). The source rock in the Hibernia K-18 well reached maturity during the Eocene (57 Ma) and has yet to reach peak generation capacity. These wells are located near the basin margin, where the present geothermal gradient is lowest, the total sedimentary column is thinnest, and the oil window is thickest.

At the Egret location, the source rocks did not reach the threshold for oil generation until the Eocene (43 Ma)

because of extensive erosion at the Avalon and Pre-Aptian unconformities and consequent shallow depth of burial.

Since the Upper Jurassic source rocks reached maturity at least as early as 106 Ma in the Ben Nevis well, there may have been leakage at the Avalon Unconformity. Powell (1984) suggested that oil generation started as early as Lower Cretaceous in the basin depocentre, and reached the same conclusion. Most of the traps were formed by structural deformation which occurred during the Albian.

There is some evidence for biodegradation of the oil trapped in the Avalon reservoir near the basin depocentre. This oil presumably migrated after structural deformation but before significant burial of the Avalon sandstone. Drill stem tests in the Hebron I-13 well show that the API gravity of the oil averages only 17.5° in the Avalon reservoir, 29° in the underlying Catalina reservoir, and 33.5° in the Jeanne d'Arc sandstone (COGLA, 1985). There is dead oil in the Avalon sandstone at the Ben Nevis well with a 22.3° API gravity. The oil is also heavy at the Mara M-54 well. Press releases from this confidential well (in Grant et al., 1986) indicate that from 1851-1857 m, API gravity = 21.6°; from 2403-2408 m, API gravity = 21.5°; and from 2704-2708 m, API gravity = 11°. In contrast, all of the reservoirs at the Hibernia field have oil with gravities of 30-50° (COGLA, 1985).

If some of the earliest-formed oil was lost at the Avalon unconformity, this would explain why most of the major

oil discoveries are located near the basin margin. Furthermore, there are gas prone potential source rocks in the Lower Cretaceous section which matured during the base of the Tertiary lacuna in the Ben Nevis area; the Jurassic source rocks are currently near the "oil floor" and may be producing wet gas (Fig. 14). This would explain the very high gas to oil ratio in the Ben Nevis reservoirs and the gas discovered at the North Dana I-43, Trave E-87, and Whiterose N-22 locations.

At the Hibernia field, oil maturation occurred well after structural deformation was complete. Because of the thick oil window, the Jurassic source rock is still at peak generating capacity.

Hydrocarbon Migration

The Jurassic source rocks are presently overpressured (Grant, et al., 1986) and were shown to have above average geothermal gradients which accelerate maturation rates. Dow (1978) points out that increased hydrocarbon generation rates would increase expulsion efficiency by concentrating hydrocarbons before expulsion. The overpressures would retard dewatering until significant quantities of hydrocarbons were formed.

Dow (1978) also notes that faulting and salt piercement can fracture high-pressure shales and release generated oil and gas to tectonically-controlled migration pathways. This

may have happened to the earliest-formed oil at the Ben Nevis I-45 and Nautilus C-92 wells. In both instances, the present overpressured zone lies stratigraphically above the top of the overpressured zones in the other wells. The overpressured zone may have migrated up through the stratigraphic section during the Avalon lacuna.

The overpressured zone remains below the top of the Verrill Canyon Shale in the other wells studied. Grant et al. (1986) suggest that the prime cause of oil migration may be episodic buildup of pressure to near lithostatic in the overpressured regime. This causes natural fracturing and consequent release of fluids into overlying reservoirs via microfractures (Plate 7) and faults (Plates 11 and 12), which close again after pressure reduction. The cyclic nature of such a phenomenon would provide an additional explanation for the variation in maturity at different levels in individual wells. Chapman (1975) notes that the migration of hydrocarbons in faults is across faults rather than up the fault plane since an abnormally pressured shale cannot support a fracture for very long.

Dow (1978) also cited periodic fracturing as a mechanism for the expulsion of oil from high pressure shales of the Gulf Coast. Doligez et al. (1986) modelled hydrocarbon migration in the North Sea Basin and found that migration from overpressured Jurassic shales was similarly governed by the structural pattern of the basin and hydraulic fracturing.

Once again, the importance of structural deformation to hydrocarbon accumulation is apparent. Grant et al. (1986) estimated that 75% of the oil potential of the East Newfoundland Shelf is associated with the trans-basin fault trend which extends from Hibernia to Ben Nevis. The structural configuration of the Jeanne d'Arc Basin probably controlled the deposition of the Hibernia member, provided structural traps, and provided migration routes for hydrocarbons and other diagenetic fluids.

Enclosure 9 is a structural fence diagram of the Hibernia member in the Hibernia field. It was constructed using Handyside and Chipman's (1983) grid with fault traces at the seismic "H" event. There is a displacement in excess of 4500 m on the Murre Fault (Arthur et al., 1982) which is not shown. Throws on the transverse faults range from 60 to 610 m and cut the Hibernia structure into a series of tilted fault blocks. The faults which cut the Hibernia member at the B-27 and K-14 locations, were observed in core (plates 11 and 12).

The Hibernia member is water-bearing in the O-35 well, contains mostly oil in the P-15 and B-27 fault blocks, and contains gas in the structurally highest B-08 fault block. The majority of these faults formed during the Avalon lacuna; McKenzie (1981) notes that some were reactivated during the Late Cretaceous.

IX PETROGRAPHY AND DIAGENESIS OF THE HIBERNIA MEMBER

The Hibernia sandstones were shown to be chemically mature with a consistent composition across the Jeanne d'Arc Basin. Furthermore, I have shown that the sandstones had a different burial-thermal history at various fault blocks. The petrography of the Hibernia member will be described and then explained in terms of time-temperature-dependent reactions and pore fluid evolution and migration.

Petrography

The petrographic data base is shown in Table 1 and a summary of the quantitative petrographic observations is included in the appendix. The best quality thin sections are from cores in the Hibernia K-14, K-18, and B-08 wells (courtesy of Robertson Research and the Atlantic Geoscience Centre). They were impregnated with blue epoxy to highlight porosity and stained with alizarin red-S and potassium ferricyanide to distinguish types of carbonate cement. Quantitative data were obtained and textural relationships were described for each of these thin sections.

Chip samples were used to make thin sections from the Hebron I-13 and Ben Nevis I-45 wells. Thin sections from the Egret K-36 well were also made from chip samples (courtesy of Dr. Jansa). It is difficult to force epoxy into the pores of chip samples and so the amount of porosity was difficult to estimate for these thin sections. Also, because the thin

sections were made from chips, only qualitative and semi-quantitative descriptions could be made.

Enclosure 10 is a plot of Hibernia sandstone porosity (measured from the sonic log) as a function of depth. The general trend is of decreasing porosity with depth. Hibernia sandstones at the Ben Nevis well have, by far, the lowest porosity. However, there are exceptions: at the Terra Nova well, sandstones have better overall porosity than at the shallower Egret well, and within individual wells there is a wide range of porosity values.

Figure 27 is a graph of grain size range versus porosity from the core thin section data for Hibernia K-14, K-18, and B-08. Porosity generally increases with increasing grain size, except for the conglomerate samples. Very fine sandstone to siltstone samples have less than 13% porosity and fine to very coarse grained sandstones have greater than 13% porosity. Data for the sandstones at the Ben Nevis well are not shown since precise measurements were not possible in the cuttings samples; however, all grain sizes have less than 11% porosity (Enclosures 7 and 10).

Enclosure 11 summarizes the quantitative petrographic data obtained from the 68 thin sections of the Hibernia K-14 well. The lithologic log and core descriptions are shown for comparison. The column for percent components ends at 65%; the remaining 35% is comprised of clasts which are undifferentiated because they have an almost unimodal quartz

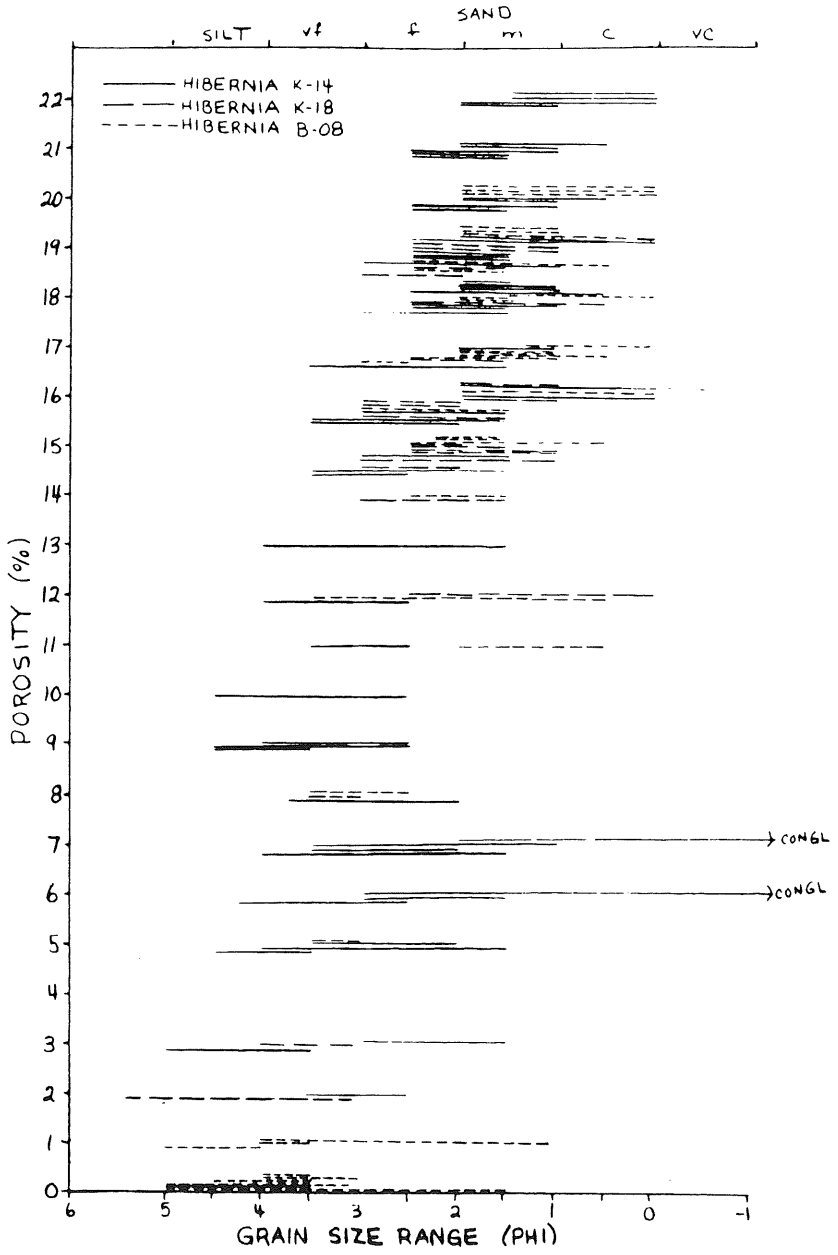

Figure 27: Graph of grain size range versus porosity from thin section data.

composition (Fig. 9). The component column is essentially a bar graph; the thickness of the "bar" for each thin section depends on the distance between thin section samples. The thin section locations are at the centre of the bar and are labeled on the gamma ray curve at the left.

Enclosure 11 shows that the channel sandstones between 3900 m and 3945 m have excellent porosity (18-22%), approximately 12% quartz overgrowths, 2% authigenic clay (mainly kaolinite), and very minor detrital clay. Authigenic kaolinite was distinguished by its euhedral, platey habit and its vermicular growth pattern (Scholle, 1979). Clay was assumed to be detrital if it was associated with carbonaceous matter and silt-sized quartz grains in lenses within the sandstones.

The highest porosity values were recorded for the very well-sorted, medium-grained sandstone body between 3900 m and 3910 m. The interpreted fault rubble observed at 3892 m is in close proximity (Plate 12). All of these channel sandstones contain hydrocarbons. One thin section (#36 at 3932.6 m), from near the top of a sandstone body, has 20% ferroan calcite and minor moldic and intragranular porosity.

The channel sandstones near the base of the log are water-bearing and have bitumen staining. They have poorer porosity than the other major sandstones and more variable amounts of porosity and cement. The relatively higher percentage of clasts shows that they are more compacted than the other channel sandstones.

The very fine sandstones and siltstones generally have low porosity, up to 17% ferroan calcite cement, common detrital clay, but no authigenic clay, and have an average of 8% quartz overgrowths. They also are more compacted than the very porous channel sandstones, with up to 80% clasts.

The quantitative petrographic data from the Hibernia K-14, K-18, and B-08 wells were averaged for the channel sandstones and floodplain siltstones to very fine sandstones. Standard deviations are also shown.

The channel sandstones have grain sizes ranging from very fine to very coarse; the average is medium-grained sandstone (1.8Ø). The mean grain size for each well is similar; differences are attributed to the number and location of samples (K-18: 2.0 ± 0.4Ø; K-14: 1.8 ± 0.6Ø; B-08: 1.6 ± 0.5Ø). The mean porosity is 17.1 ± 3.2%. The K-14 well has a slightly better average porosity (17.0 ± 4.6%) than the B-08 (16.6 ± 2.3%) and K-18 (16.2 ± 1.9%) wells.

In 97% of the channel sandstone samples there is only 0-1% ferroan calcite, whereas there is up to 20% ferroan calcite in a few finer-grained samples near the tops of sandstone bodies. Quartz overgrowths comprise 11.4 ± 1.4% of the thin sections. This figure is not as reliable as other estimates because the overgrowths are in optical continuity with the quartz grains and may only be distinguished if they are rimmed with clay. Also, the distinctive euhedral shape of the overgrowths may be altered by dissolution.

Authigenic kaolinite comprises $0.8^{+}_{-}0.8\%$ of the thin sections, whereas high birefringent clay comprises $1.1^{+}_{-}1.1\%$. There is a trace to 2% authigenic pyrite and organic carbon in all samples.

The floodplain siltstones to very fine sandstones have 0-18% porosity; the mean is $5.9^{+}_{-}5.0\%$. There are variable amounts of ferroan calcite: an average of 10% in 7 samples and 0-1% in 22 samples. Quartz overgrowths comprise $7.4^{+}_{-}4.0\%$ of the thin sections and detrital clay comprises $4.6^{+}_{-}4.5\%$ (not including argillaceous streaks). There is no authigenic clay. Nodular siderite cement locally comprises 3%, and pyrite and organic carbon comprise 0-7% of the fine-grained sediments.

The textural relationships seen in the thin sections will be summarized with the help of plates 13-29. Note that PPL and XN designate plane polarized light and crossed nicols, respectively.

Plate 13 is a photomicrograph of a conglomerate at the base of a thin sandstone in the Hibernia K-14 well (Enclosure 11). It shows abundant siderite/pyrite nodules, also found in the channel sandstones. These intraclasts are derived from the floodplain; thin sections from the finer sediments clearly show that the authigenic cements surround very fine quartz grains to form a nodule. The growth of these nodules in the floodplain sediments indicates reducing and slightly acidic conditions.

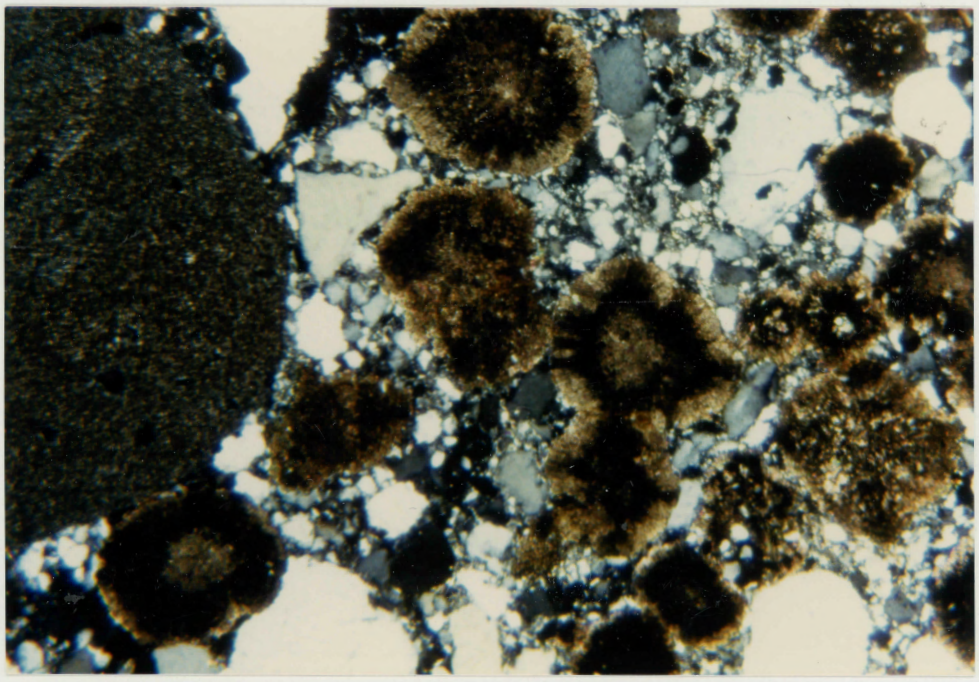

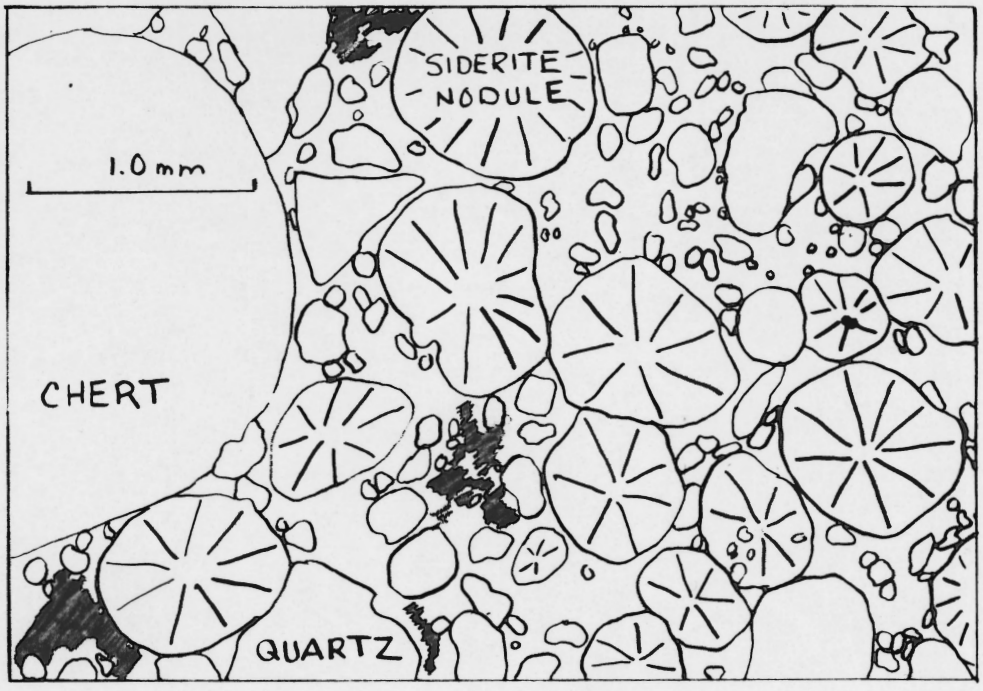

Plate 13: Conglomerate with abundant detrital siderite/ pyrite nodules. Hibernia K-14, TS 54, 3964.6 m, XN.

Plate 14 shows good porosity developed in fine-grained sandstone of the Hibernia K-18 well. Abundant quartz overgrowths are easily distinguished in this thin section because they are outlined by very fine rims of clay. Most of these overgrowths are interlocking and have euhedral terminations; they are clearly authigenic. The plate also shows irregularly distributed secondary porosity with clays outlining the positions of former grains. A siltstone clast, partially replaced by authigenic kaolinite, suggests that sedimentary rock fragments may have been leached to form the secondary porosity.

Plates 15 to 18 are examples of the severe porosity reduction which accompanies extensive calcium carbonate cementation, most common in the Ben Nevis I-45 well.

Plate 15 shows euhedral dolomite rhombs cementing a fine to medium-grained sandstone in the Ben Nevis well. Dolomite is not a common cement in the Hibernia sandstone; it was found with certainty only in the Ben Nevis well.

Extensive ferroan calcite cementation and common replacement of plagioclase occurs in fine-grained sandstones above the Hibernia member in the Egret K-36 well (Plate 16). The underlying, coarser-grained sandstones have up to 22% porosity. This suggests that ferroan calcite was leached from the coarser-grained, more permeable Hibernia sandstones.

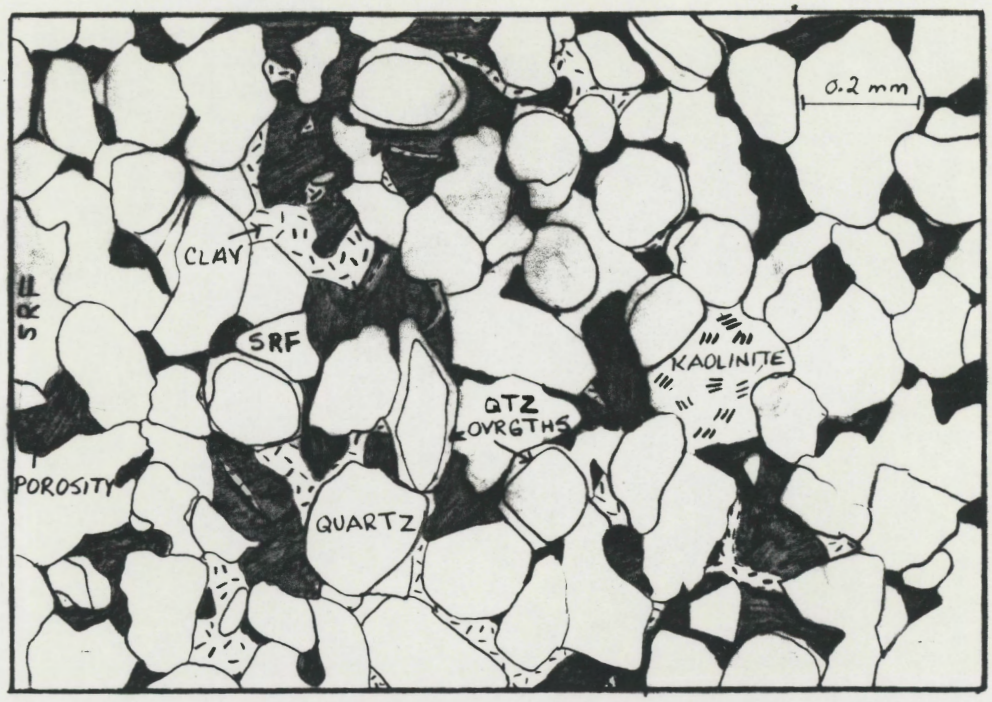

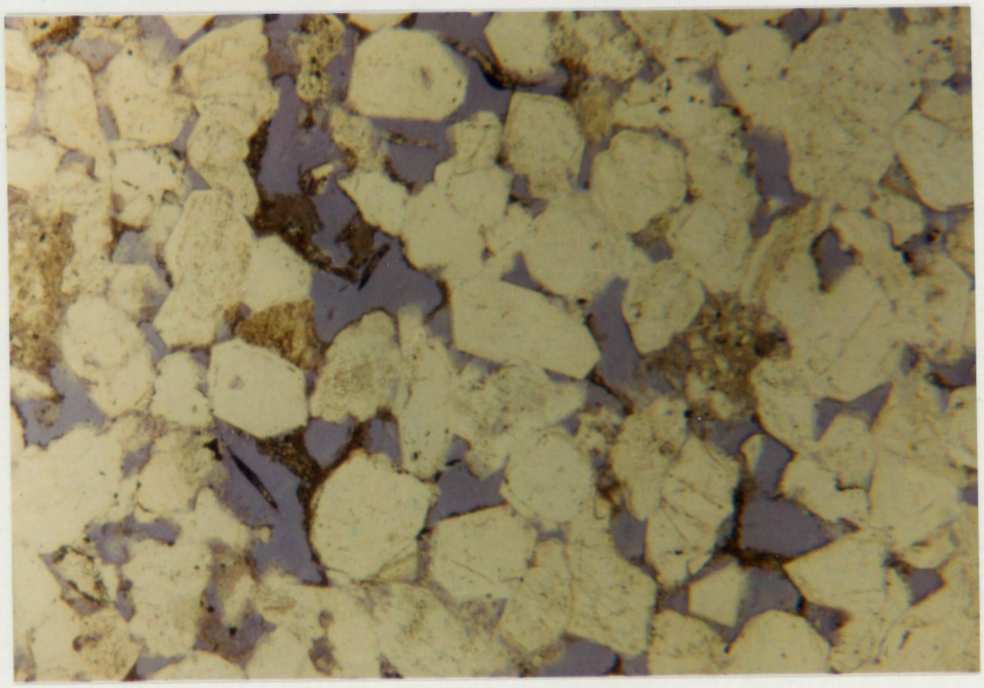

Plate 14: Abundant quartz overgrowths, secondary porosity outlined by pre-dissolution clay, and a grain replaced by kaolinite. Fine-grained sandstone, Hibernia K-18, TS 15, 3826.6 m, PPL.

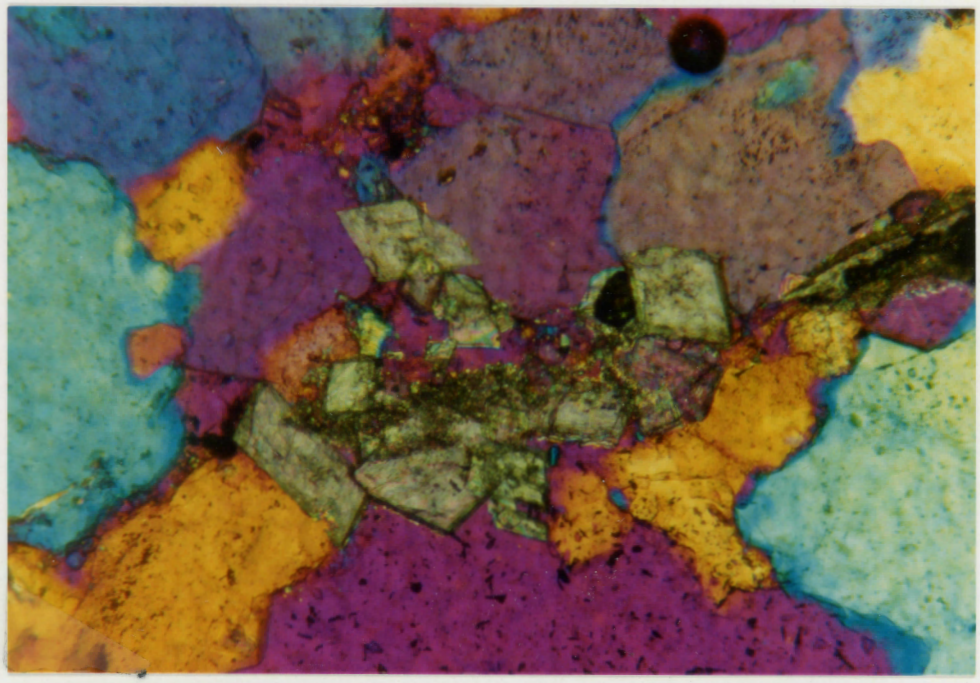

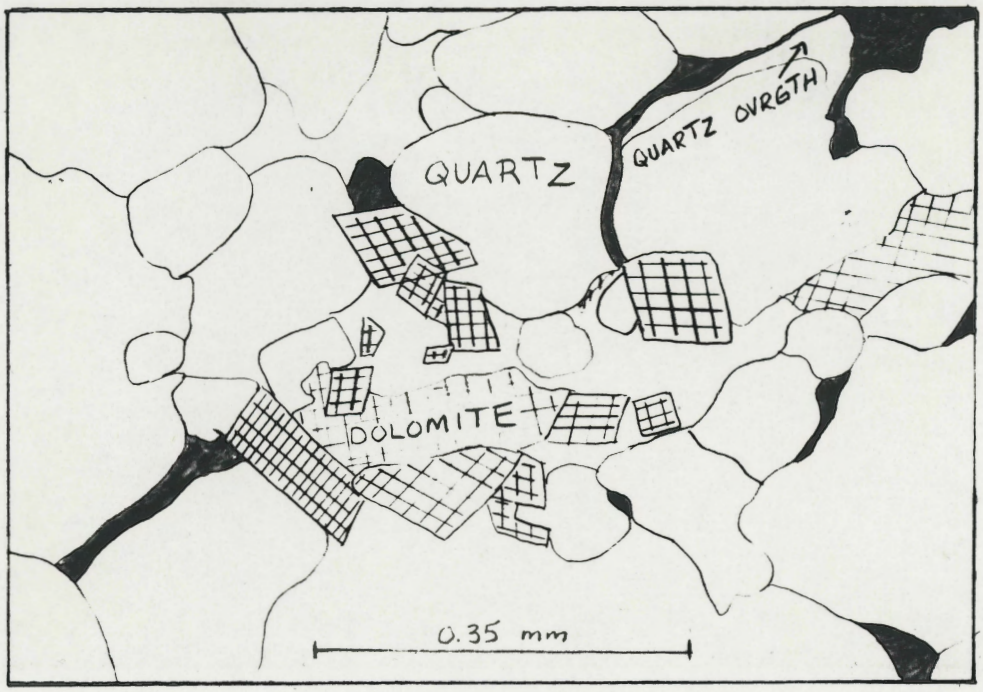

Plate 15: Dolomite rhombs in fine to medium-grained sandstone, Ben Nevis I-45, TS 11, 4195-4200 m, XN with mica plate.

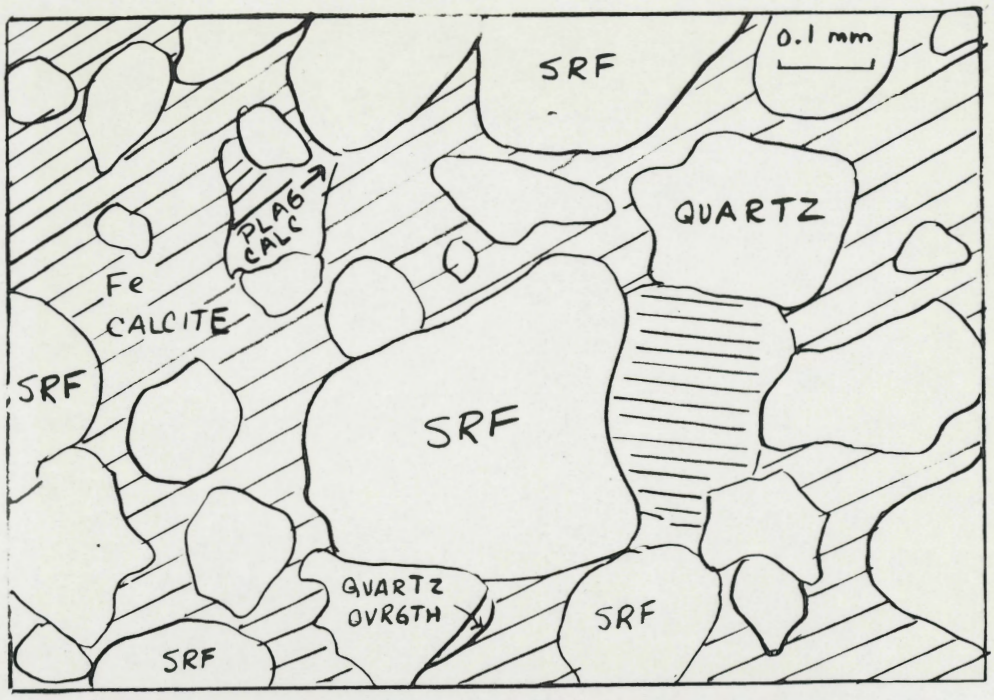

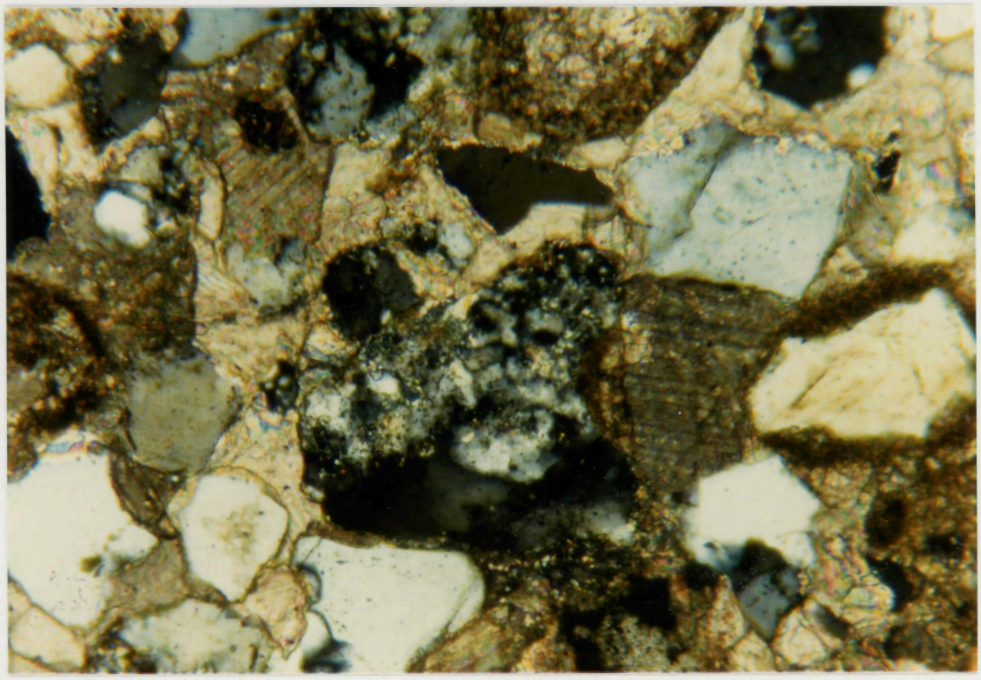

Plate 16: Extensive ferroan calcite cementation and replacement in fine-grained sandstone above the Hibernia member, Egret K-36, TS 4, 5190'-5200', XN. Note the rounded detrital quartz overgrowth and ferroan calcite pseudomorphs after plagioclase.

Plate 17 shows extensive calcite cementation and replacement of plagioclase in the Ben Nevis well. Rare detrital quartz overgrowths are abraded and do not interlock, providing evidence for a sedimentary provenance. The low degree of packing in this poorly sorted sandstone indicates that either the cement was very early or the sandstones were undercompacted at the time of cementation.

Plate 18 shows extensive pyrite and ferroan calcite cement in very fine to fine-grained sandstone of the Ben Nevis well. As in the previous plate, the sandstone has a low degree of mechanical compaction. The quartz grains are corroded and have no visible overgrowths.

In plate 19, evidence for secondary porosity includes a honeycombed feldspar grain and corroded quartz grains. There are minor patches of ferroan calcite and pyrite, reminiscent of the previous photograph. The clay appears to be authigenic and partially fills the secondary pores. However, it forms around the partially dissolved grain in the upper left hand side of the photograph. Probably, detrital clay recrystallized after the porosity was generated.

Plate 20 shows a honeycombed siltstone grain with detrital quartz overgrowths. It is associated with authigenic kaolinite and intragranular porosity. Siltstone grains partially replaced by kaolinite and pyrite are shown

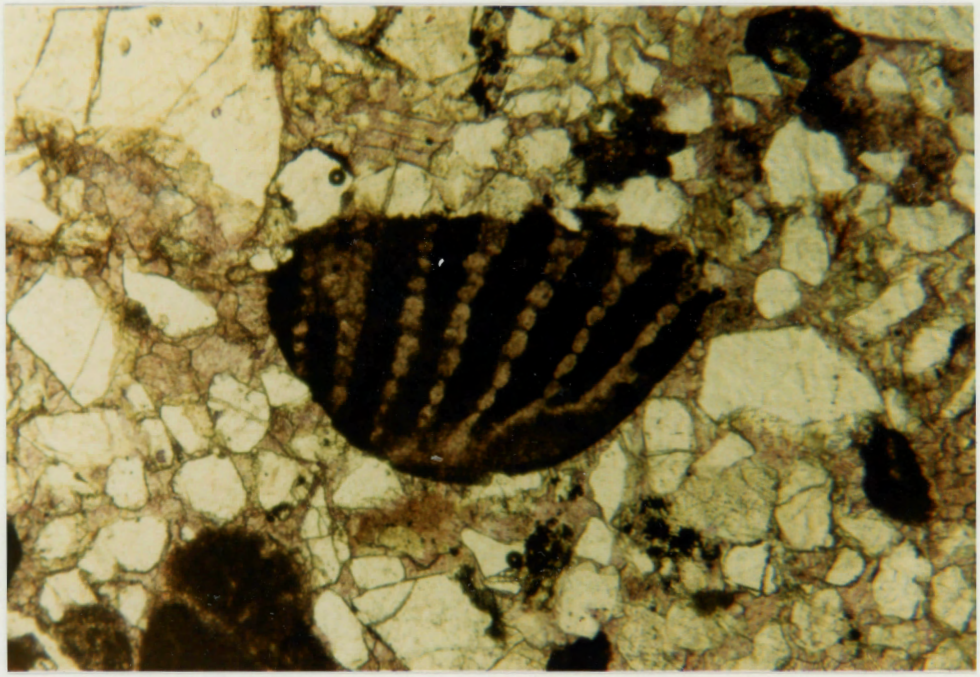

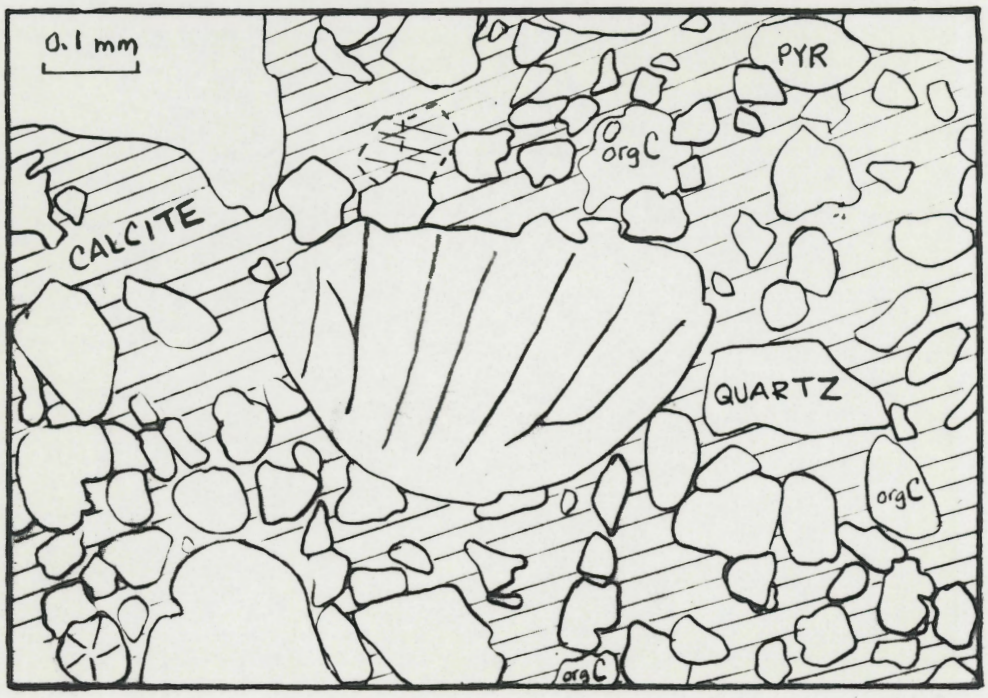

Plate 17: Unidentified microfossil in a poorly sorted sandstone with extensive calcite cementation and grain replacement. Rare detrital quartz overgrowths are abraded and do not interlock. Ben Nevis I-45, TS 14, 4325-4330 m.

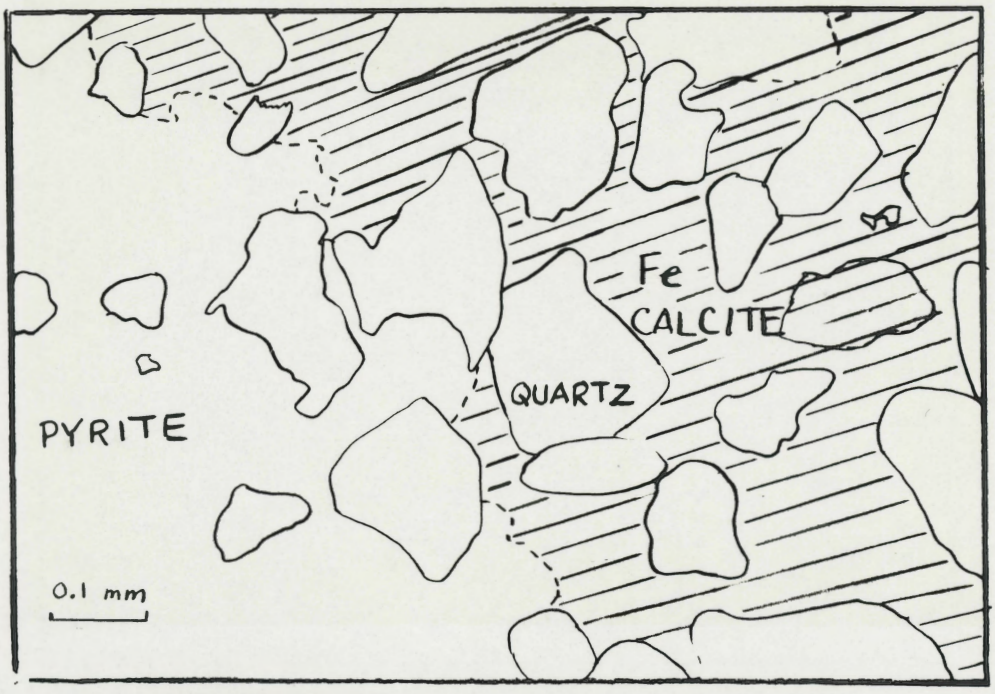

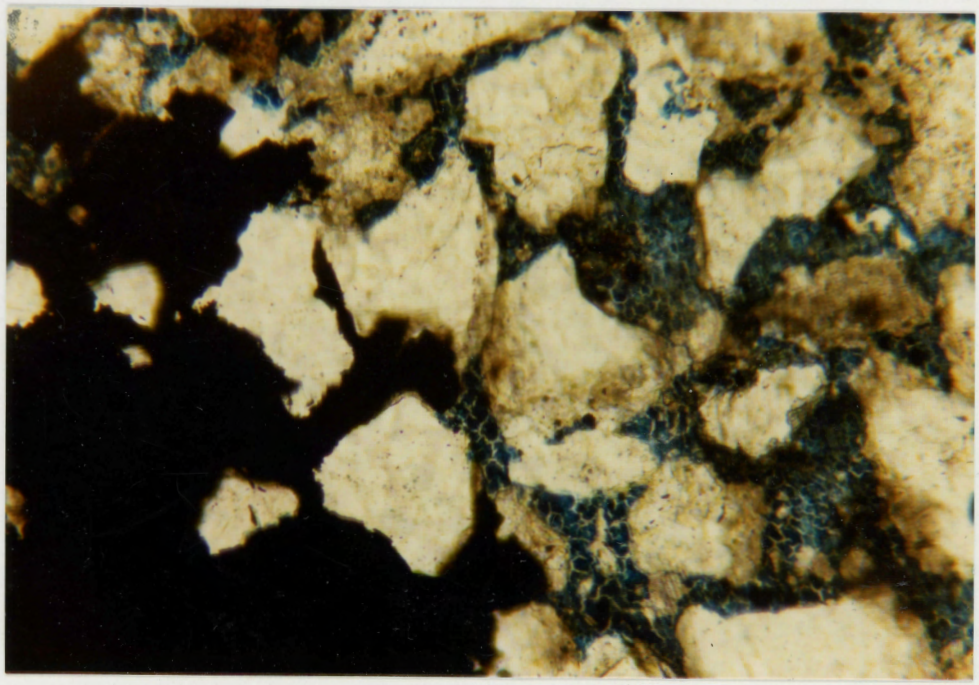

Plate 18: Pyrite and ferroan calcite cement in very fine to fine-grained sandstone, Ben Nevis I-45, TS 10, 4180-4185 m, PPL. Note the low degree of mechanical compaction.

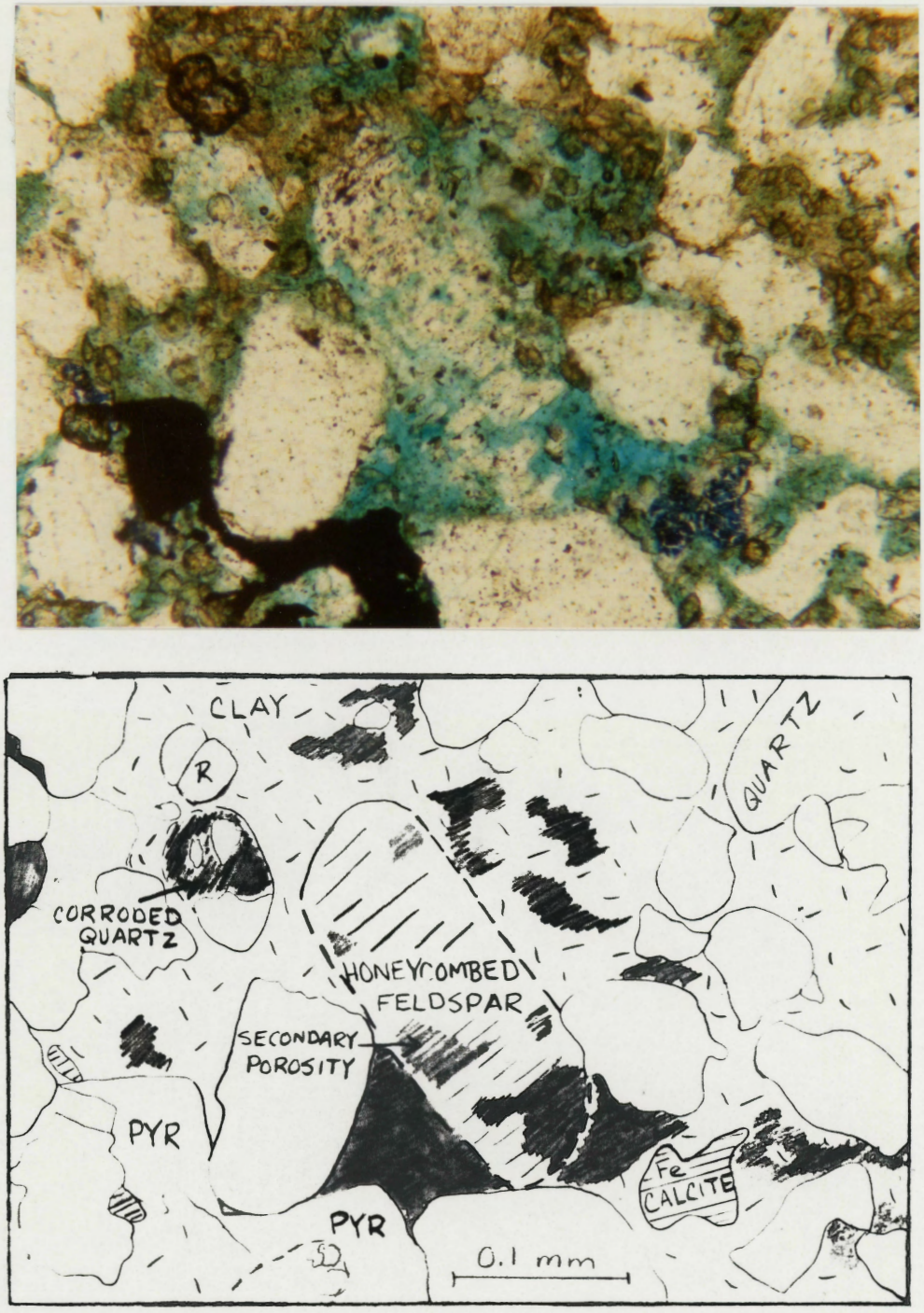

Plate 19: Honeycombed feldspar, corroded quartz grains, and patches of pyrite and ferroan calcite cement, fine-grained sandstone, Hibernia K-14, TS 8, 3874.8 m, PPL. Authigenic clay may have recrystallized from detrital clay, causing authigenic rutile (R) growth.

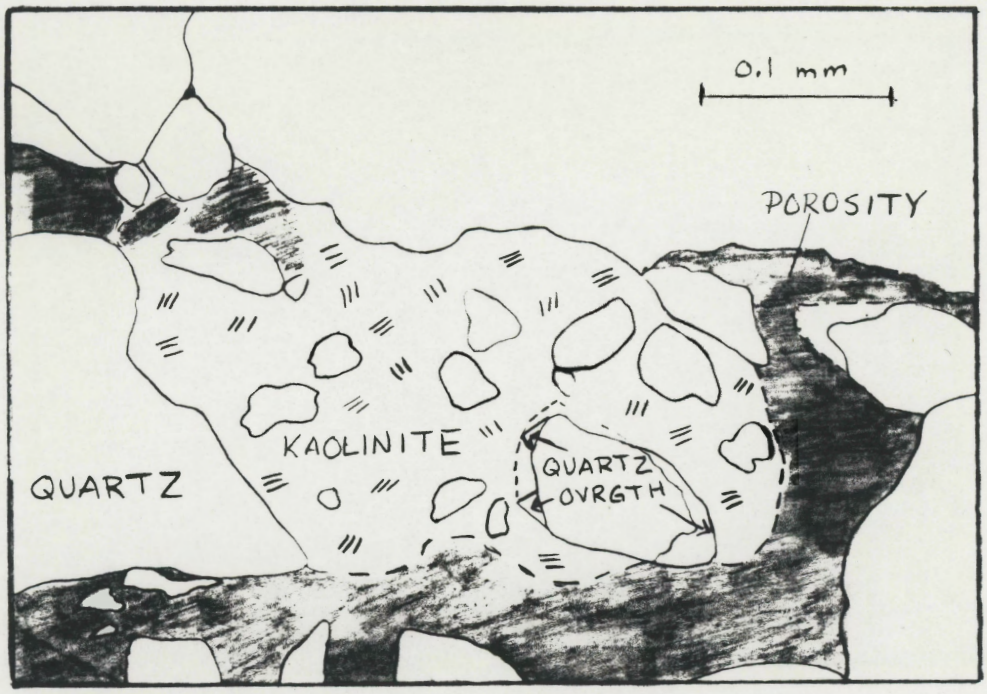

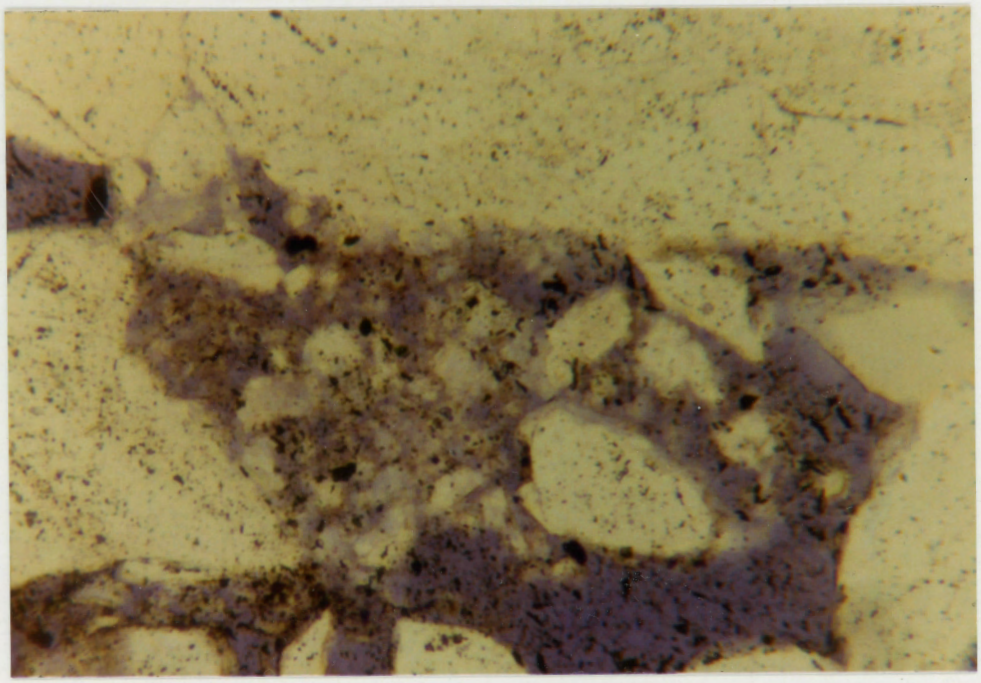

Plate 20: Honeycombed sedimentary rock fragment (siltstone) with detrital quartz overgrowths and authigenic kaolinite. Hibernia K-18, TS 5, 3810.25 m, PPL.

in Plate 21. The surrounding quartz grains are very corroded and associated with secondary porosity.

Plate 22 shows ferroan calcite cement replacing a siltstone clast. The adjacent pore is very irregular in shape and was probably formed by the dissolution of ferroan calcite. The quartz overgrowth (upper right) is slightly corroded and surrounded by ferroan calcite. This suggests that the silica cementation preceded the calcite cementation.

Ferroan calcite cement is associated with authigenic kaolinite in Plate 23. The grain mold and elongate pores are good evidence for secondary porosity. The porosity was most likely created by the dissolution of ferroan calcite.

Plate 24 shows a grain replaced by ferroan calcite, pyrite, and kaolinite. Vermicular growths of authigenic kaolinite partially fill a secondary pore. The difference in crystal form may be a result of grain replacement versus unrestricted growth in a secondary pore. Note the honeycombed grain (upper right).

Plate 25 shows a diagenetic front between ferroan calcite cement with minor clay, and clay cement. The clay is probably authigenic kaolinite which formed small crystals in this very fine-grained sandstone. Kaolinite commonly occurs as a replacement of ferroan calcite.

Plate 26 shows good evidence for secondary porosity: grain molds, honeycombed sedimentary rock fragments, corroded quartz grains, and elongate pores. Authigenic kaolinite partially fills the secondary porosity.

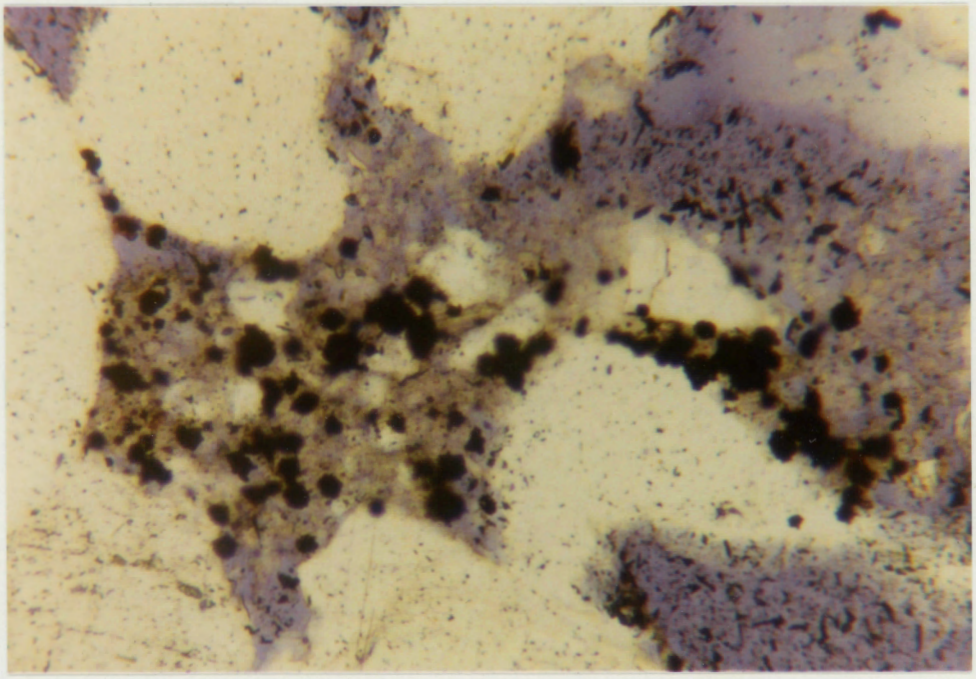

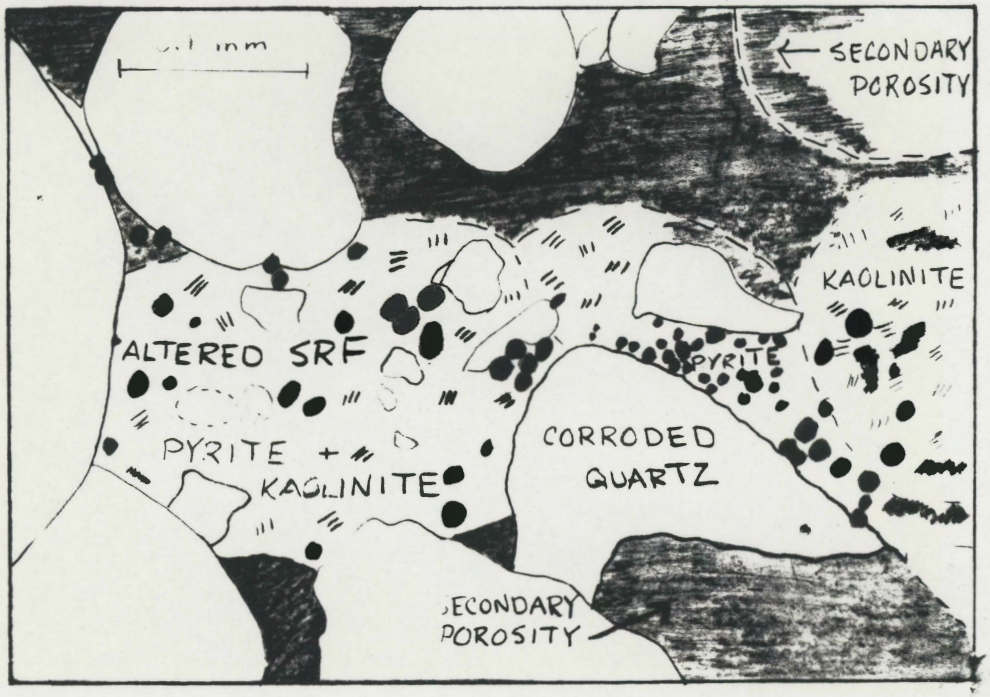

Plate 21: Sedimentary rock fragments (siltstone) partially replaced by authigenic kaolinite and pyrite. Also note the secondary porosity assoicated with corroded quartz grains. Hibernia K-18, TS 5, 3810.25 m, PPL.

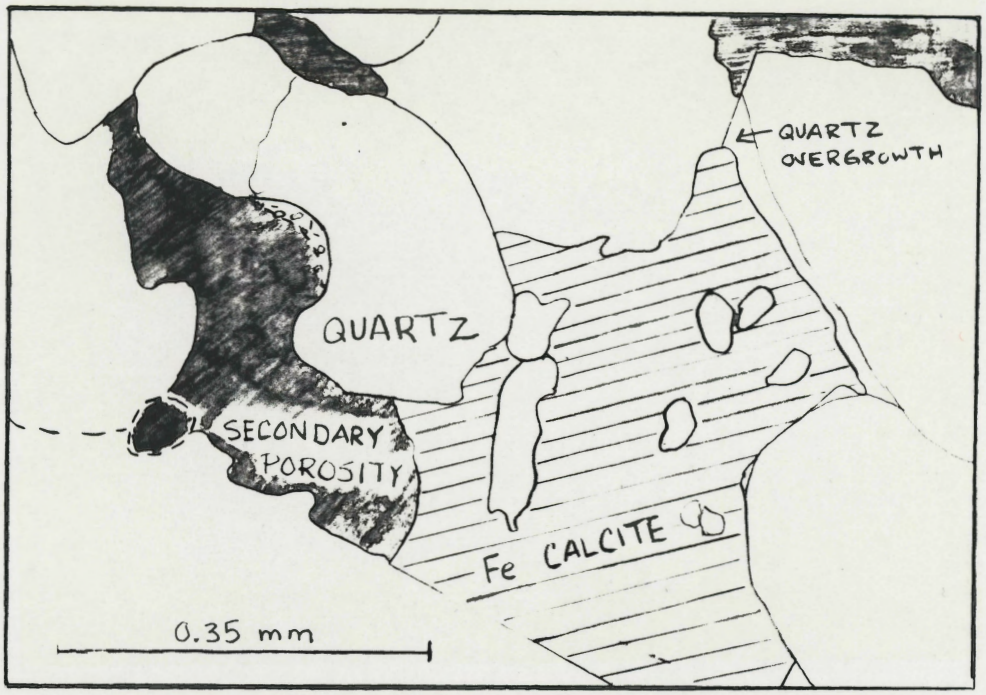

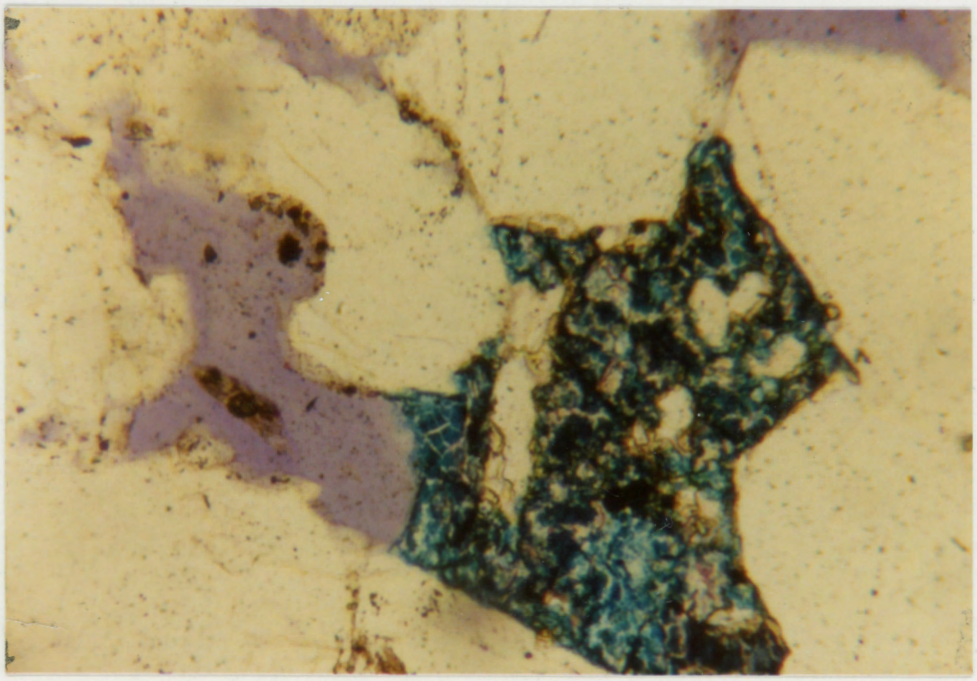

Plate 22: Ferroan calcite replacing a siltstone clast. The adjacent pore is very irregular in shape and was probably formed by dissolution of ferroan calcite. Hibernia K-18, TS 3, 3807.3 m, PPL.

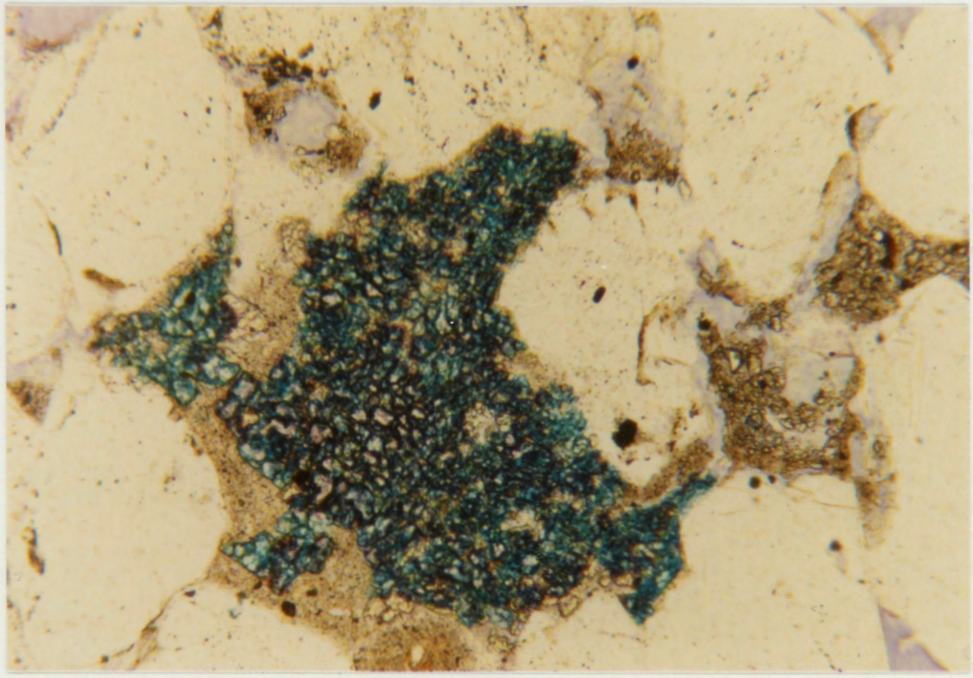

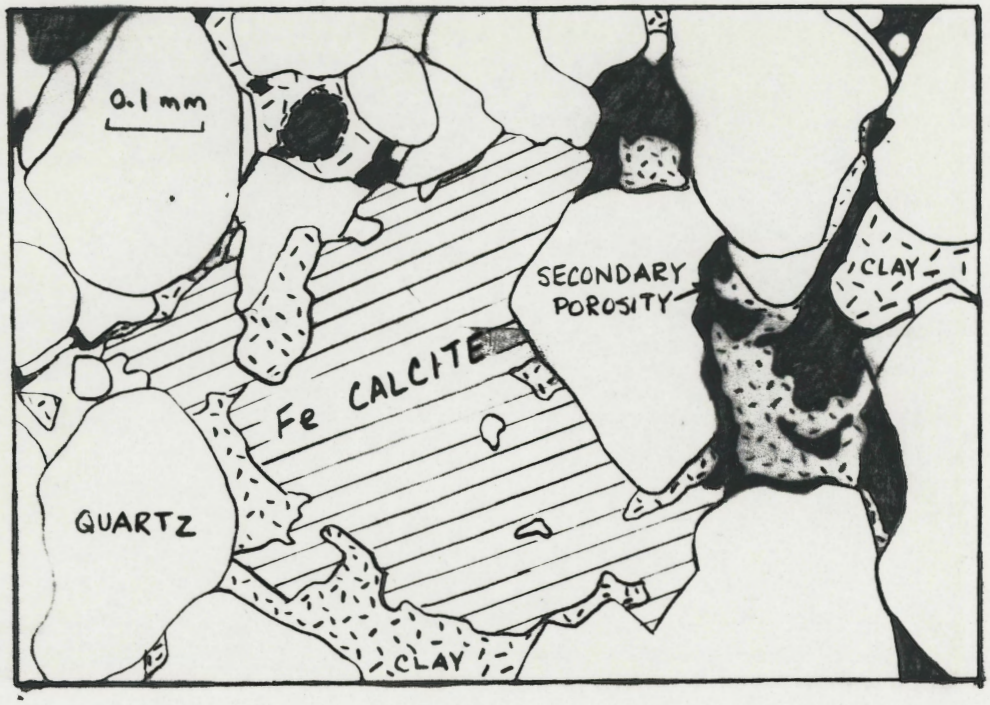

Plate 23: Ferroan calcite cement and authigenic kaolinite in fine-grained sandstone, Hibernia K-18, TS 15, 3826.6 m, PPL. The grain mold (upper centre) and elongate pores (right) are good evidence for secondary porosity.

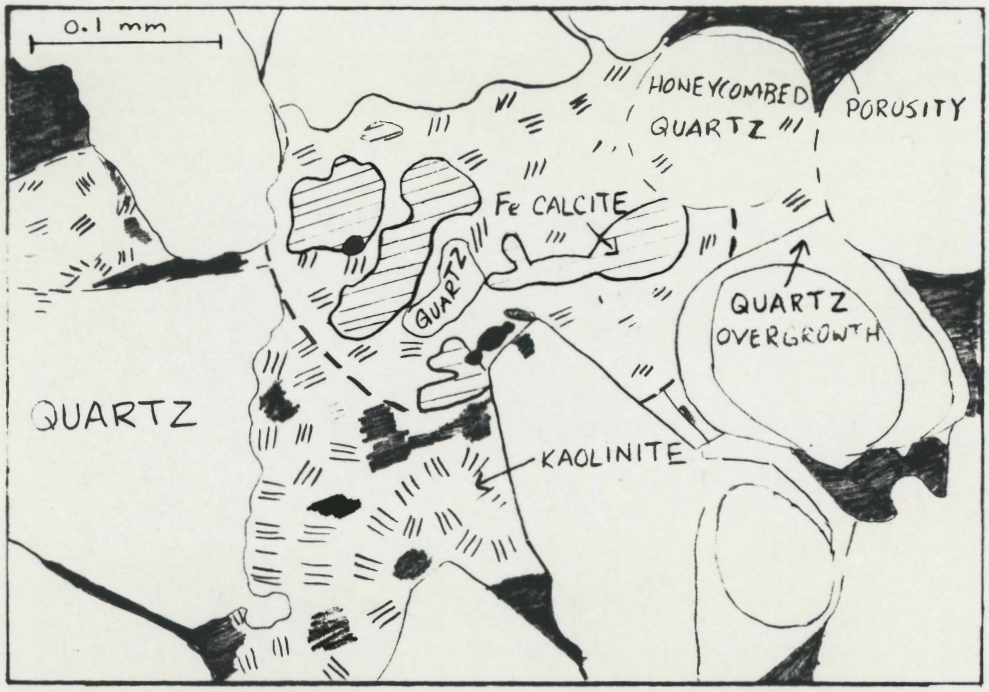

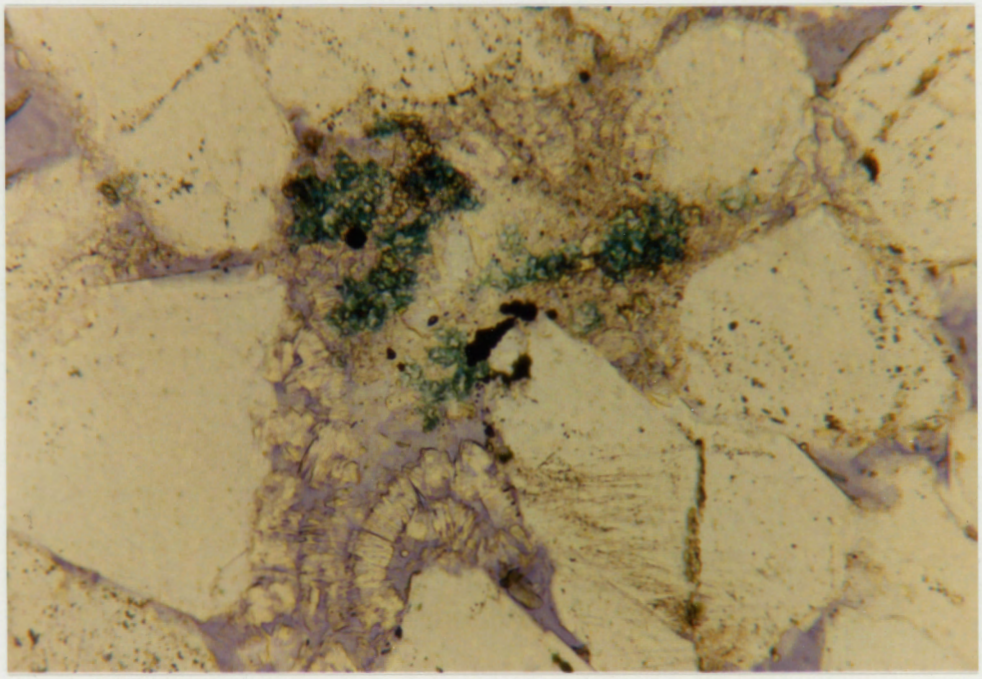

Plate 24: Remnant quartz grain, ferroan calcite, pyrite, and kaolinite mark the position of a former clast (upper center); vermicular growths of authigenic kaolinite partially fill secondary pore (lower center). Fine-grained sandstone, Hibernia K-18, TS 15, 3826.6 m, PPL.

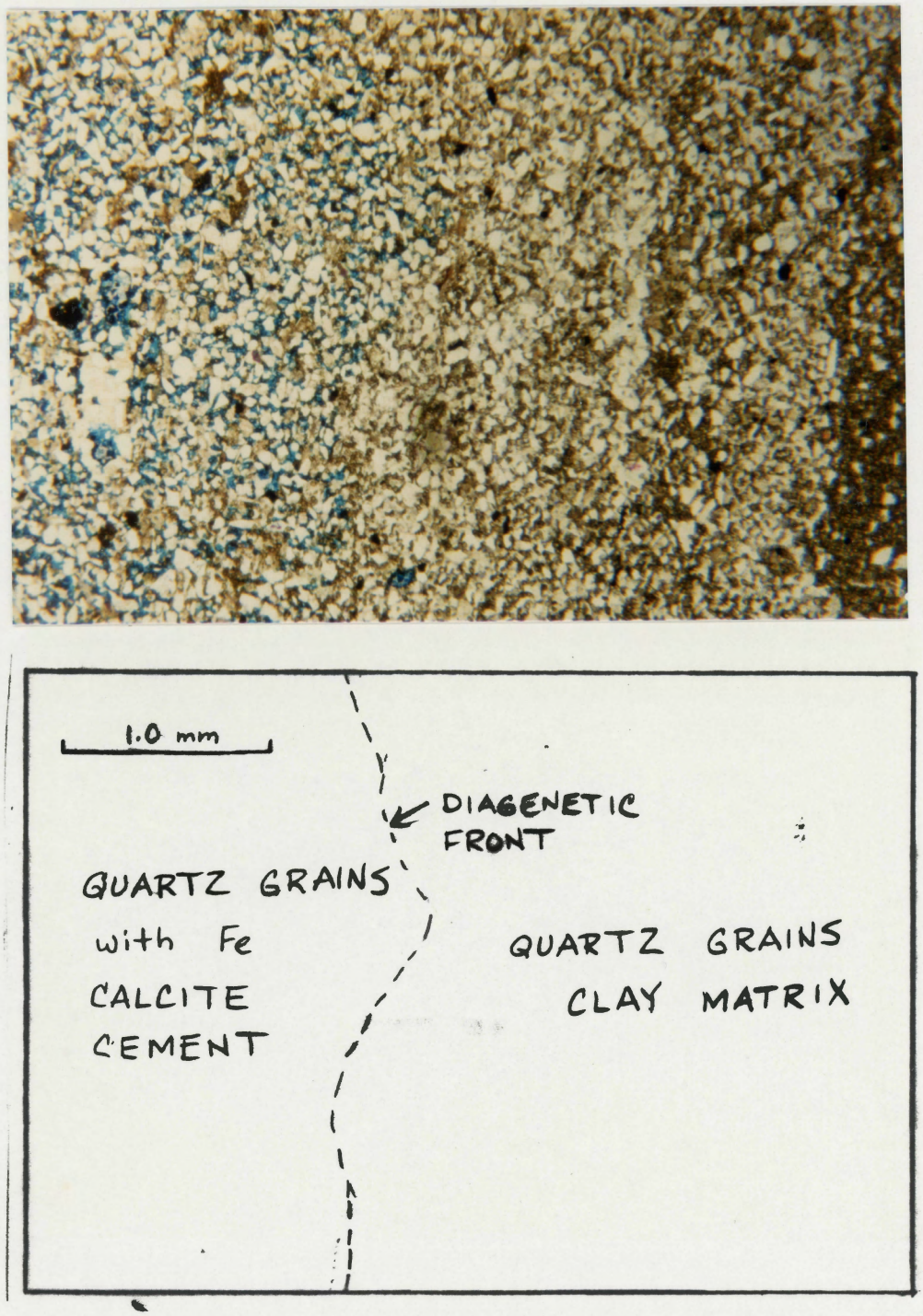

Plate 25: Diagenetic front in very fine-grained sandstone, Hibernia B-08, TS 11, 3489.96 m. PPL.

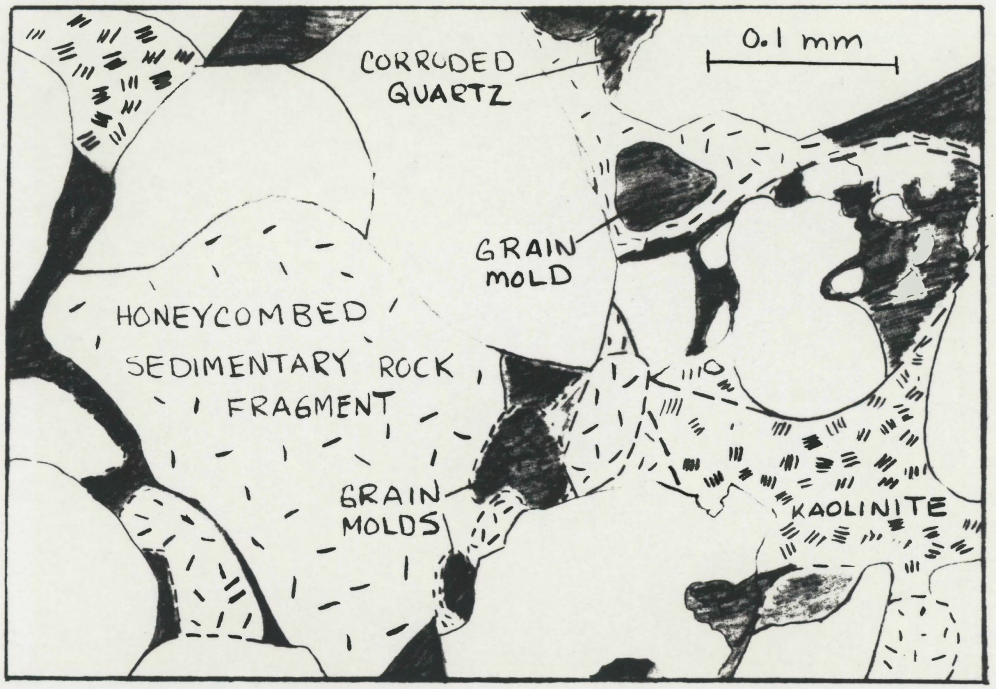

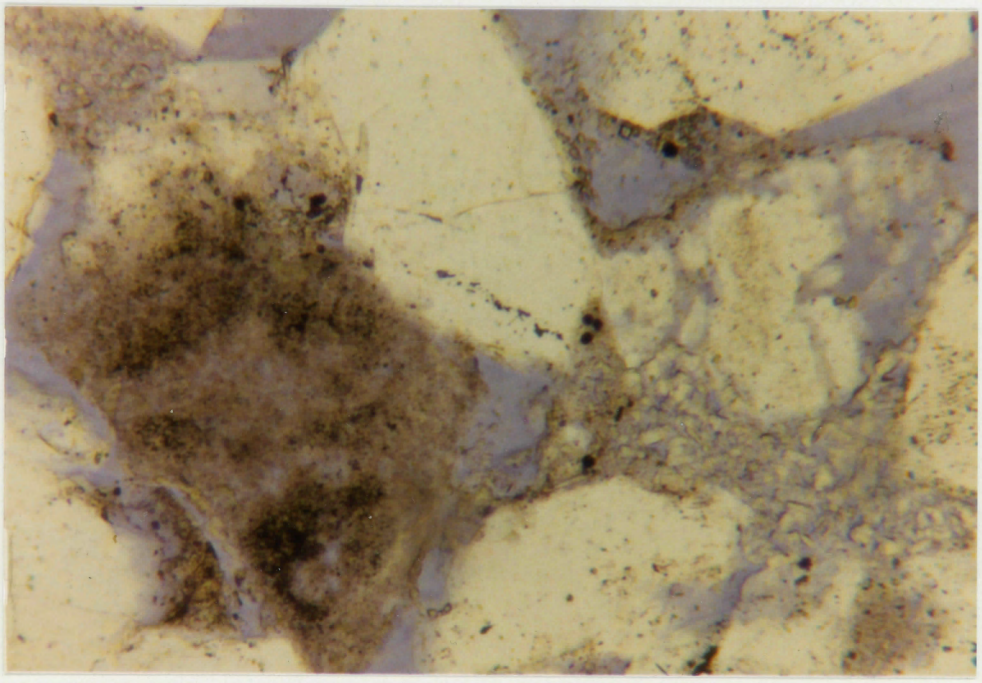

Plate 26: Grain molds outlined by detrital clay, honeycombed sedimentary rock fragments, corroded quartz grains, and elongate pores are evidence of secondary porosity. Authigenic kaolinite partially fills secondary porosity. Hibernia K-18, TS 15, 3826.6 m. PPL.

Ghost grains and corroded quartz overgrowths provide additional evidence for secondary porosity in plate 27. The abundant quartz overgrowths are outlined by very fine rims of impurities and can also be distinguished by their euhedral shape.

Plates 28 and 29 show the rare laumontite cement found in one thin section of the Hibernia K-14 well. The thin section otherwise exhibits excellent porosity. This zeolite mineral is believed to have precipitated from fluid moving through a nearby fault (at 3892 m).

Diagenetic Interpretation

Porosity profiles of the wells show that the Hibernia sandstones are mostly very porous in the Hibernia, Egret, and Hebron wells. However, the Hibernia member is overpressured in the Ben Nevis well and is heavily cemented with calcite, ferroan calcite, and kaolinite.

There is a general trend of decreasing porosity with depth (Enclosure 10), which could be explained by a gradual reduction in primary porosity with burial. However, within individual wells there are dramatic differences in porosity caused by the presence or absence of calcite cement; there is no gradual increase in the amount of calcite cement with depth.

According to Schmidt and McDonald's (1980) criteria, there is no doubt that the majority of the porosity in the

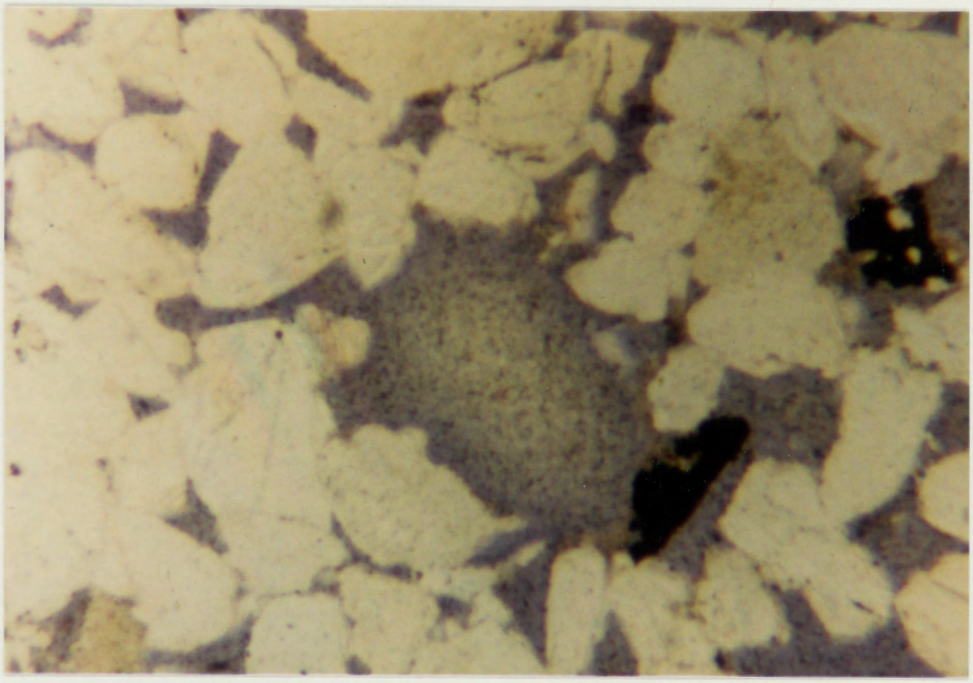

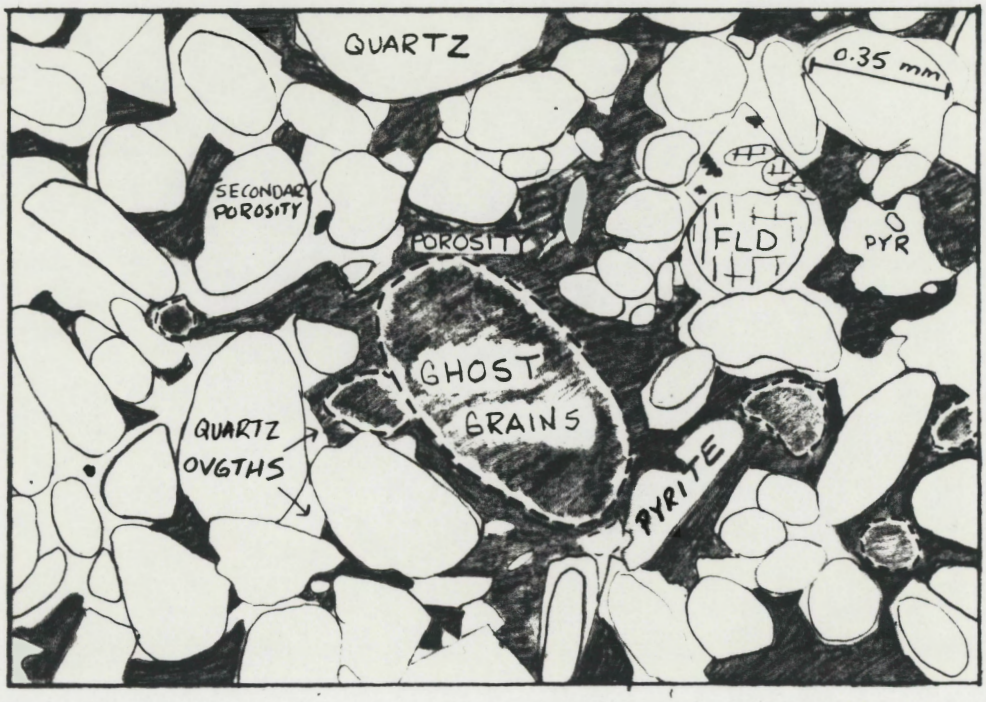

Plate 27: Extensive silica cement in poorly sorted sandstone, Hibernia K-18, TS 12, 3816.2 m, PPL. Ghost grains and corroded quartz overgrowths are evidence of secondary porosity.

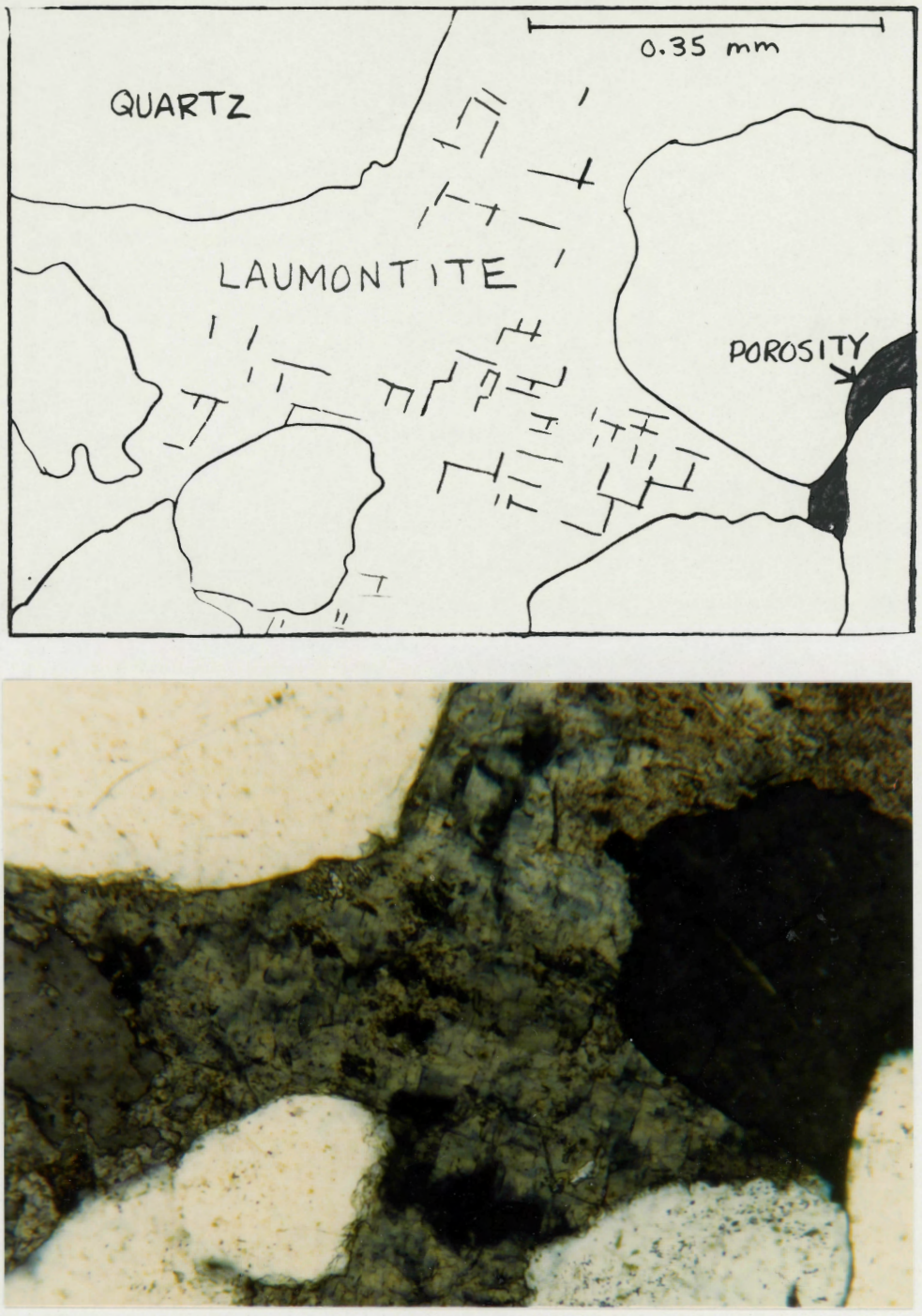

Plate 28: Laumontite cement in medium-grained sandstone, Hibernia K-14, TS 28, 3923.8 m, XN. Note the two cleavages at 90° and the very low birefringence characteristic of this zeolite mineral.

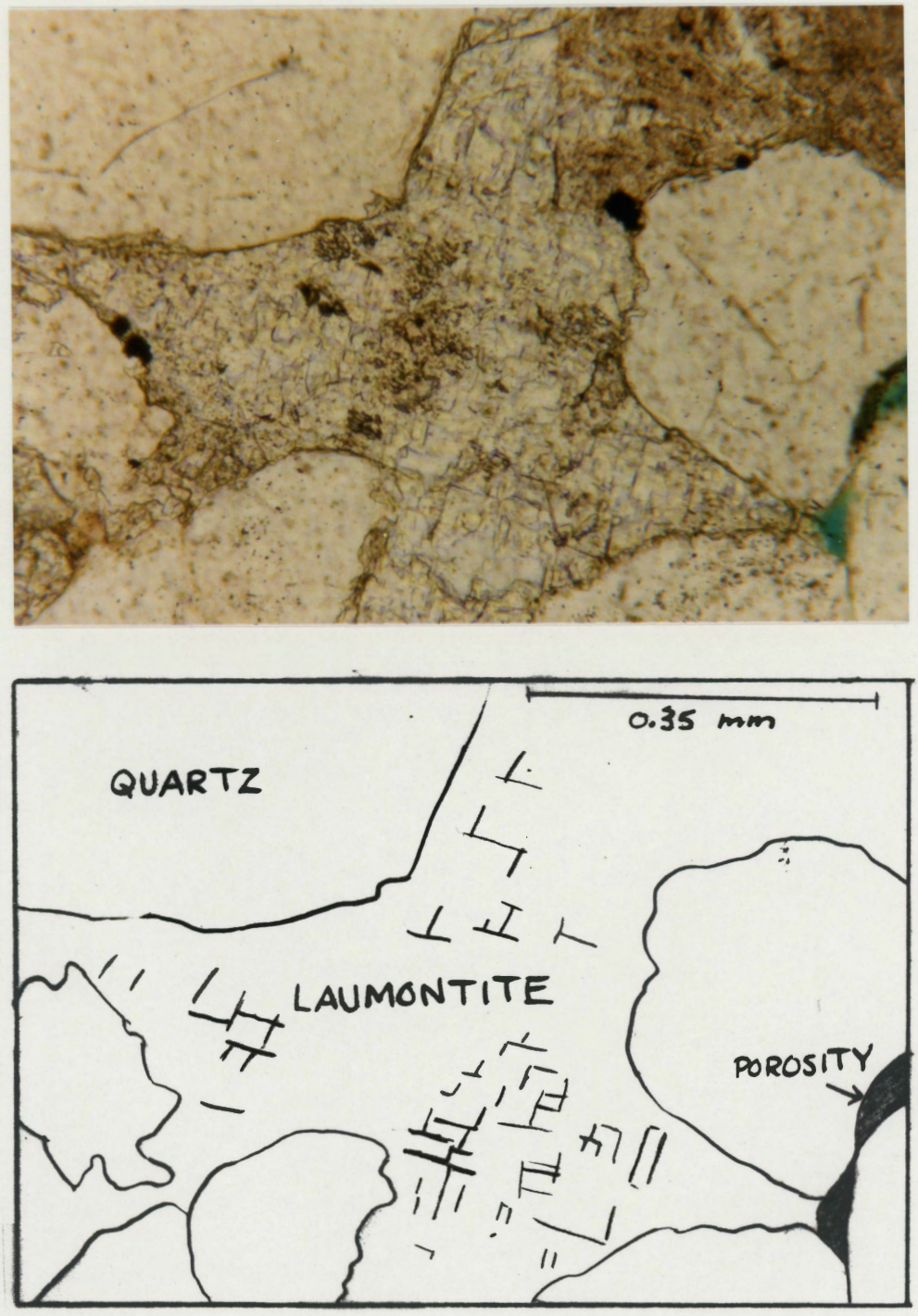

Plate 29: Laumontite cement in medium-grained sandstone, Hibernia K-14, TS 28, 3923.8 m, PPL. Note the characteristic colourless to dirty brown colour, relief slightly lower than quartz, and two cleavages at 90°.

Hibernia sandstone is secondary in origin. The petrographic evidence includes the presence of: grain molds, ghost grains, honeycombed grains, corroded grains, floating grains, irregularly-shaped pores, elongate pores, oversized pores, and irregularly distributed porosity.

Within the wells which developed extensive secondary porosity, the lithofacies exerted some control on the amount of porosity. The very fine sandstones and siltstones were shown to have less than 13% porosity, whereas the coarser channel sandstones have 14-22% porosity. The grain size probably determined the amount of residual primary porosity and permeability which would have allowed perculation of porosity-producing fluids. Similarly, sorting and sandstone thickness are important depositional controls of porosity. Within the very porous channel sandstones, tight streaks, with extensive calcite cement, are located near the top, in the finest-grained sandstones.

The textural evidence does not suggest a unique sequence of diagenetic events. However, a generalized paragenetic sequence is proposed:

Early Diagenesis

The floodplain sediments were deposited in a reducing environment, as indicated by the formation of siderite and the preservation of coal. Rapid early burial (70-90 m/Ma) enhanced the preservation potential of the organic carbon and caused pronounced anaerobic early diagenesis.

Early diagenesis of organic-rich sediment can be described in terms of bacterial reduction zones (Gautier et al., 1985). In the absence of oxygen, aerobic respiration ceases, and the less energetically favorable, nitrate and sulfate reduction occur. Nitrate reduction is not associated with mineral precipitation; however pyrite framboids are the principal products of sulfate reduction. There may have been a limited supply of sulfate in the brackish to fresh Hibernia pore water and so the final stage of early diagenesis, methanogenesis, probably was reached quickly.

In the absence of oxygen, nitrogen, and sulphate, methanogenic micro-organisms produce biogenic methane from organic material (Gautier et al., 1985). Therefore, any iron will be incorporated into carbonate to form siderite or ferroan calcite. Nodular siderite cement is very common in the fine-grained floodplain deposits. At least 45% original porosity was present in these sediments prior to dewatering. The volume percent carbonate within a concretion formed during early diagenesis closely approximates the porosity of the sediment during the time the concretion grew (Gautier and Claypool, 1984).

Middle-Stage Diagenesis

Textural evidence suggests that a major phase of silica cementation preceded a major phase of ferroan calcite precipitation. Abundant authigenic quartz overgrowths are

very commonly corroded and replaced by ferroan calcite cement.

The sources of silica may be a combination of the following: (1) dissolution of quartz grains at contact points by pressure solution, (2) silica dissolution in circulating pore fluids by flow over quartz grains in sandstones, (3) silica liberated by the transformation of clay minerals, and (4) liberation of silica during other mineral reactions (such as feldspar dissolution with kaolinite formation, or replacement of montmorillonite by kaolinite or illite) (Leder and Park, 1986). Fine-grained Hibernia sediments have undergone only minor pressure solution and so (1) is not important as a source of silica. The other three sources may have contributed silica to the Hibernia sandstones.

Calculations have shown that clay transformations could be volumetrically the most significant potential source of silica (Leder and Park, 1986). Mass balance calculations, based on the fluid volume generated by compaction of shales and clay reactions, indicate that a large volume of fluid must be recycled within the system or supplied by recharge from outside the system, such as through faults (Leder and Park, 1986).

A large volume of fluid may have passed through the Hibernia member from the underlying very thick section of shales. A major phase of silica cementation may be

associated with the early compaction and dewatering of these shales. Although compaction was never completed in this presently overpressured section, initial fluid release would have been volumetrically the most significant (Galloway, 1984). The remaining fluid, subjected to yet higher temperatures, may have been sufficient to maintain the overpressures.

Quartz overgrowths generally form in abundance at temperatures of 80°C or more (Franks and Forrester, 1984). The smectite to illite transformation occurs between 60°C and 100°C (Bjorlykke, 1984) and may have provided an important source of silica. The Verrill Canyon and Mic Mac shales may have always had a steeper geothermal gradient than the Hibernia member (page 72). The cooling of a hot, silica-saturated solution from the shales, could lead to precipitation in the overlying Hibernia member. There may have also been a lowering of pore pressure associated with the release of fluids from the overpressured shale section, causing silica precipitation. The lowering of the pH of a saturated solution may not be a relevant process for silica precipitation (Leder and Park, 1986).

Plate 14 shows abundant quartz overgrowths associated with probable recrystallized clay in a fine-grained sandstone. The clay surrounds the secondary porosity and may have recrystallized before the dissolution event. Plate 19 also shows probable recrystallized clay surrounding

secondary porosity. However some of the clay partially infills the pores, suggesting that clay recrystallization continued after secondary porosity development.

A major phase of ferroan calcite precipitation clearly post-dates silica cementation (e.g. Plate 22). Clay transformations may have released the iron and may have reduced the aluminum concentration in the shale water so that plagioclase could also be replaced by calcite (Seibert et al., 1984). The temperature increase due to burial may have resulted in precipitation of calcite cement (Franks and Forester, 1984).

Late-Stage Diagenesis

The maturation of organic matter (to R_o=0.5) is probably responsible for several later-stage mineral reactions. Maturation reactions result in the evolution of significant amounts of carbon dioxide and carboxylic acid. Both of these can create secondary porosity by the dissolution of calcite. The activity of both is greatest prior to hydrocarbon generation, at approximately 100°C (Crossey et al., 1984; Franks and Forrester, 1984; Surdam et al., 1984). The porosity formed by the maturation process may be retained during further burial if lower rates of cementation result from reduced pore-water flow and/or displacement of pore water by hydrocarbons (Franks and Forrester, 1984).

Kaolinite is almost always associated with the secondary porosity (Plates 20, 21, 23, 24, 26). It may form

from the excess aluminum in solution as a result of plagioclase dissolution. Kaolinite cement was exceptionally abundant in the overpressured sandstones of the Ben Nevis I-45 well. Under overpressured conditions the stability of the kaolinite field expands (Kaiser, 1984).

The lower porosity in the Hibernia sandstones in the Ben Nevis well can be related to the maturation history of the underlying source rock. According to the burial-thermal history curves, the shales had a temperature of 100°C at 60 Ma. This was a time of peak carbon dioxide and carboxylic acid generation. However, by 38 Ma, a temperature of 125°C was reached and there was a significant decline in the amount of carbon dioxide generated and the thermal degradation of short-chained carboxylic acids was imminent. This would have allowed a late stage of ferroan calcite cementation in the undercompacted, overpressured Hibernia sandstones (Plates 17 and 18). Temperature generally dominates the effect of fluid pressure on calcite stability (Franks and Forester, 1984).

The lower geothermal gradient at the Hibernia wells allowed much more time for porosity-producing organic reactions. The organic-rich shales are still at peak carbon dioxide/carboxylic acid generating capacity. Even the water-bearing sandstones near the base of the Hibernia K-14 log (Enclosure 11) are porous.

The Hibernia member overlies an overpressured zone in all wells with extensive secondary porosity. The geopressured/hydropressured interface is probably a zone of mixing of diagenetic pore fluids and a site of extensive secondary porosity development. Faults would also be active sites for diagenetic reactions. The best secondary porosity in the Hibernia K-14 well is in a channel sandstone at 3900 m to 3982 m, very near the interpreted fault at 3892 m. Traces of laumontite were found only in this sandstone unit. Laumontite is one of the few zeolites which is not restricted to sedimentary rocks (Scholle, 1979). Most of it may have been dissolved with the calcite. Waters rich in carbon dioxide or carboxylic acid can cause replacement of laumontite by kaolinite and quartz (Crossey, et al., 1984).

CONCLUSION

Plate tectonic theory has provided a useful model with which to describe the structure, stratigraphy, and thermal-burial histories of sediments in the Jeanne d'Arc Basin. This model can also be used to predict diagenesis as a result of structurally-controlled paths of fluid migration, temperature/pressure regimes, and the petrography of the original sediment. Therefore, the sedimentology and diagenesis of the Hibernia member was studied in the context of basin analysis.

Unique geological conditions in the Jeanne d'Arc Basin are responsible for the giant Hibernia oil field. Two rifting episodes produced an exceptionally deep depocenter with up to 14 km of sediment.

The Hibernia member was deposited during an overall regression caused by an input of large volumes of sediment from the surrounding craton. Deposition was in channels and floodplains of a non-marine to brackish water environment. A contemporaneous eustatic sea level rise coupled with high sedimentation rates and subsidence caused rapid vertical aggradation, as in anastomosed fluvial systems. Eventually, the sediment supply could not keep pace with the rising sea level and the Hibernia member was capped by shales.

The Hibernia member overlies a thick section of overpressured shales which provided a source rock for

hydrocarbons and large quantities of fluid available for diagenetic reactions. Burial and thermal history curves show that the source rock reached maturity first at the Ben Nevis well and hydrocarbon migration may have begun before the structural traps were formed during the Albian. Geothermal gradients were much lower near the basin margin, at the Hibernia field, where the source rocks are still generating hydrocarbons. Therefore, there was no leakage of hydrocarbons at the pre-Aptian and Avalon unconformities in this area.

The higher geothermal gradient at the Ben Nevis well was also responsible for the destruction of secondary porosity. The thermal degradation of carboxylic acids and the reduced activity of carbon dioxide at temperatures above 100°C, allowed a late stage of ferroan carbonate cement. Organic maturation in shales below the Hibernia field is still causing the generation of porosity-producing organic acids.

By studying the burial and thermal history of the basin, it is possible to relate diagenetic reactions to an absolute time and temperature scale. This is considered to be one step better than simply noting the relative paragenetic sequence of diagenetic events. However, data on the carbon and oxygen isotopes would help to ascertain the temperature of formation of the mineral phases and is a recommendation for future work. Also, the petrography of

the other reservoirs should be studied to compare the effects of mineralogy and greater distance from the overpressured zone.

The most prospective area for hydrocarbon exploration is probably along faults in the shallower portions of the basin. These areas would have thick oil windows caused by a relatively low geothermal gradient. The source rock would have only recently reached maturity and migration would have occurred after structural deformation. Furthermore, the geochemistry would still favour the production of secondary porosity by carboxylic acids and carbon dioxide. The faults would provide conduits for fluid migration as well as potential traps.

APPENDIX

The following tables document the quantitative data from 68 thin sections of the Hibernia K-14 well (displayed on Enclosure 11), 21 thin sections from the Hibernia K-18 well, and 32 thin sections from the Hibernia B-08 well. Approximately 200 points per slide were counted for one in ten thin sections, providing a check on the visual estimates. Porosity estimates were also compared to core plug measurements by Core Laboratories.

The grain size is reported as a range which includes approximately 80% of the clasts. Grain size was determined by visual comparison with a grain size chart under the microscope. Since the thin sections do not necessarily bisect the centre of individual grains, the apparent grain sizes were divided by 0.7 to obtain the reported values.

Thin Section Data: Hibernia K-14

TS	DEPTH	GRAIN SIZE	PHI	QTZ OVGTH	Fe CALC	AUTH KAOL	AUTH CLAY	DTL CLAY	PYR	Corg/ BIT
1	3861.5	3.7-2.0	8	5	tr		3	10	tr	1
2	3862.1	3.5-2.5	15	10	tr		1	2	tr	1
3	3862.5	Shale	0	0	tr			73		5
4	3863.4	3.5-2.5	2	8	15		1	1	tr	tr
5	3865.0	4.0-2.5	9	9	tr	tr		5	1	1
6	3872.2	3.0-1.5	16	12	tr	2			tr	tr
7	3874.1	4.0-1.5	5	7	17		tr		tr	1
8	3874.8	3.5-2.5	11	9	3		8		tr	tr
9	3881.2	4.5-2.5	6	10				1	1	
10	3884.6	3.5-2.0	7	10			2	4	tr	2
11	3885.3	4.0-1.5	7	10			2	2	1	tr
12	3886.4	4.5-3.5	5	3			1	8	1	
13	3898.5	2.0-1.5	18	12	tr	1	1		tr	
14	3900.9	2.0-1.0	18	11	tr	tr	tr		tr	tr
15	3901.8	2.0-1.0	18	12		1	1			
16	3902.5	2.0-1.0	16	12		1	1		tr	
17	3903.8	2.0-1.0	15	11		3	tr	3	2	tr
18	3904.7	2.0-1.0	17	12		1	tr	1	1	
19	3905.4	2.5-1.5	20	12	tr	1	tr		tr	
20	3906.0	2.0-1.0	20	13		1	tr	tr	1	tr

TS	DEPTH	GRAIN SIZE	PHI	QTZ OVGTH	Fe CAL	AUTH KAOL	AUTH CLAY	DTL CLAY	PYR	Corg/ BIT
21	3906.8	2.5-1.5	21	12		tr	tr		1	tr
22	3909.7	4.5-2.5	9	12			tr	3	2	tr
23	3911.4	4.5-3.5	9	9			1	2	2	1
24	3919.4	2.0-0.0	19	12		3				
25	3920.3	2.0-0.5	21	12		1				
26	3921.1	2.0-0.0	22	12		1				
27	3922.3	2.0-0.0	20	12		1	tr			
28	3923.8	2.0-0.0	22	12		1			tr	
29	3924.5	1.5-0.0	22	12		1			tr	
30	3925.3	2.0-0.5	19	12		1			tr	
31	3925.6	2.0-0.5	20	12		1	tr		tr	tr
32	3929.5	contaminated with drilling mud								
33	3930.4	3.5-1.5	17	9	tr	2	1	1	tr	
34	3931.5	2.0-1.0	17	12	tr	1	tr	4	tr	tr
35	3932.4	2.0-1.0	18	7	tr		tr	3	tr	
36	3932.6	3.0-1.5	3	8	20		tr		tr	
37	3933.0	2.5-1.5	21	12	tr	1	tr	tr	tr	
38	3934.6	2.5-1.5	18	12	tr	2	1		tr	
39	3935.1	2.5-1.5	19	12	tr	tr		tr	tr	tr
40	3938.1	2.5-1.0	21	12	tr	1	tr		tr	tr
41	3938.8	2.5-1.0	20	12	tr		tr		tr	
42	3939.4	2.5-1.0	19	13	tr	tr			tr	
43	3940.1	2.5-1.5	19	12	tr	1			tr	
44	3940.2	2.5-1.5	19	12	tr	1	1		tr	
45	3940.3	3.0-1.0	19	13	tr	1	1	2	tr	tr
46	3941.0	2.5-1.0	18	12	tr	2				
47	3942.3	2.0-1.0	21	12	tr	1	1		tr	
48	3943.0	2.5-1.0	19	12		1		1	tr	
49	3944.6	2.5-0.5	18	12		2			tr	
50	3959.1	3.0-1.5	6	12	7	2		tr	2	3
51	3961.6	3.5-2.0	16	12	tr	tr	tr	0.5	tr	0.5
52	3962.2	2.0--1.0	7	3	tr	1			tr	1
53	3963.6	3.5-2.0	?5	10				2		4
54	3964.6	3.0--1.0	?6	4		3	2			
55	3965.1	3.2-1.5	16	12	tr	2			tr	2
56	3965.7	5.0-3.5	?3	2					1	
57	3965.8	3.0-1.5	15	10	tr	1	1	0.5	tr	2.5
58	3966.3	4.0-1.5	13	10	tr	2	tr		1	3
59	3967.1	3.0-1.5	18	10	tr	tr			tr	2
60	3967.3	4.5-2.5	10	6	tr	tr		3	1	4
61	3968.8	4.0-2.5	12	8	tr				1	2
62	3969.0	3.5-1.0	7	13		2		1	1	3
63	3969.6	2.0-0.0	16	12	tr	1			tr	1
64	3970.4	2.0-0.0	20	12		tr			tr	2
65	3970.9	5.0-3.5	?0	3				12	tr	7
66	3971.1	2.0-1.0	22	9					tr	
67	3971.6	2.0-0.5	18	10	tr	1			tr	2
68	3971.7	2.0--0.5	16	12					tr	2

Thin Section Data: Hibernia K-14, con'd

TS	SID NOD	MONO QTZ	POLY QTZ	CHT	SH	SS	PLAG	K-SPAR	MUSC	HVY MNLS
*1		64	3	2	1		2	tr		tr Z,T
2		62	4	2	tr		3	tr	tr	tr Z,R
*3		19	2	tr		1	tr	tr		
4		66	3	2		1	1	tr	tr	tr Z,R,T
5		65	6	3	tr	tr	1	tr	tr	tr Z,R,T
6	tr	63	4	2	tr	1	tr		tr	tr Z,T
7		63	3	2	tr		1	tr	tr	tr Z,R
8		62	4	3	tr		tr			tr T,R
9	3	75	2	1			tr	tr	tr	1% Z,T,R
10	tr	72	2	1	tr		tr		tr	tr Z,T,R
11	tr	71	5	2	tr		tr		tr	tr Z,R
12	3	75	tr				tr		3	1% Z,T,R
13	tr	62	2	2	tr	2	tr	tr		tr T
14		63	3	2	tr	3	tr	tr		
15		62	1	2	tr	3	tr	tr		
16		64	1	2	tr	3	tr	tr		tr Z,T
17	1	60	1	1	tr	3	tr		tr	tr Z,T
18	tr	62	1	2	tr	3	tr		tr	tr Z
19	tr	60	1	3	tr	3	tr		tr	tr Z,T
20	tr	61	2	1	tr	1	tr			
21	tr	60	2	1	tr	3	tr	tr		tr R
22	4	65	1	2	tr	1	tr	tr	0.5	.5 Z,T,R
23	tr	71	2	2			tr	tr	1	tr Z,R,T
24		62	2	2	tr					tr Z
25		61	3	2	tr					tr Z
26		60	3	2		tr				
27		61	4	2						
28		61	3	1						tr R
29		60	3	1		1				
30		61	6	1	tr					
31		61	5	1	tr					
32		contaminated with drilling mud								
33		62	4	2	1	1	tr		tr	tr Z,R,T
34		60	4	2	tr	tr	tr		tr	tr Z
35		62	5	3	1	1	tr	tr		tr Z,T
36		63	3	2		1	tr			tr Z,T
37		60	4	2	tr				tr	tr Z
38		62	2	1	tr	2				tr Z,T
39		63	3	1	tr	2				tr Z,T
40	tr	62	2	1		1	tr			tr T
41	tr	61	4	2	tr	1	tr			
42	tr	62	3	2	tr	1				tr Z,T
43	tr	61	4	2	tr	1		tr		
44	tr	61	4	2	tr	tr		tr		tr T
45	tr	59	3	2			tr		tr	tr R,Z,T
46	tr	61	4	2	1	tr	tr		tr	tr Z,T

TS	SID NOD	MONO QTZ	POLY QTZ	CHT	SH	SS	PLAG	K-SPAR	MUSC	HVY MNLS
47	tr	59	3	2	tr	1	tr			
48	tr	61	3	2	tr	1				
49	tr	61	4	1	tr	2				
50	1	61	4	2	tr		tr			tr Z,T,R
51	tr	66	2	2				tr	tr	1% Z,T,R
52		13	2	1	(67% rock fragments, 5% sid nod)					
53	tr	73	4	2			tr		tr	tr Z,T,R
54		28	1	1	(30% rock fragments, 25% sid nod)					
55		59	5	4	tr			tr	tr	tr R
56		88		2			tr		2	2% Z,T,R
57		64	3	2	tr	1			tr	tr Z,T,R
58	tr	65	4	2	tr				tr	tr Z,R
59		64	2	3		1				tr R
60		69	4	3			tr	tr	tr	tr Z,R
61		72	3	2			tr		tr	tr Z,T,R
62		66	4	2	tr	1	tr		tr	tr Z,R
63		62	5	3						
64		61	4	1			tr	tr		
65	tr	70	1	1			1		3	2%R,trZ,T
66		61	6	2	tr					
67		64	4	1				tr		
68		64	4	1		1				

* Thin sections with 1% calcareous fossils.

TS=Thin Section Number
PHI=Porosity
QTZ OVGTH=Authigenic Quartz Overgrowths
Fe CALC=Ferroan Calcite Cement
AUTH KAOL=Authigenic Kaolinite Cement
AUTH CLAY=Other Authigenic Clay Cement
DTL CLAY=Detrital Clay Matrix
PYR=Pyrite
Corg/BIT=Organic Carbon (Plant Remains) and Bitumen
SID NOD=Siderite Nodules
MONO QTZ=Monocrystalline Quartz
POLY QTZ=Polycrystalline or Metamorphic Quartz
CHT=Chert Clasts
SH=Shale Clasts
SS=Siltstone or Sandstone Clasts
PLAG=Plagioclase Feldspar Clasts
K-SPAR=Potasium Feldspar Clasts
MUSC=Muscovite

Heavy Minerals:
Z=Zircon
T=Tourmaline
R=Rutileneral:
S=Sphene

Note: Thin sections 3, 4, 7, 23, 31, 36, 43, 44, 53, 54, 56, 59, 61, 65, and 67 were made by D. Brown; all others were made by Robertson Research.

Thin Section Data: Hibernia K-18

TS	DEPTH	GRAIN SIZE	PHI	QTZ OVGTH	Fe CALC	AUTH KAOL	AUTH CLAY	DTL CLAY	PYR	Corg/ BIT
1	3797.1	5.5-3.0	2	2				4	2	2
2	3798.8	4.0-3.0	3	6			5		1	tr
3	3807.3	2.5-1.5	17	12	2	1	2		tr	
4	3808.9	2.5-2.0	15	11	3	1		2	tr	
5	3810.2	3.0-1.5	16	12		2			tr	
6	3811.5	3.0-2.0	19	12		1		2	0.5	0.5
7	3812.6	2.5-1.5	19	12		tr		2		tr
8	3813.4	2.5-1.5	17	13		1		1	1	2
9	3814.3	2.0-1.0	16	12		1	2		1	1
10	3814.7	2.5-0.0	12	9		1	2		3	1
11	3815.6	2.5-1.0	19	12				1	tr	2
12	3816.2	2.5-0.5	18	12		tr	1		tr	tr
13	3817.0	1.5-0.5	19	10			1		1	
14	3823.7	3.0-1.5	14	12		1		2	tr	2
15	3826.6	3.0-2.0	16	14	tr	3		1		tr
16	3827.1	3.0-2.0	15	13	tr	2	2			
17	3828.7	3.0-2.0	16	12	tr	1	2			
18	3831.1	2.5-1.5	15	12	tr	1	2	1	tr	
19	3832.8	3.0-1.0	15	12		1	3			
20	3834.2	2.5-1.0	15	12	tr	2	1	1	tr	tr
21	3834.8	2.5-1.0	15	12	1	2	2		tr	

TS	SID NOD	MONO QTZ	POLY QTZ	CHT	SH	SS	PLAG	K-SPAR	MUSC	HVY MNLS
1		80	2	2			tr		4	2% R,Z
2		81	2	2			tr		tr	2% R,T
3	tr	57	3	4	1					1% R,T,Z
4	tr	59	4	2	1					2% R,T,S,Z
5	tr	63	2	3		2				tr Z,T,S
6	tr	60	2	2		1	tr			tr R,T
7	1	59	3	2		2				tr Z,T,S
8	tr	58		3		4				
9	tr	59	2	3	1	2				tr T
10	1	67	2	2						
11	1	60	2	2		1				
12	tr	64	1	2	2					
13		65	3	1						
14	tr	65	2	2						tr T,Z
15	tr	59	2	2	1	2	tr		tr	tr T
16		64	1	2	1					tr Z
17	tr	62	2	3	1	1				
18	tr	65	2	2	1	1				
19	tr	64	2	1	2					tr Z
20	tr	62	2	3	1	1				tr Z
21	tr	62	3	3						

Thin Section Data: Hibernia B-08

TS	DEPTH	GRAIN SIZE	PHI	QTZ OVGTH	Fe CALC	AUTH KAOL	AUTH CLAY	DTL CLAY	PYR	Corg/ BIT
1	3480.2	5.0-3.0						60	tr	tr
2	3481.2	3.5-2.5	8	13		tr		5		
3	3482.4	2.5-1.5	15	12		1	1	1	tr	tr
4	3483.0	1.5-0.0	17	11		1	1		0.5	0.5
5	3483.3	2.0-0.0	19	11	tr	tr	tr	1		tr
6	3483.7	2.0-1.0	16	11	tr	tr		2	1	2
7	3484.3	3.0-2.5	17	10		1	4			
8	3484.8	3.5-3.0	8	tr	tr		20		tr	
9	3485.3	5.0-4.0	1	8	tr			2	1	tr
10	3485.7	3.5-3.0	5	12	1					
11	3490.0	4.5-3.5	tr	4	20			4		
12	3491.9	4.0-3.5	1	4	2			3		
13	3495.2	4.0-3.5	tr	4	7			5	tr	
14	3552.0	2.5-0.5	15	11	tr		1		0.5	0.5
15	3554.5	2.0-0.5	17	9		tr	1		tr	tr
16	3554.9	3.5-0.5	12	12				4	1	
17	3555.2	2.0-1.0	17	10			tr		tr	
18	3555.9	2.5-1.0	17	13		tr	1			
19	3556.3	3.0-1.5	16	12		tr	tr		tr	tr
20	3556.9	2.0-0.5	11	13				4	tr	tr
21	3557.3	2.5-1.5	15	11	tr	tr		tr		
22	3558.8	5.0-1.5	0	2				tr		tr
23	3559.4	4.0-1.0	1	6				2	1	tr
24	3559.7	2.0-1.5	18	12		tr	1		tr	
25	3560.0	2.0-1.5	18	12				1	tr	tr
26	3560.3	2.5-1.5	14	12			1		tr	
27	3606.5	1.5-0.0	18	7		2	1			
28	3617.2	4.0-3.0	tr	10				3	1	tr
29	3620.3	2.5-1.5	19	12	tr	tr	tr		2	
30	3621.7	2.5-0.5	19	12			tr			tr
31	3622.7	2.0-0.0	20	10			1			
32	3623.2	2.0-0.0	19	10		1	tr		tr	

TS	SID	MONO QTZ	POLY QTZ	CHT	SH	SS	PLAG	K-SPAR	MUSC	HVY MNLS	
1		40		tr			tr		tr	tr	Z
2	tr	70		3			1	tr	tr	tr	T,Z
3	tr	63	2	3	1	1					
4	tr	61	2	2	3	1					
5	tr	65	2		1	1					
6	1	61	1	1	2	2					
7	tr	62	3	2			0.5	0.5	tr	tr	R,Z,T
8		72		tr	tr			tr			
9		86							1	1%	R,T,Z

TS	SID NOD	MONO QTZ	POLY QTZ	CHT	SH	SS	PLAG	K-SPAR	MUSC	HVY MNLS
10	tr	78			3		tr		tr	1% Z,R,T
11	10cmt	62					tr		tr	
12		84		3			1		1	1% R,Z
13		83					tr		1	tr T,R,Z
14	tr	65	2	2	2	1	tr			tr Z
15		68	2	2	1		tr			
16		65	2	2	1	1	tr			tr Z,T
17	tr	67	4	1		1				
18	tr	63	3	1	1	1				
19	tr	66	2	2	1	1	tr			tr Z
20	tr	64	4	2	1	1	tr			tr Z,T
21	tr	67	3	3		1				tr Z,T
22		94	1						3	tr Z,R
23		88	1	tr			tr		1	tr Z, R
24	tr	64	3	2			tr			tr Z,R,T
25	tr	62	3	2	tr	2		tr	tr	
26	tr	67	3	3		tr				
27	tr	66	3	2		1				
28		80	1	3			tr		1	1% Z,T,R
29	tr	62	2	1						2% Z,T,R
30	tr	63	2	3		1			tr	tr Z
31		61	4	2	1	1				tr Z
32	tr	67	3							

REFERENCES

Arthur, K.R., Cole, D.R., Henderson, G.G.L., and Kushnir, D.W.(1982) Geology of the Hibernia discovery: in Halbouty, M.T.(editor), The Deliberate Search for the Subtle Trap, American Association of Petroleum Geologists, Memoir 32, pp. 181-195.

Avery, M.P., Bell, J.S., and McAlpine, K.D. (1986) Vitrinite reflectance measurements and their implications for oil and gas exploration in the Jeanne d'Arc Basin, Grand Banks, Eastern Canada: in Current Research, Part A, Geological Survey of Canada Paper 86-1A, pp. 489-498.

Benteau, R.I. and Sheppard, M.G. (1982) Hibernia - a petrophysical and geological review: Journal of Canadian Petroleum Technology, pp 59-72.

Bjorlykke, K. (1984) Formation of secondary porosity: how important is it?: in MacDonald, D.A. and Surdam, R.C. (editors), Clastic Diagenesis, American Association of Petroleum Geologists Memoir 37, pp. 277-286.

Brown, D. (1985) Stratigraphy of the Hibernia Member, Missisauga Formation, of the Hibernia oil field: unpublished M.Sc. thesis, Carleton University, 78 p.

Canadian Oil and Gas Lands Administration (1985) Offshore Schedule of Wells (1966-1984): Energy Mines and Resources Canada.

Cant, D.J. (1982) Fluvial facies models and their application: in Scholle, P.A. and Spearing, D. (editors), Sandstone Depositional Environments, American Association of Petroleum Geologists, pp. 115-137.

Chapman, R.E. (1975) Petroleum geology of regressive sequences: in Structural Types and Associated Oil and Gas Occurrences, National Conference On Earth Science, Banff,Alberta, pp. 3-62.

Chapman, D.S. and Willett, S.D. (1986) Analysis and interpretation of thermal data in sedimentary basins (abstract): Atlantic Geoscience Society Symposium on the Basins of Eastern Canada, programme with abstracts, p. 32.

Coleman, J.M. and Prior, D.B (1980) Deltaic Sand Bodies, American Association of Petroleum Geologists, Continuing Education Course Note Series #15, 171 p.

Crawford, F.D. (1972) Arenaceous Deposits: Sedimentation and Diagenesis: 1972 National Conference on Earth Science, 285 p.

Crossey, L.J., Frost, B.R., and Surdam, R.C. (1984) Secondary porosity in laumontite-bearing sandstones: in MacDonald, D.A. and Surdam, R.C.(editors), Clastic Diagenesis, American Association of Petroleum Geologists Memoir 37, pp. 225-237.

Curray, J.R. (1964) Transgressions and regressions: in Miller, R.L. (editor), Papers in Marine Geology (Sheppard Commemorative Volume), McMillan, New York, pp. 175-203.

Curtis, C.D. and Coleman, M.L. (1986) Controls on the precipitation of early diagenetic calcite, dolomite and siderite concretions in complex depositional sequences: in Gautier, D.L. (editor), Roles of Organic Matter in Sediment Diagenesis, Society of Economic Paleontologists and Mineralogists, Special Publication no. 38, pp. 23-33.

Demaison, G.J. and Moore, G.T. (1980) Anoxic environments and oil source bed genesis: American Association of Petroleum Geologists Bulletin 64, pp. 1179-1209.

Doligez, B., Undgerer, P., Chenet, P.Y., Burrus, J., and Bessis, F. (1986) Reconstruction of paleopressures; hydrocarbon formation and migration in the North Sea Basin (abstract): Atlantic Geoscience Society Symposium on Basins of Eastern Canada, programme with abstracts, p. 38.

Dow, W.G. (1978) Petroleum source beds on continental slopes and rises: in Watkins, J.S., Montadert, L., and Dickerson, P.W.(editors), Geological and Geophysical Investigations of Continental Margins, American Association of Petroleum Geologists Memoir 29, pp. 423-442.

Ervine, W.B. (1985) A Synthesis of Hydrocarbon Maturation Data for the East Coast Newfoundland Basin: Geological Survey of Canada Open File 1178, 74 p.

Folk, R.L. (1974) Petrology of Sedimentary Rocks: Hemphill Publishing Company, 182 p.

Franks, S.G. and Forester, R.W. (1984) Relationships among secondary porosity, pore-fluid chemistry and carbon dioxide, Texas Gulf coast: in MacDonald, D.A. and Surdam, R.C.(editors), Clastic Diagenesis, American Association of Petroleum Geologists Memoir 37, pp. 63-79.

Galloway, W.E. (1984) Hydrologic regimes of sandstone diagenesis: in MacDonald, D.A. and Surdam, R.C.(editors), Sandstone Diagenesis, American Association of Petroleum Geologists Memoir 37, pp. 3-13.

Gautier, D.L. and Claypool, G.E. (1984) Interpretation of methanic diagenesis in ancient sediments by analogy with processes in modern diagenetic environments: in MacDonald, D.A., and Surdam, R.C.(editors), Sandstone Diagenesis, American Association of Petroleum Geologists Memoir 37, pp. 111-123.

Gautier, D.L., Kharaka, Y.K. and Surdam, R.C. (1985) Relationship of Organic Matter and Mineral Diagenesis: Society of Economic Paleontologists and Mineralogists Short Course 17, 158 p.

Grant, A.C., McAlpine, K.D., and Wade, J.A. (1986) Offshore geology and petroleum potential of eastern Canada: in Energy Exploration and Exploitation, 4, Elsevier Applied Science Publishers Ltd., England, pp. 5-52.

Graves, W. (1986) Bit-generated rock textures and their effect on evaluation of lithology, porosity, and shows in drill-cutting samples: American Association of Petroleum Geologists Bulletin, v. 70, pp. 1129-1135.

Gretener, P.E. (1981) Pore Pressure: Fundamentals, General Ramifications, and Implications for Structural Geology (Revised): American Association of Petroleum Geologists Education Course Note Series #4, 131 p.

Handyside, D.D. and Chipman, W.I. (1983) A preliminary study of the Hibernia field: Journal of Canadian Petroleum Technology, pp. 67-78.

Heroux, Y., Chagnon, A., and Bertrand, R. (1979) Compilation and correlation of major thermal maturation indicators: American Association of Petroleum Geologists Bulletin, v.63, no. 12, pp. 2128-2144.

Issler, D.R. (1984) Calculation of organic maturation levels for offshore eastern Canada - implications for general application of Lopatin's method: Canadian Journal of Earth Science, v.21, pp. 477-488.

Jansa, L.F. and Wade, J.A. (1975) Geology of the continental margin off Nova Scotia and Newfoundland: in Offshore Geology of Eastern Canada, Geological Survey of Canada Paper 74-30, v.2, pp. 51-105.

Kaiser, W.R. (1984) Predicting reservoir quality and diagenetic history in the Frio Formation (Oligocene) of Texas: in MacDonald, D.A., and Surdam, R.C.(editors), Sandstone Diagenesis, American Association of Petroleum Geologists Memoir 37, pp. 195-215.

Keen, C.E. (1979) Thermal history and subsidence of rifted continental margins - evidence for wells on the Nova Scotian and Labrador Shelves: Canadian Journal of Earth Science, v.16, pp. 505-522.

Keen, C.E. (1983) Salt diapirs and thermal maturity: Scotian Basin: Bulletin of Canadian Petroleum Geology, v.31, pp.101-108.

Keen, C.E. and Barrett, D.L. (1981) Thinned and subsided continental crust on the rifted margin of eastern Canada: crustal structure, thermal evolution and subsidence history: Canadian Geophysical Journal, v.65, pp. 443-465.

Keen, C.E. and Lewis, T. (1982) Measured radiogenic heat production in sediments from continental margin of eastern North America: implications for petroleum generation: American Association of Petroleum Geologists Bulletin, v.66, pp. 1402-1407.

Keen, C.E., Beaumont, C., and Boutilier, R. (1982) A summary of thermo-mechanical model results for the evolution of continental margins based on three rifting processes: in Watkins, J.S. and Drake, C.C.(editors), Continental Margin Geology, American Association of Petroleum Geologists Memoir 34, pp. 725-728.

Kent, D.V. and Gradstein, F.M. (1984) A Jurassic to Recent chronology: in Tucholke, B.E. and Vogt, P.R. (editors), The Western Atlantic region, Volume M of The Geology of North America: Boulder, Colorado, Geological Society of America.

Leder, F. and Park, W.C. (1986) Porosity reduction in sandstone by quartz overgrowth: American Association of Petroleum Geologists Bulletin, v. 70, pp. 1713-1728.

LePichon, X., Sibuet, J.C., and Francheteau, J. (1977) The fit of the continents around the North Atlantic Ocean: Tectonophysics, v. 38, p. 169-209.

Masson, D.G. and Miles, P.R. (1984) Mesozoic Seafloor Spreading Between Iberia, Europe and North America: Marine Geology, v. 56, pp. 279-287.

Masson, D.G. and Miles, P.R. (1986) Development and hydrocarbon potential of Mesozoic sedimentary basins around margins of North Atlantic: American Association of Petroleum Geologists Bulletin, v. 70, pp. 721-729.

McKenzie, R.M. (1981) The Hibernia...A classic structure: Oil and Gas Journal, v. 79, pp. 240-246.

McMillan, M.J. (1982) Canada's east coast: the new super petroleum province: Journal of Canadian Petroleum Technology, pp. 95-109.

Medioli, F.S. and Scott, D.B. (1986) Lucustrine Thecamoebians (mainly Arcellaceans) as potential tools for paleolimnological interpretations: Publication no. 18, Center for Marine Geology, Dalhousie University, 53 p.

Pitman, W.C. and Talwani, M. (1972) Sea-floor spreading in the North Atlantic: Geological Society of America Bulletin, v. 83, pp. 619-646.

Powell, T.G. (1984) Hydrocarbon-Source Relationships Jeanne d'Arc and Avalon Basins, Offshore Newfoundland: Geological Survey of Canada Open File 1094.

Pokorny, V. (1978) Ostracodes: in Haq, B.V. and Boersma, A.(editors), Introduction to Marine Micropaleontology, pp. 109-150.

Rayer, F.G. (1981) The Hibernia Oil Discovery, A Classical Structural Trap in a Pull-Apart Basin: a paper presented to the LXIII ARPEL Experts Meeting, Rio de Janiro, Nov. 9-12, 1981, 10 p.

Robertson Research (1985): unpublished consultants' report.

Royden, L. and Keen, C.E. (1980) Rifting process and thermal evolution of the continental margin of eastern Canada determined from subsidence curves: Earth and Planetary Science Letters, v. 51, pp. 343-361.

Schmidt, V. and McDonald, D.A. (1980) Secondary Reservoir Porosity in the Course of Sandstone Diagenesis: A.A.P.G. Continuing Education Course Note Series 12, 125 p.

Scholle, P.A. (1979) Constituents, Textures, Cements, and Porosities of Sandstones and Associated Rocks: American Association of Petroleum Geologists Memoir 28, 201 p.

Sherwin, D.F. (1973) Scotian Shelf and Grand Banks: in McCrossan, R.G.(editor), Future Petroleum Provinces of Canada - Their Geology and Potential, Canadian Society of Petroleum Geologists Memoir 1, pp. 519-559.

Siebert, R.M., Moncure, G.K., and Lahann, R.W. (1984) A theory of framework grain dissolution in sandstones: in MacDonald, D.A. and Surdam, R.C.(editors), Sandstone Diagenesis, American Association of Petroleum Geologists Memoir 37, pp. 163-175.

Smith, D.G. (1983) Anastomosed fluvial deposits: modern examples from western Canada: in Collinson, J.D. and Lewin, J. (editors), Modern and Ancient Fluvial Systems, Special Publication of the International Association of Sedimentologists, v. 6, pp. 155-168.

Smith, D.G. and Putnam, P.E. (1980) Anastomosed river deposits: modern and ancient examples in Alberta, Canada: Canadian Journal of Earth Science, v. 17, pp. 1396-1406.

Surdam, R.C., Boese, S.W. and Crossey, L.J. (1984) The chemistry of secondary porosity: in MacDonald, D.A. and Surdam, R.C.(editors), Sandstone Diagenesis, American Association of Petroleum Geologists Memoir 37, pp. 127-149.

Swift, J.H., Switzer, R.W., and Turnbull, W.F. (1975) The retaceous Petrel Limestone of the Grand Banks, Newfoundland: in Yorath, C.J., Parker, E.R., and Glass, D.J. (editors), Canada's Continental Margins and Offshore Petroleum Exploration, Canadian Society of Petroleum Geologists Memoir 4, pp. 181-194.

Tankard, A.J. and Welsink, H.J. (in press) Extensional Tectonics and Stratigraphy of the Mesozoic Grand Banks of Newfoundland.

Vail, P.R. and Mitchum, R.M. (1978) Global cycles of relative changes of sea level from seismic stratigraphy: in Watkins J.S., Montadert, L., and Dickerson, P.W.(editors), Geological and Geophysical Investigations of Continental Margins, American Association of Petroleum Geologists Memoir 29, pp. 469-472.

Walker, R.G. and Cant, D.J. (1979) Sandy fluvial systems: in Walker, R.G. (editor), Facies Models, Geoscience Canada, Reprint Series 1, pp. 23-31.

Weir, L.A. and Furlong, K.P. (1986) Thermal evolution of sedimentary basins: intrabasinal effects (abstract): Atlantic Geoscience Society Symposium on the Basins of Eastern Canada, programme with abstracts, p. 124.

Williamson, M.A. (1987) A Quantitative Foraminiferal Biozonation of the Late Jurassic and Early Cretaceous of the East Newfoundland Basin: Micropaleontology, v. 33, no. 1, pp. 37-65.

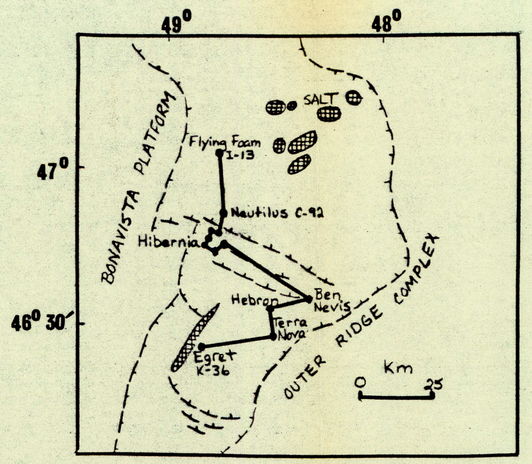

WELL LOCATIONS — JENNE D'ARC BASIN

ENCLOSURE 1

TIME — SPACE DIAGRAM

22 Km | 8 Km | 3 Km | 3Km | 3 Km | 5 Km | 5 Km | 38 Km | 14 Km | 10 Km | 25 Km

FLYING FOAM I-13 | NAUTILUS C-92 | HIBERNIA B-08 | HIBERNIA K-18 | HIBERNIA B-27 | HIBERNIA O-35 | HIBERNIA K-14 | HIBERNIA P-15 | BEN NEVIS I-45 | HEBRON I-13 | TERRA NOVA K-08 | EGRET K-36

PERIOD / AGE: CRETACEOUS — MAASTRICHTIAN, CAMPANIAN, SANTONIAN, CONIACIAN, TURONIAN, CENOMANIAN, ALBIAN, APTIAN, BARREMIAN, HAUTERIVIAN, VALANGINIAN, BERRIASIAN; JURASSIC — TITHONIAN, KIMMERIDGIAN, OXFORDIAN

UPPER CRETACEOUS SANDSTONE

DAWSON CANYON FORMATION

PETREL LIMESTONE

(marlstone)

LOGAN CANYON FORMATION

(mostly shale)

AVALON LACUNA

UPPER AVALON SANDSTONE

PRE-APTIAN LACUNA

LOWER AVALON SANDSTONE

LIMESTONE

MISSISAUGA FORMATION

(mostly shale)

limestone + shale (minor sandstone)

CATALINA SANDSTONE

"B" LIMESTONE

"B" LMST

B LIMESTONE

HIBERNIA SANDSTONE

VERRILL CANYON SHALE

"J" MARKER

MIC MAC FORMATION

JEANNE D'ARC SANDSTONE

JEANNE D'ARC SANDSTONE

↓KIMMERIDGIAN UNCONFORMITY (SHORT-LIVED LACUNA)

LIMESTONE AND SHALE

TD=12,084 | TD=4435 | TD=5039 | TD=5117 | TD=4380 | TD=4802 | TD=4462 | TD=4407 | TD=4723 | TD=4932 | TD=4500 | TD=11,000

C.E. FITZGERALD

STRATIGRAPHIC COLUMN OF THE HIBERNIA MEMBER

IN THE WELL

MOBIL ET AL HIBERNIA K-14

ENCLOSURE 2

SPUDDED: AUG. 9, 1983

RIG RELEASED: JAN. 15, 1984

LOCATION: N 46° 43′ 40″ W 48° 47′ 36″
OFFSHORE, NEWFOUNDLAND

STATUS: SUSPENDED OIL WELL

Logs are measured from the rotary table, 32.9m above sea level.

T.D. is 4462m R.T.

LEGEND

DRILL STEM TESTS

- G Gas Recovery
- O Oil Recovery
- W Water Recovery
- Casing

OIL STAINING

- Pervasive
- Spotted
- Questionable

SORTING

- W Well Sorted
- M Moderately Sorted
- P Poorly Sorted

ROUNDING

- R Well Rounded
- r Subrounded
- a Subangular
- A Angular

LITHOLOGY

- Sandstone
- Siltstone
- Shale/Mudstone
- Coal

ACCESSORIES

- Siliceous
- Calcareous
- Dolomitic
- Carbonaceous/Coaly
- Plant fragments/Roots
- P Pyritic
- Siderite Nodules
- Shale Clasts
- B Bitumen

SEDIMENTARY STRUCTURES

- Large scale Cross bedding
- Small scale Cross bedding
- Contorted Laminations
- Flame Structures, Sandballs, Loadcasts
- Bioturbated

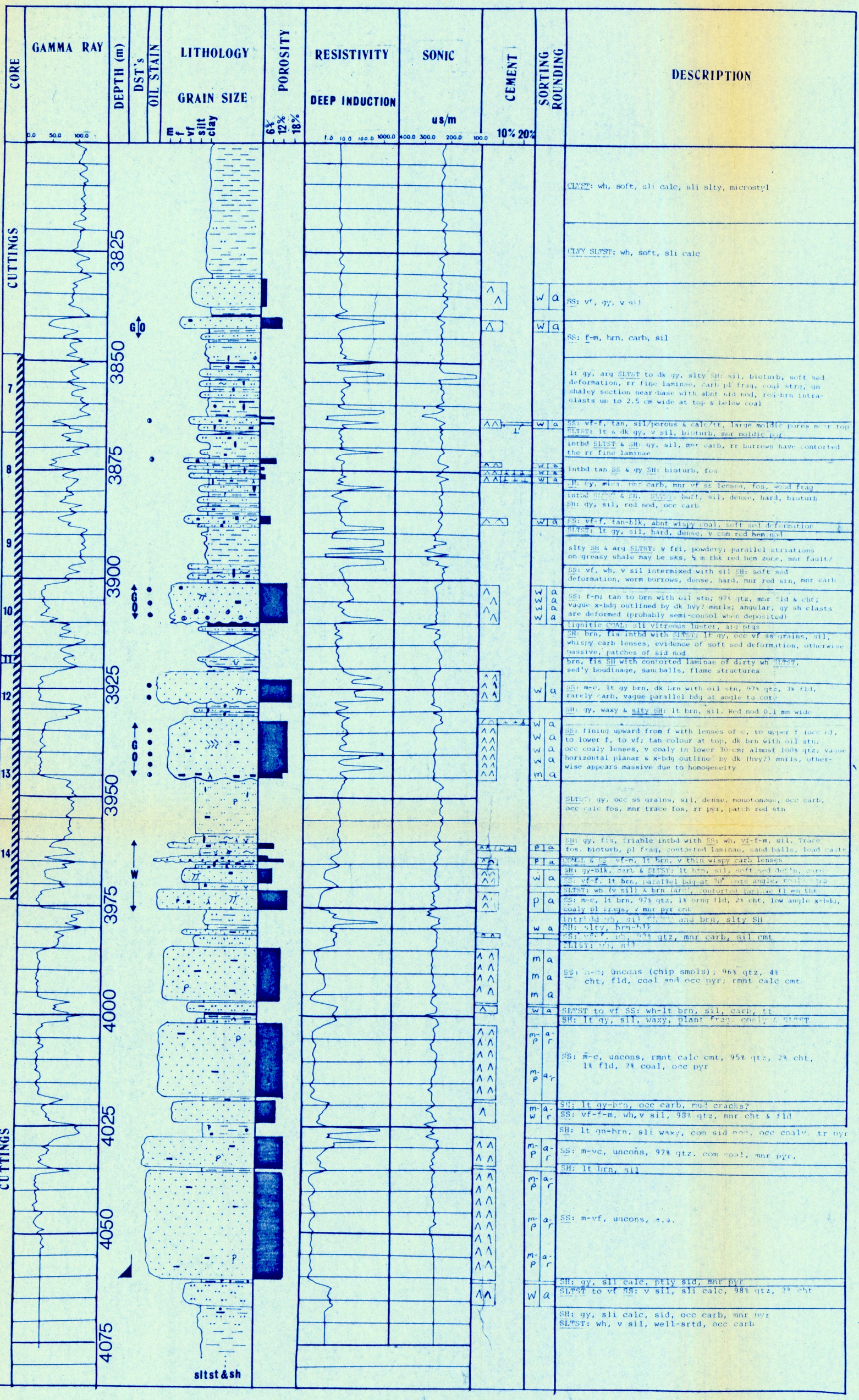

STRATIGRAPHIC COLUMN OF THE HIBERNIA MEMBER

IN THE WELL

MOBIL ET AL HIBERNIA K-18

ENCLOSURE 3

SPUDDED: FEB 26, 1981

RIG RELEASED: NOV. 6, 1981

LOCATION: N46° 47'35" W48° 47'17"
OFFSHORE, NEWFOUNDLAND

STATUS: SUSPENDED OIL WELL

Logs are measured from the rotary table, 27 m above sea level.

T.D. is 5039 m R.T.

LEGEND

DRILL STEM TESTS

G Gas Recovery
O Oil Recovery
W Water Recovery

OIL STAINING

● Pervasive
◑ Spotted
○ Questionable

SEDIMENTARY STRUCTURES

- Large scale Cross bedding
- Small scale Cross bedding
- ~ Contorted Laminations
- Flame Structures, Sandballs, Loadcasts
- Bioturbated

LITHOLOGY

- Sandstone
- Siltstone
- Shale / Mudstone
- Coal

ACCESSORIES

- ∧ Siliceous
- ⊥ Calcareous
- ∠ Dolomitic
- Carbonaceous / Coaly
- λ Plant fragments / Roots
- P Pyritic
- •• Siderite Nodules
- ⌀⌀ Shale Clasts

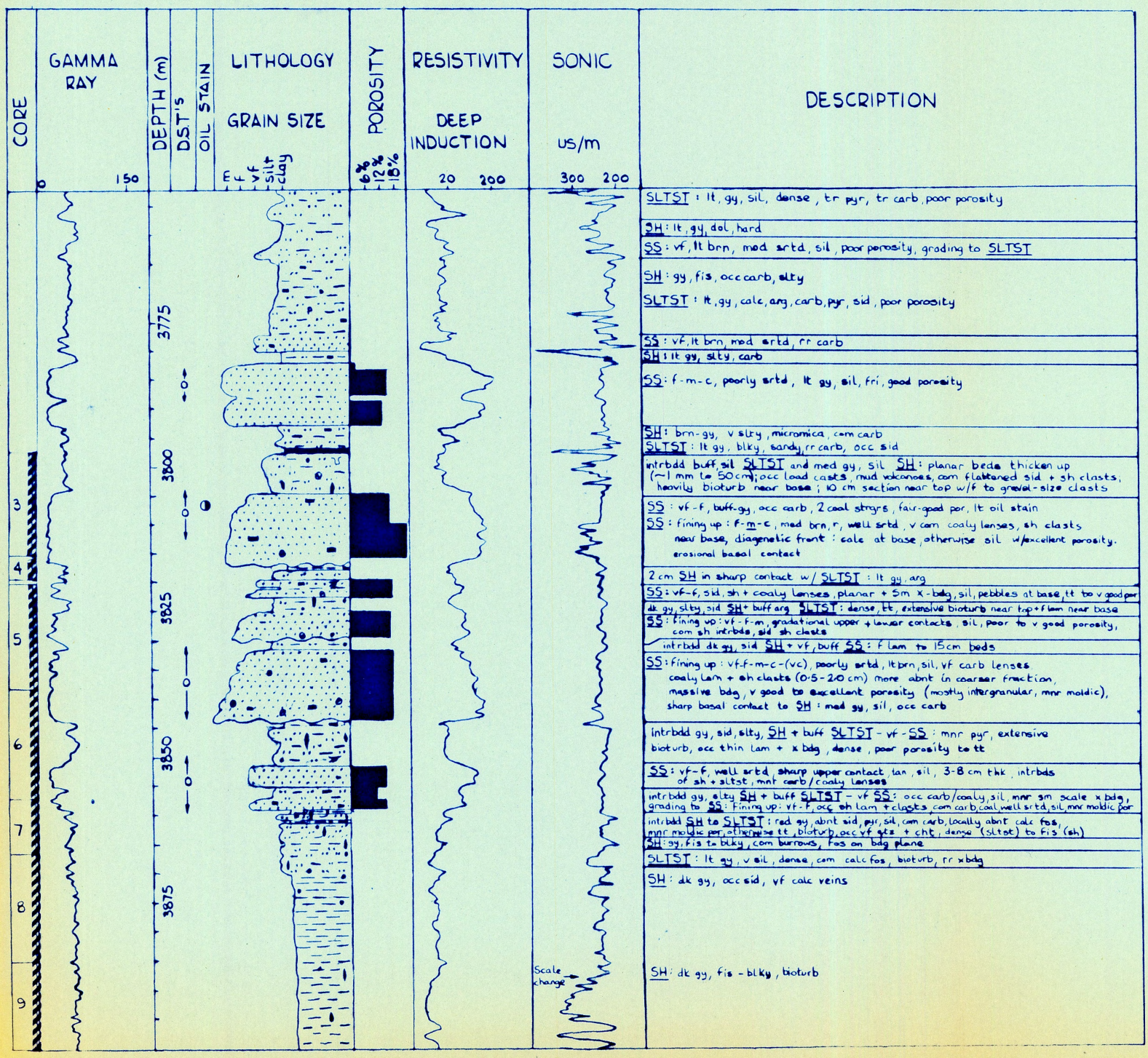

STRATIGRAPHIC COLUMN OF THE HIBERNIA MEMBER

IN THE WELL

MOBIL ET AL HIBERNIA B-08

ENCLOSURE 4

SPUDDED: MARCH 19, 1980

RIG RELEASED: JAN. 6, 1981

LOCATION: N 46°47'06" W48°45'30" OFFSHORE, NEWFOUNDLAND

STATUS: SUSPENDED OIL WELL

Logs are measured from the rotary table, 27.4 m above sea level.

T.D. is 4435 m R.T.

LEGEND

DRILL STEM TESTS

G Gas Recovery
O Oil Recovery
W Water Recovery

OIL STAINING

- ● Pervasive
- ◑ Spotted
- ○ Questionable

SEDIMENTARY STRUCTURES

- Large scale Cross bedding
- Small scale Cross bedding
- ~ Contorted Laminations
- Flame Structures, Sandballs, Loadcasts
- Bioturbated

LITHOLOGY

- Sandstone
- Siltstone
- Shale/Mudstone
- Coal

ACCESSORIES

- ∧ Siliceous
- ⊥ Calcareous
- ⊿ Dolomitic
- ▬ Carbonaceous/Coaly
- λ Plant fragments/Roots
- P Pyritic
- •• Siderite Nodules
- ●● Shale Clasts

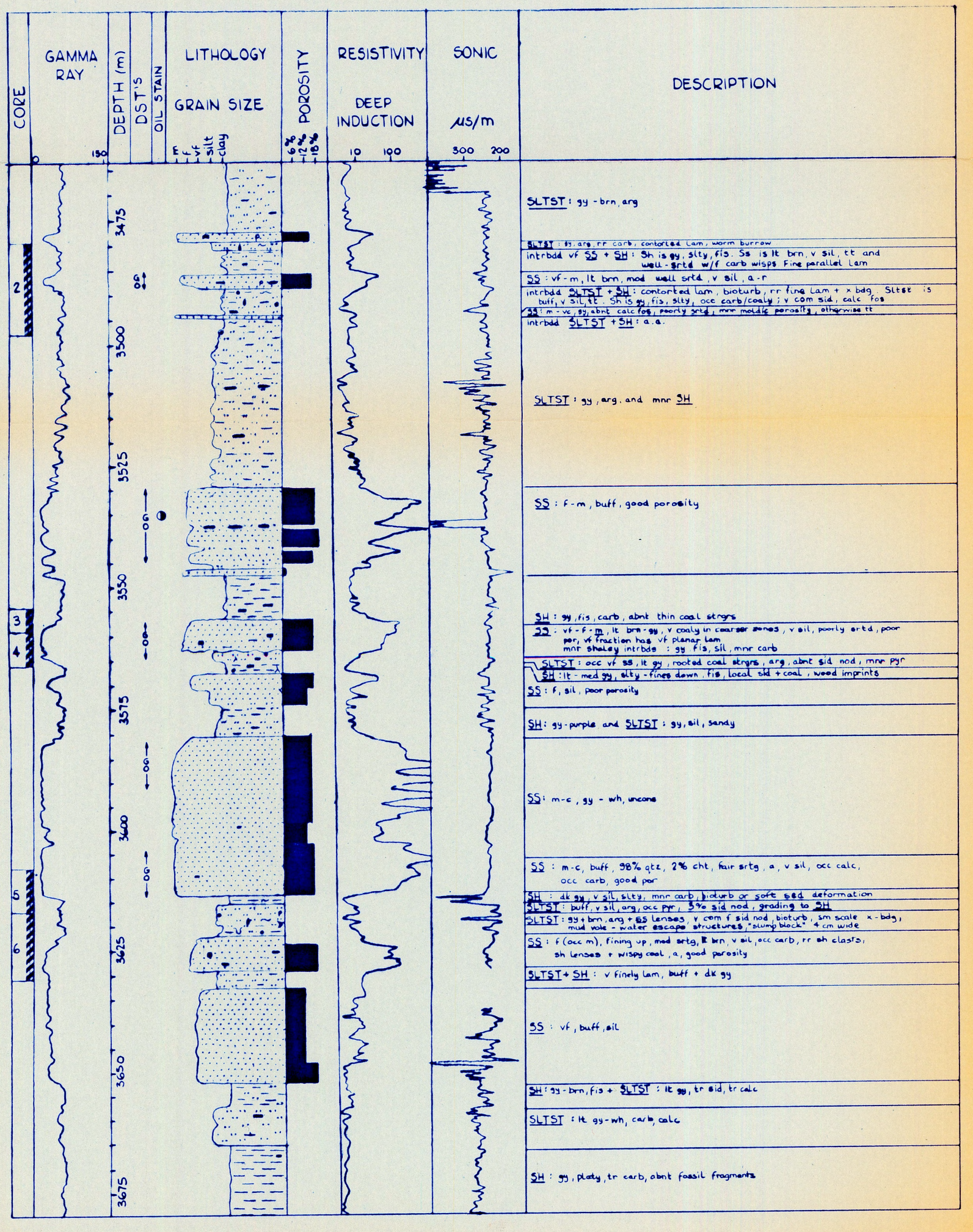

STRATIGRAPHIC COLUMN OF THE HIBERNIA MEMBER

IN THE WELL

MOBIL ET AL HIBERNIA B-27

ENCLOSURE 5

SPUDDED: AUG. 8, 1983

RIG RELEASED: DEC. 17, 1983

LOCATION: N 46° 46' 10" W 48° 48' 28"
OFFSHORE, NEWFOUNDLAND

STATUS: SUSPENDED OIL WELL

Logs are measured from the rotary table, 27 m above sea level.

T.D. is 4380 m R.T.

LEGEND

DRILL STEM TESTS

G Gas Recovery
O Oil Recovery
W Water Recovery

OIL STAINING

● Pervasive
◑ Spotted
○ Questionable

SEDIMENTARY STRUCTURES

- Large scale Cross bedding
- Small scale Cross bedding
- Contorted Laminations
- Flame Structures, Sandballs, Loadcasts
- Bioturbated

LITHOLOGY

- Sandstone
- Siltstone
- Shale / Mudstone
- Coal

ACCESSORIES

- Siliceous
- Calcareous
- Dolomitic
- Carbonaceous / Coaly
- Plant fragments / Roots
- P Pyritic
- Siderite Nodules
- Shale Clasts
- Inferred fault

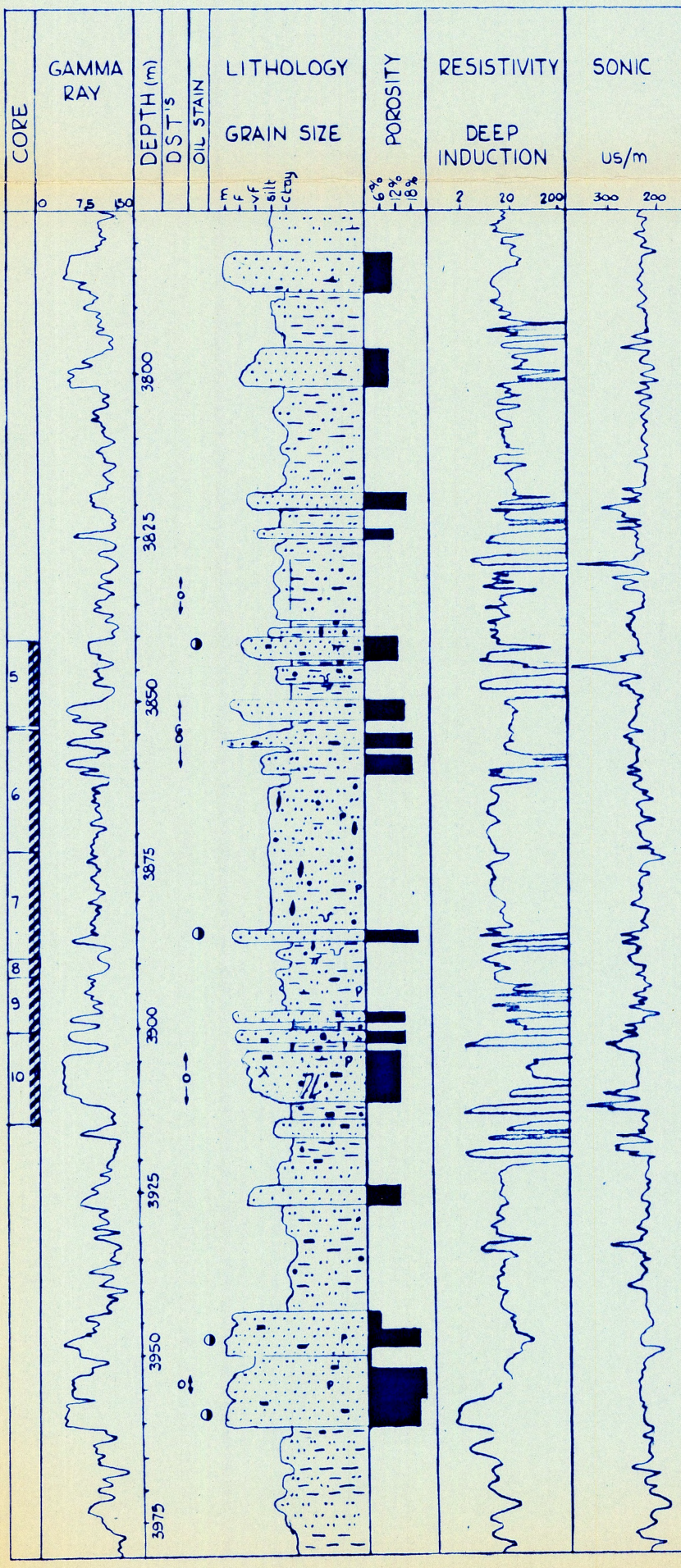

DESCRIPTION

SLTST : wh - gy, calc, arg

SS : m, uncons, well srtd, wh, sil
SS : vf-f, well srtd, wh, dol, carb, tr coal

SH : lt gy - gn, waxy, sil + SLTST strgrs

SS : vf-f-m, wh, dol, poor porosity

SH : lt gy - gn, rr mauve, waxy, sil, fis
SLTST : wh-brn, arg, sil, tt

SS : vf-f, wh, uncons, fri, sil, poor porosity
SH : lt + dk gy, waxy, sil, hard SLTST strgrs
SS : vf, wh brn, poor porosity

SH : lt brn - dk gy, rubbly to v hard, sil, partly carb and
SLTST : to vf SS : locally abnt m grains, buff, v sil, dense, sid conc in burrows

SS : f (occ m), well srtd, lt brn, v sil, occ arg, carb/coaly streaks, sm scale x-bdg, poor to good porosity
intrbdd dk gy, silty SH + wh, arg SLTST - vf SS : abnt coal, abnt sid, v deformed bdg
SH : gy, sil, fis, silty, finely lam w/ SLTST, sm scale x-bdg
SS : f-m, lt brn, sil, occ coaly wisps, good porosity
SH : lt gy, sil, vfis, poss slickensiding
SS : m-c, lt brn, mod srtd, sil, occ coaly, v good porosity

SLTST : lt-med gy, well srtd, tt, v sil, partly arg, sid, bioturb, locally abnt calc fossils, rubbly near base, pos fault

SLTST : gy, sil, sid intrbdd w/ vf buff SS + gy, silty SH. Bioturb, deformed bdg, fault or slump features

SS : f-m, mod brn, sil, mod well srtd, v good porosity
intrbdd dk gy SH - lt gy SLTST - vf SS : sid, rr planar lam + x-bdg, extensive bioturb, local sh/slt clasts + qtz pebbles, fault gouge, sm faults offsetting lam
intrbdd buff SLTST to vf - f SS and dk gy SH : abnt coaly lam, com pyr, diagenetic contact : sil + calc cmt, tt
SS : f-m, gy, well srtd, sil, pyr, sh intraclasts, rr coal inclusions w/ intrbds of SH : dk gy w/ red brn sid lenses, fis, warm burrow
SS : vf - f - (m), gy, pyr, large coaly inclusions, plant remains, calc cmt, poor por
Rubble : vf SS + SLTST, sil, v com sid nod, no calc cmt, fault breccia, poss laumontite - fault mnl
SH : dk gy, carb, v abnt sid nod, sheared, red iron staining
SLTST : lt gy, carb, sil, dense, monotonous
SH : lt - dk gy, blky, sid nod
SLTST : gy, mnr coal
SS : f, lt gy, partly uncons, sil, fair porosity

intrbdd SH + SLTST : lt - dk gy, carb, sid, sil

SS : f-m-c, mod srtd, mostly uncons, sil, pyr, coaly, good porosity
SLTST to vf SS : lt gy, sil, mnr carb
SS : f-m-c, mod srtd, mostly uncons, sil, pyr, coaly, good porosity

SH : med gy, silty, blky, carb and
SLTST : lt gy, arg, sil, tt

STRATIGRAPHIC COLUMN OF THE

HIBERNIA MEMBER

IN THE WELL

MOBIL ET AL HEBRON I-13

ENCLOSURE 6

SPUDDED: JAN. 14, 1981

RIG RELEASED: SEPT. 12, 1981

LOCATION: N46° 32′ 34″ W48° 31′ 46″
OFFSHORE, NEWFOUNDLAND

STATUS: SUSPENDED OIL WELL

Logs are measured from the rotary table, 27.3 m above sea level.

T.D. is 4723.5 m R.T.

LEGEND

DRILL STEM TESTS
- G Gas Recovery
- O Oil Recovery
- W Water Recovery
- Casing

OIL STAINING
- Pervasive
- Spotted
- Questionable

SORTING
- W Well Sorted
- M Moderately Sorted
- P Poorly Sorted

ROUNDING
- R Well Rounded
- r Subrounded
- a Subangular
- A Angular

LITHOLOGY
- Limestone
- Sandstone
- Siltstone
- Shale/Mudstone
- Coal

ACCESSORIES
- Siliceous
- Calcareous
- Dolomitic
- Carbonaceous/Coaly
- Plant fragments/Roots
- P Pyritic
- Siderite Nodules
- Shale Clasts

THIN SECTIONS | GAMMA RAY & SP (GR 0.0 50.0 100.0; SP -100.0 -50.0 0.0 50.0) | DEPTH (m) | DST's, OIL STAIN | INTERPRETED LITHOLOGY GRAIN SIZE (m f vf silt clay) | POROSITY (6% 18%) | RESISTIVITY DEEP INDUCTION (1 10 100 1000) | SONIC µs/m (400.0 300.0 200.0) | CEMENT (10% 20%) | SORTING ROUNDING | CUTTINGS LITHOLOGY (20% 40% 60% 80%) | CUTTINGS DESCRIPTION

1
2
3
4
5
6
7
8
9
10
11
12
13
14
15
16
17
18
19
20
21
22
23
24
25
26

3000
3025
3050
3075
3100
3125
3150
3175
3200
3225
3250
3275
3300
3325
3350
3375
3400
3425
3450
3475
500

OIL

5% LMST: wh, fr orng, ool, pel, pt biocl
30% SS: vf-f, oil stn 20% SLTST: dk gy, calc

30% LMST: a.a. 10% SLTST: dk gy, calc
60% SS: f, wh-brn, occ oil stn, 95% qtz

25% LMST: a.a. 5% SLTST: dk gy, calc
70% SS: f, occ m, a.a.

20% LMST: a.a. 5% SLTST: dk gy, calc
75% SS: f, oil stn, less calc cmt, good por

15% LMST: a.a. 10% SS: f, calc
75% SS: f, oil stn, sil cmt, good por

15% LMST: a.a. 5% SLTST: dk gy
65% SS: f, oil stn, sil 15% SS: f, calc, tt

15% LMST: a.a. 20% SS: f, wh, calc, tt
65% SS: f, brn, oil stn, sil, fair por

15% LMST: a.a. 25% SS: f, wh, calc, tt
45% SS: f, brn, a.a. 15% carb SH & gy SLTST

20% SS: vf-f, calc 20% SH: dk gy, calc, carb
60% SS: f, gy-brn, oil stn, sil

75% SS: vf-f, calc 5% SS: f, gy-brn, oil stn
20% SH: gy-blk, calc, carb/coaly

75% SS: vf-f, calc 5% SS: f, gy-brn, oil stn
20% SH: gy-blk, calc, carb/coaly

60% vf SS to SLTST: wh-gy, calc
35% SH: dk gy, calc 5% sil SS & calc strg

55% vf SS to SLTST: wh-gy, calc
25% SH: a.a. 10% SS: f, sil 10% calc strg

90% SS: vf to f, gy, calc, poor por
5% SH: dk gy, calc 5% calc strg

25% SS: m, uncons 40% vf SS to SLTST: calc
30% SS: f, calc & sil, var por 5% SH: dk gy

45% SS: m-c, uncons, qtz ovgth, resd calc cmt
30% SS: f, wh, calc 25% SS: vf, gy, calc, tt

65% SS: m, uncons, qtz ovgth, resd calc cmt
10% SS: vf-f, wh-gy, calc, tt 5% SS: f, sil

35% SS: m-c, uncons, qtz ovgth, resd calc cmt
10% SS: f-m, sil & calc cmt 5% SH & calc strg

70% SS: m-c, uncons, a.a. 5% SH: blk, pyr
25% SS: vf-f-m, wh to brn, pl frag

75% SS: m-c, uncons, a.a. 5% SS: f, sil
20% SS: vf-f-m, sil & calc cmt, var por

80% SS: m-c, uncons, resd calc cmt
20% SS: f-m, sil & calc cmt

80% SS: m-c, uncons, qtz ovgth 5% SS: vf-f
15% SS: m-c, calc, comp same as uncons ss

85% SS: m-c, uncons, resd calc cmt, mnr pyr
10% SS: m, calc 5% SS: vf-f, calc, tt

80% SS: m, uncons, occ orng fld, coal, pyr
15% SS: f-m, var sil & calc 5% vf SS-SLTST

65% SS: m-c-vc, uncons, cht, occ coal, pyr
33% SS: f-m, var calc cmt 2% SLTST: calc, tt

43% SS: m, uncons & cons 45% SS: f, sil
5% SS: vf, calc, tt 7% qy pyr SH & CLYST str

25% SS: m, uncons 15% SS: m, calc, var por
50% SS: vf-f, calc 10% SH: lt gy-gn, sil

45% SS: m, uncons 10% SH: dk gy, sil
45% SS: vf-f, sil & calc cmt, poor-fair por

60% SS: vf-f, a.a.
40% SH: lt-dk brn-gy, sil

15% SS: m, uncons 50% SS: vf, calc, poor por
10% SLTST: tan 25% SH: brn-gy, sil

70% SS: vf-f, sil, var por 5% wh calc strg
15% SH: lt gy-gn, mnr coal, pyr 10% SLTST

80% SS: vf, sil, tt
20% SH: gy-brn

80% SS: vf, sil, tt
20% SH: gy-brn

45% SS: vf, sil, poor por
10% SH: gy-brn, fis 5% calc strg & calc ss

45% SS: vf, mostly sil cmt, poor por
10% SH: gy, fis, coaly 5% calc strg/calc ss

27% SS: vf, a.a. 60% SH: gy 2% COAL
4% SS: uncons, a.a. 2% sid nod 3% calc strg

40% SS: vf-f, wh, mostly sil cmt, poor por
55% SH: gy, fis, pyr 5% wh calc strg

34% SS: vf-f, wh, calc, tt
65% SH: gy, fis, pyr 1% sid nod

34% SS: vf-f, wh, calc, tt 3% wh calc strg
65% SH: gy-gn, pyr 1% sid nod

20% SS: vf-f, calc, var por
80% SH: dk gy to sli gn, fis, plty

20% SS: vf-f, calc, var por
80% SH: dk gy-gn, fis, plty, occ sid nod

10% SS: vf-f, tt 5% LMST: cream, pt biocl
85% SH & SLTST: dk gy occ sid nod

15% vf SS to SLTST: wh, sil, tt
85% SH: gy

15% vf SS to SLTST: a.a.
85% SH & SLTST: dk gy/mnr LMST: orng & wh

25% vf SS to SLTST: wh, sil, tt
40% SH: gn-gy 15% SLTST: gy-blk

30% vf SS to SLTST: a.a.
70% SH & SLTST: gy mnr COAL

30% vf SS to SLTST: wh, sid nod, sil, tt
50% gy SH & dk gy SLTST/mnr orng LMST/wh CLY

50% SS: vf-f, wh, sid nod, sil, poor por
40% SH: gy-gn 10% SLTST: dk gy

35% vf SS-SLTST: wh, sil, tt 50% SH: gn-gy
5% SS: f, sil 10% SLTST: dk gy-blk, mnr COAL

15% SS: vf-f, wh 3% SLTST: dk gy-blk
82% SH: gn-gy, splty mnr LMST: wh & orng

3% SS: vf-f, sil & mnr calc cmt
90% SH to SLTST: dk gy 4% LMST/CLYST

22% SS: vf-f 4% LMST, CLY 2% sid nod
55% SLTST: dk gy 15% SH: lt gy 2% SH: gn

30% vf SS to SLTST: wh, mnr oil stn, sil
10% SLTST: dk gy 45% SH: gn-gy 15% COAL

36% vf SS-SLTST: wh, sil 4% SLTST: dk gy-blk
55% SH: gn-gy 3% COAL & pyr 2% sid nod

33% vf SS-SLTST: wh, sil 5% SLTST: dy gy-blk
25% gy SH 15% brn SH 20% gn SH 2% orng LMST

35% SLTST: wh 50% SH to SLTST: lt gy
15% SLTST: blk mnr LMST/CLY sid nod

30% SLTST: wh
70% lt gy SH & dk gy SLTST mnr gn SH

25% SS, vf, sil, poor por
30% SH: red 15% SH:gn 30% SH: cream-gy

21% SS: vf, wh, sil & calc cmt 12% SH: red
5% SS: f 37% SH: gy-brn 23% SH: gn 2% LMST

15% SS: vf-f, wh, oil stn, sil 2% LMST
18% SS: vf, a.a. 65% SH: gy-brn, gn, red

(poor spl) 10% SS: vf-f, a.a. 50% SH: a.a.
20% SS: vf, a.a. 20% uncons ss, lmst, coal

(poor spl) 30% SS: f, s&p 33% SH: brn-gy
4% SH: red 6% SH: gn 22% lmst, ss, coal

23% SLTST to vf SS: wh-gy 40% SH: gy-brn
4% SS: f, s&p 7% SH: red & gn 2% LMST

35% SS: vf, gy 40% SH: lt & dk gy 2% SH: red
3% SH: gn 2% LMST mnr sid nod, pr

45% SS: vf, gy, sil & calc cmt
15% COAL 40% SH: lt gy, sid nod

65% SS: vf, wh, calc, tt 30% SH: gn-gy
3% SH: red-brn 2% COAL

70% SS: vf, wh 15% SH: gn-gy
15% SLTST: dk gy

30% SS: vf, wh, sil 25% SLTST: dk gy
30% SS: f, wh, calc, tt 15% SH: gn-gy

30% SS: vf, wh, sil 50% SH-SLTST: gy
20% SS: f, wh, calc, tt

40% SS: vf, wh-tan, sil 55% SH: gy
5% SS: f, a.a. 2% SH: lt gn, com sid/lim

30% SS: vf, wh-tan, sil 65% SH-SLTST: gy
5% SS: f, wh, calc, tt occ sid/lim

15% SS: vf, wh-tan, sil & calc cmt
5% SH-SLTST: gy occ lt gn sh, sil, lmst

5% SS: m, pt uncons, wh, calc & sil cmt
10% SS: vf-f, wh-gy 65% SH: gy mnr coal

65% SS: m, uncons, clr-smky qtz, mnr fld, cht
10% SS: vf, wh-tan 25% SH: gy, abnt sid nod

65% SS: m-c, uncons, 65% qtz, 10% fld, cht
10% SS: vf, wh-tan, sil 15% SH: gy

5% SS: m-c, uncons, a.a. 10% SLTST: wh, sil
30% SS: vf, wh-tan, sil 45% SH: dk gy

90% SS: vf, wh-smky, 90% qtz, sil
10% SLTST: wh-gy 40% SH: dk gy

30% SS: vf, wh, sil
35% SLTST: gy 35% SH: gy

25% SS: vf, wh, sil 35% SLTST: gy
35% SH: gy 5% COAL & carb SH

10% SS: vf, wh, sil
90% SS: f, 97% qtz, sil 70% SH: gy

5% SS: vf, wh, sil
95% SH: gy

5% SS: vf, wh, sil, 97% qtz
20% SLTST: dk gy 15% SH: lt gy

90% SS: vf, wh, sil, 97% qtz
5% SLTST: dk gy 15% SH: lt gy

25% SS: vf, a.a. 40% SLTST: gy
10% SH: gy-gn 15% SH: red

10% SS: f, sil, good por 30% SLTST: gy
20% SS: vf, a.a. 35% SH: gy-gn 5% CLYST intbd

5% SS: a.a. 35% SLTST: dk gy, sil
35% SS: vf, wh, 97% qtz, sil 25% SH: gn-gy

40% SS: vf-f, wh, 97% qtz, sil
10% SLTST: dk gy, sil 10% SH: gn-gy

40% SS: vf, wh, sil 33% SH: lt gy, sid nod
15% SH: dk gy-blk, carb, coaly 2% SH: red

40% SS: vf, wh, sil 33% SH: lt gy, sid nod
15% SH: dk gy-blk, carb, coaly 2% SH: red

40% SS: vf, wh, sil, occ dol, coal
40% SH-SLTST: lt & dk gy, mica, sil, pl frag

40% SS: vf, wh, sil occ dol, coal
40% SH-SLTST: lt & dk gy, mica, sil, pl frag

90% SH: dk gy, silty, fis, pl frag, mnr coal
5% SS: vf, a.a. 5% sid nod & rest SH

40% SH: dk gy, silty, fis, dol
40% SS: vf-f, sil

20% SS: m-c, uncons, clr-smky-yel qtz
20% SS: vf, coaly, sil cmt 70% SH: a.a.

20% SS: f-m, clr-gy qtz, occ cht, fld, coaly
20% SS: f-c, uncons, comp a.a. 60% SH: a.a.

90% SS: m-c, uncons, 97% qtz, 3% fld & cht
5% SS: f-c, carb, pl frag, sil 5% SH: a.a.

90% SS: m-c, uncons, a.a. 5% SH: a.a.
5% SS: f-c, carb, pl frag, sil

75% SS: m-c, uncons 10% SH, ool LMST, DOL
25% SS: f-c, 80% qtz, 20% cht, sil

45% SS: m-c, uncons, 98% clr-smky qtz
25% SS: vf-m 27% SH: dk gy, sil 3% wh CLYST

75% SS: vf-f, carb, coaly 25% SH: dk gy
17% SS: uncons, a.a. 3% wh CLYST

95% SS: vf-f, wh, coaly 25% SH: dk gy
17% SH: uncons, a.a. 3% wh CLYST

42% SS: f, carb
15% SH: dk gy 3% DOL/LMST

95% SH: dk gy, fis, sil, splty, ool
3% wh DOL 2% SS & COAL

95% SH: dk gy, fis, sil, splty, dol
5% SLTST: tan, calc

100% SH: dk gy, fis, dol, fossil

STRATIGRAPHIC COLUMN OF THE

HIBERNIA MEMBER

IN THE WELL

MOBIL ET AL BEN NEVIS I-45

ENCLOSURE 7

SPUDDED: JAN. 10, 1980

RIG RELEASED: SEPT. 10, 1980

LOCATION: N 46° 34′ 40″ W 48° 21′ 10″
OFFSHORE, NEWFOUNDLAND

STATUS: SUSPENDED OIL & GAS WELL

Logs are measured from the rotary table, 26.82 m above sea level.

T.D. is 4932 m R.T.

LEGEND

DRILL STEM TESTS

- G Gas Recovery
- O Oil Recovery
- W Water Recovery
- Casing

OIL STAINING

- Pervasive
- Spotted
- Questionable

SORTING

- W Well Sorted
- M Moderately Sorted
- P Poorly Sorted

ROUNDING

- R Well Rounded
- r Subrounded
- a Subangular
- A Angular

LITHOLOGY

- Sandstone
- Siltstone
- Shale/Mudstone
- Coal

ACCESSORIES

- Siliceous
- Calcareous
- Dolomitic
- Carbonaceous/Coaly
- Plant fragments/Roots
- P Pyritic
- Siderite Nodules
- Shale Clasts

ENCLOSURE 8

LITHOFACIES RELATIONSHIPS WITHIN THE HIBERNIA MEMBER

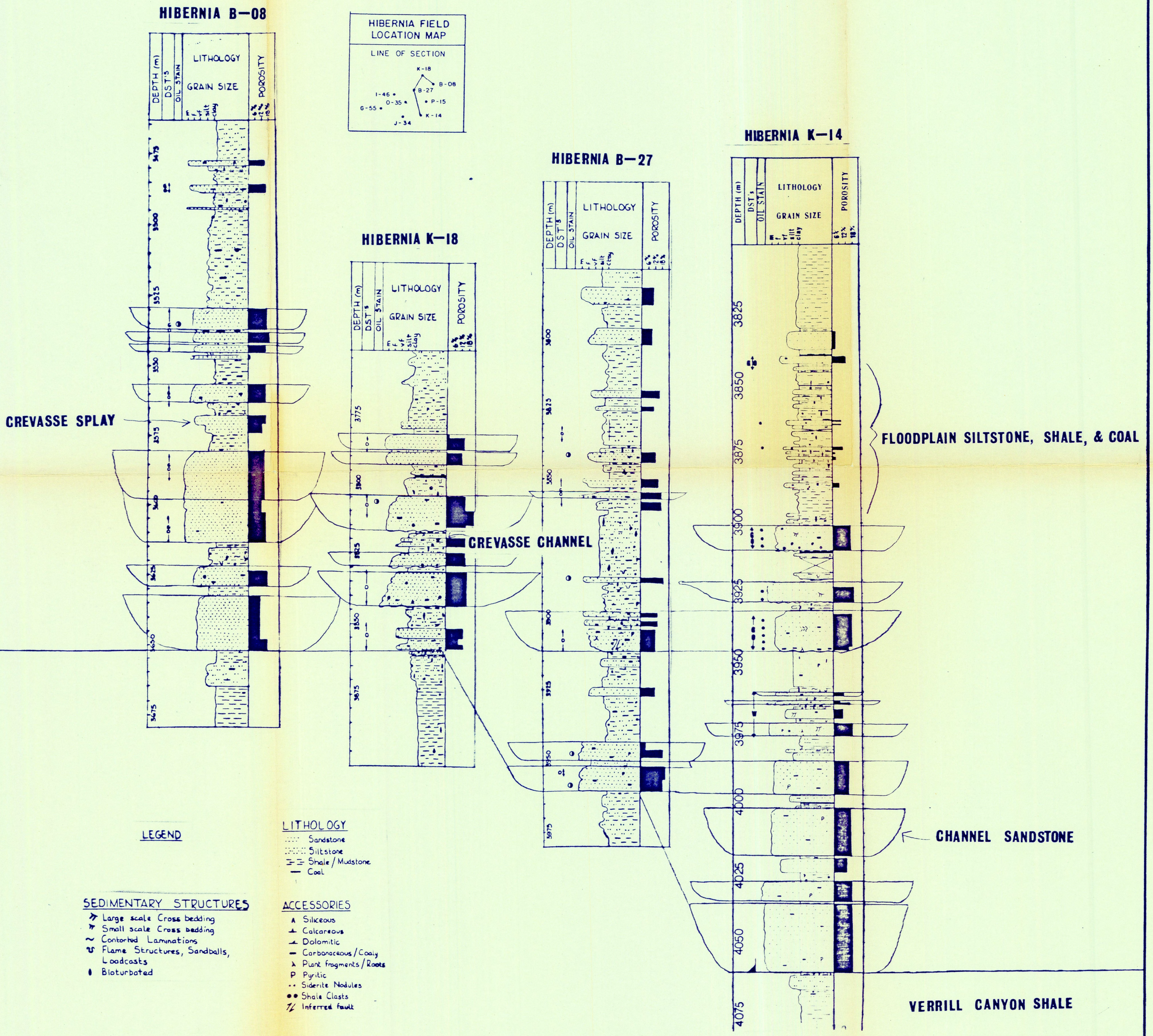

C.E. FITZGERALD

ENCLOSURE 9

STRUCTURAL FENCE DIAGRAM:

HIBERNIA MEMBER,

HIBERNIA FIELD

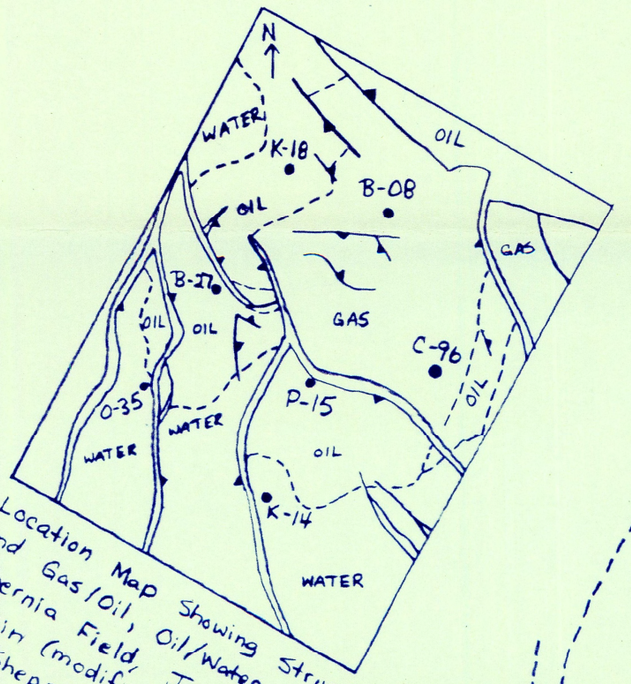

Location Map Showing Structure and Gas/Oil, Oil/Water Contacts Hibernia Field, Jeanne d'Arc Basin (modified from Benteau and Sheppard, 1982 and Handy-Side and Chipman, 1983).

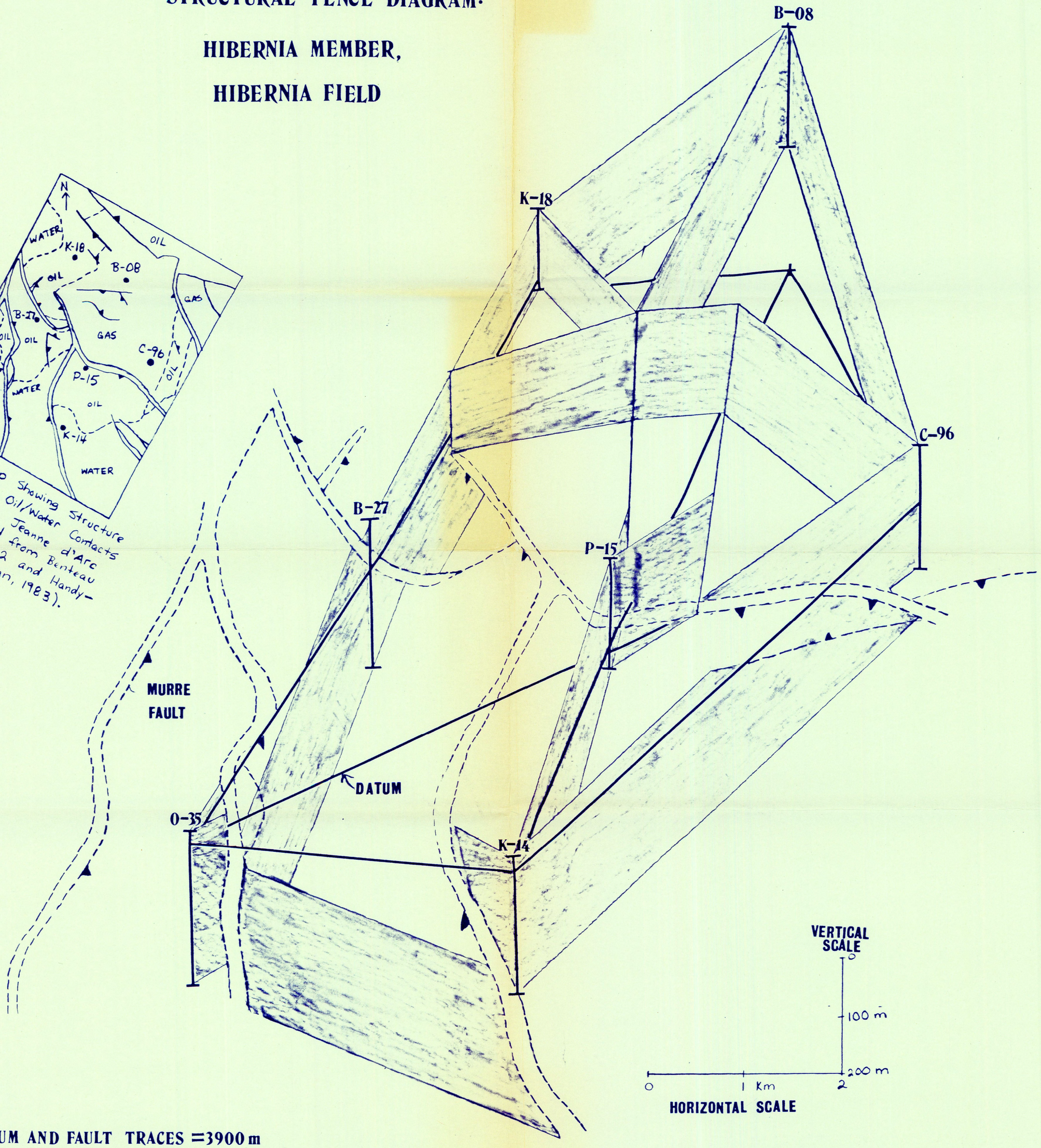

DATUM AND FAULT TRACES =3900 m

C.E. FITZGERALD

DEPTH VS SANDSTONE POROSITY

FOR THE HIBERNIA MEMBER IN WELLS:

Egret K-36
Terra Nova K-08
Hebron I-13
Hibernia B-08
Hibernia K-18
Hibernia K-14
Ben Nevis I-45

ENCLOSURE 10

POROSITY

(from sonic log)

Pocket #991
Item 3

CORE DESCRIPTION &

PETROGRAPHIC DATA

FROM THE

HIBERNIA MEMBER

IN THE WELL

MOBIL ET AL HIBERNIA K-14

ENCLOSURE 11

LEGEND

LITHOLOGY

- Sandstone
- Siltstone
- Shale/Mudstone
- Coal

ACCESSORIES

- ^ Siliceous
- ⊥ Calcareous
- ⊿ Dolomitic
- ▬ Carbonaceous/Coaly
- λ Plant fragments/Roots
- P Pyritic
- •• Siderite Nodules
- Shale Clasts

SEDIMENTARY STRUCTURES

- Large scale Cross bedding
- Small scale Cross bedding
- Contorted Laminations
- Flame Structures, Sandballs, Load casts
- Bioturbated

CORE | GAMMA RAY & THIN SECTION LOCATIONS (GR 0.0 50.0 100.0) | LITHOLOGY GRAIN SIZE (m f vf silt clay) | DEPTH (m) | CORE DESCRIPTION | PETROGRAPHIC DATA: GRAIN SIZE RANGE (PHI) 0 1 2 3 4 | PERCENT COMPONENTS 5 10 15 20 25 30 35 40 45 50 55 60

7

3850

lt gy, arg SLTST to dk gy, slty SH: sil, bioturb, soft sed def'n, rr fine lam, carb plant frag, coal strg, gn shaley section near base with abnt sid nod, red-brn intraclasts up to 2.5 cm diam

SH: gy, v fis, flakey, sil

SS: vf, tan, sil, patchy calc cmt, large moldic pores near top

SLTST: lt & dk gy, v sil, rr carb/coaly lenses near base, bioturb, mnr moldic por

8

SH: gy, slty and SLTST: wh, sil, mnr carb. Burrows have contorted the rr fine lam.

3875

SS: vf-f, tan, well srtd, mnr carb, sil, fair-poor por, spotty oil stn

SH: gy, intrbdd with SS: vf, wh, sil, calc, bioturb, fos

SS: vf, tan, well srtd, sil, calc, local moldic por, overall poor por

slty SH: wh & gy, v sil, tr calc cmt, carb, wood frag, bioturb, fos

SLTST: buff, dense, v sil, mnr carb & pyr, mnr fos bioturb, red stn at lw contact

9

SLTST: buff, dense, v sil, mnr arg ptg, mnr bioturb

intrbdd SLTST & SH: Sltst is buff, homogen, dense, hard, v sil. Sh is slty, gy, carb, v sil, fri, red nod & mnr soft sed def'n

SS: vf-f, abnt wispy coaly lenses, occ arg lenses, v sil, tt to poor por, soft sed def'n

SLTST: lt gy, hard, dense, v sil, v com red nod (hem?) ½ mm diam

slty SH and arg SLTST: v fri, pwdy, parallel striations (sks?), greasy, oxidized zone ½ m thk-stnd red, pos fault

SS: vf, wh, v sil and SH: dk gy, sil; soft sed def'n, bioturb, dense, hard, mnr red stn, mnr carb

3900

10

: f-m, tan, mnr carb, sil cmt, a, well-srtd, good por, large-scale x-bdg

SS: f; sh clasts (A, gy, deformed); a, mod-well srtd, carb near top, less sil cmt than surrounding ss, good por

SS: f-m, tan, sil cmt, a, mod-well srtd, good por, lt oil stn, vague parallel inclined bdg (large-scale x-bdg) outlined by hvy mnls

COAL 13 cm; SH: lt brn, fis, occ carb, slty at gradational lw contact

SLTST: tan-lt gy, carb, patches sid nod, intrbds of brn, fis SH

11

brn, fis SH with contorted lam of dirty wh

SLTST: sed'y boudinage, sand balls

12

SS: m-c, lt gy-brn, mod well srtd, mostly qtz, mnr fld, rr carb, vague large scale x-bdg

3925

sharp basal contact

SH: gy, waxy and slty SH: gy-lt brn, sil. Sid nod 0.1 mm diam.

SS: fining up, f-vf, tan, well srtd, 98% qtz, abnt sil cmt, 30 cm section of calc cmt, tt

13

SS: f, brn, 98% qtz, occ coaly lenses, well srtd, good por, even oil stn; vague horizontal & parallel bdg outlined by dk hvy mnls, large-scale herringbone pattern

lw 30 cm: mostly f, lenses of c, v coaly, plant frags, patchy oil stn

sharp basal contact

3950

SLTST: gy, v arg, v sil, occ carb, mnr pyr, monotonous, dense, mnr fos & bioturb, tt

SH & vf SS: gy & wh, bioturb, soft sed def'n &

SS: gy; vf (m) at base to m to vf (m) at top; v com contorted coaly lenses: v sil, patchy calc & com bit cmt, poor por

CONGL & SS: sh & sid clasts up to 5 cm long, matrix of m ss, fining up: f to vf

14

SH: lw 15 cm is blk, carb, rest is lt gy, fis

SLTST: gradational lw contact, gy-lt brn (arg) & wh (slty) lam, sil, micromic

SS: lt brn, arg lam, large-scale x-bdg, coal & carb lenses mostly in top half, v sil-esp around carb lenses, mnr bit

SLTST: lam (1 mm thk, wh (slty) & brn (arg) lam, v sil, musc

SS: lt brn, 97% qtz, 2% cht, 1% fld, coaly plant frag, mnr pyr, mod-poor srtg

3975

PETROGRAPHIC DATA — PERCENT COMPONENTS

- POROS, Corg, Fe CALCITE, DETRITAL CLAY, CLASTS
- POROS, QTZ OVRGTHS, CLASTS
- Fe CALCITE, QTZ OVRGTH, CALC FOS, AUTH CLAY, CLASTS
- SID, QTZ OVRGTHS, Corg, POROS, PYR, DTL CLAY, CLASTS
- POROSITY, QTZ OVGTHS, CLASTS
- SIDERITE, AUTH CLAY, POROSITY, QTZ OVRGTHS, DTL CLAY, PYR, CLASTS
- AUTH CLAY, POROSITY, QTZ OVRGTHS, CLASTS
- Fe CALCITE, QTZ OVRGTHS, POROSITY, DETRITAL CLAY, AUTHIGENIC CLAY, CLASTS
- Fe CAL, QTZ OVRGTH, PYR, CLASTS
- AUTH CLAY, POROSITY, CLASTS
- Corg, DTL CLAY, POROSITY, QTZ OVRGTHS, BITUMEN